UNIVERSITÉ DE NEUCHÂTEL
FACULTÉ DES SCIENCES

INSTITUT DE GÉOLOGIE
CENTRE D'HYDROGÉOLOGIE

Geometry and hydraulic parameters of karst aquifers: A hydrodynamic modeling approach

THÈSE

présentée à la Faculté des Sciences
de l'Université de Neuchâtel
pour obtenir le titre de
DOCTEUR ÈS SCIENCES

par

Attila Kovács

Soutenue le 17 Novembre 2003 devant le jury composé de:

Prof. Pierre Perrochet	Université de Neuchâtel (Suisse)	Directeur
Dr. Pierre-Yves Jeannin	Université de Neuchâtel (Suisse)	Codirecteur
Prof. László Király	Université de Neuchâtel (Suisse)	Expert
Prof. Martin Sauter	Georg-August-Universität Göttingen (Allemagne)	Expert
Prof. Daniel Hunkeler	Université de Neuchâtel (Suisse)	Expert

IMPRIMATUR POUR LA THESE

Geometry and hydraulic parameters of karst aquifers: a hydrodynamic modeling approach

M. Attila KOVACS

UNIVERSITE DE NEUCHATEL

FACULTE DES SCIENCES

La Faculté des sciences de l'Université de Neuchâtel, sur le rapport des membres du jury

MM. P. Perrochet (directeur de thèse), L. Kiraly, D. Hunkeler, P.-Y. Jeannin (La Chaux-de-Fonds) et M. Sauter (Göttingen D)

autorise l'impression de la présente thèse.

Neuchâtel, le 4 décembre 2003

La doyenne:

Martine Rahier

ABSTRACT

This thesis presents a method for characterizing flow systems in karst aquifers by acquiring quantitative information about the geometric and hydraulic parameters of a karst conduit network from spring hydrograph analysis. The investigation method applied consisted of constructing simple conceptual models of karst systems, and deducing analytical formulae describing the connection between aquifer parameters and hydrograph recession coefficient. The resulting formulae were then applied for evaluating input parameters for numerical models of the Bure aquifer (Jura, Switzerland). The comparison between model simulation results and real-world data permitted to test the applicability of the analytical formulae. The Bure test site also provided as a basis for evaluating some general characteristics of conduit networks by steady-state numerical models.

Analytical formulae identified two, significantly different flow domains, depending on the overall configuration of aquifer parameters. During the baseflow recession of mature karst systems, the conductivity of karst conduits does not influence the drainage of the low-permeability matrix. In this case the drainage process is influenced by the size and hydraulic parameters of the low-permeability blocks alone. This flow condition has been defined as matrix-restrained flow regime (MRFR). During the baseflow recession of premature karst systems and the flood recession of mature systems, the recession process is dependent not only on the hydraulic parameters and the size of the low-permeability blocks, but also on conduit conductivity, and the total extent of the aquifer. This flow condition has been defined as conduit-influenced flow regime (CIFR).

Steady-state numerical models demonstrated that field observations concerning the spatial geometry of karst conduits are generally insufficient, and that observed conduit networks must be extended to the entire domain in order to correctly reflect observed hydraulic response.

Analytical formulae demonstrated the drawbacks of equivalent models. While equivalent discrete-continuum models of premature karst systems may reflect their real hydraulic response, there is only one adequate parameter configuration for mature systems that yields appropriate recession coefficient. Consequently, equivalent discrete-continuum models are inadequate for simulating global response of mature karst systems. The global response of equivalent porous medium models corresponds to the transition between matrix-restrained and conduit-influenced flow regimes. Consequently, the equivalent porous medium approach cannot be directly applied for modeling karst aquifers.

Integrated numerical models demonstrated that retarded recharge due to epikarstic storage can considerably decrease the baseflow recession coefficient of the entire aquifer. In such cases, the estimation of aquifer parameters from global response using analytical formulae equally requires information about the separate hydraulic behavior of the subcutaneous layer.

A comprehensive hydrogeological revaluation and numerical modeling of the Bure aquifer demonstrated that the Malm Astarte Marls do not interrupt the hydraulic continuity of the aquifer. GIS-based calculations extended shallow karst zones in the area of Buix and Croix. The active conduit subsystems discharging to karst springs are far more extensive than observations would suggest. The Milandrine cave belongs to a mature karst system, where considerable water storage can be assigned to the epikarst layer.

RÉSUMÉ

Ce travail présente une approche pour caractériser les systèmes d'écoulement des aquifères karstiques. La méthode développée permet d'acquérir des informations quantitatives sur la géométrie et les paramètres hydrauliques du système sur la base d'une analyse de l'hydrogramme des sources. L'application de la méthode a exigé l'établissement d'un modèle conceptuel simple des systèmes karstiques et le développement de formules analytiques décrivant la relation entre les paramètres de l'aquifère et le coefficient de tarissement de l'hydrogramme. Les formules obtenues ont été utilisées pour évaluer les paramètres d'input nécessaires pour le modèle numérique de l'aquifère de Bure (Jura, Suisse). La comparaison entre le résultat des simulations et les données de terrain ont permis de vérifier l'applicabilité des formules analytique. Le site de test de Bure a également servi de base pour évaluer certaines caractéristiques générales du réseau de conduits grâce à des simulations réalisées en régime permanent.

Les formules analytiques ont permis d'identifier deux domaines différents de régimes d'écoulement pendant le tarissement dépendant de la configuration générale des paramètres de l'aquifère. Pour les systèmes karstiques bien développés, lors du tarissement, la perméabilité des conduits karstiques n'influence pas le drainage de la matrice peu perméable de l'aquifère. Dans cette situation, les processus de drainage sont uniquement influencés par la taille et les paramètres hydrauliques des volumes peu perméables. Ce régime d'écoulement dominé par les écoulements dans la matrice est appelé MRFR (matrix-restrained flow regime). Pour les systèmes karstiques précoces lors du tarissement et pour les systèmes karstiques bien développés lors des décrues, les processus de récession ne sont pas uniquement dépendants de la taille et des paramètres hydrauliques des volumes peu perméables, mais également des caractéristiques des conduits et de l'extension totale de l'aquifère. Ce type de condition a été appelé CIFR (conduit-influenced flow regime).

Les modèles numériques en conditions permanentes ont montré que les observations de terrain concernant la géométrie des conduits sont généralement insuffisantes, et que le réseau des conduits observé doit être étendu au domaine entier pour permettre de traduire correctement la réponse hydraulique observée.

Les formules analytiques utilisées démontrent les faiblesses des modèles équivalents. Les modèles équivalents continus discrets, permettent généralement de simuler le comportement global des systèmes karstiques précoces. Par contre une seule et unique configuration des paramètres hydrauliques permet de refléter la réponse globale des systèmes karstiques bien développés. Les modèles équivalents continus discrets ne sont pas donc adéquats pour décrire la réponse globale des systèmes karstiques bien développés. La réponse globale des modèles équivalents poreux correspond à la transition entre les régimes d'écoulements contrôlés par les volumes peu perméables et ceux contrôlés par les conduits. En conséquence, l'approche en milieu poreux équivalent ne peut pas être directement utilisée pour modéliser les systèmes karstiques.

Les modèles numériques intégrant l'épikarst ont montré l'influence du stockage dans cette zone sur le coefficient de récession de l'ensemble de l'aquifère. Dans un tel cas, l'estimation des paramètres de l'aquifère à partir de la réponse globale en utilisant des formules analytiques nécessite donc également des informations particulières concernant le fonctionnement de la zone épikarstique.

Une réévaluation complète de l'hydrogéologie et la modélisation numérique de l'aquifère de Bure a démontré que les Marnes à Astartes n'interrompent pas la continuité hydraulique de l'aquifère. Les calculs basés sur un SIG ont mis en évidence la présence d'un karst peu

profond dans la région de Buix et Croix. Les réseaux karstiques actifs des bassins alimentant les sources sont nettement plus étendus que les observations le laissent supposer. La grotte de la Milandrine appartient à un système karstique bien développé où la zone épikarstique joue un rôle de stockage important.

ZUSAMMENFASSUNG

In dieser Doktorarbeit wird eine Methode zur Charakterisierung von Fließsystemen in Karstgrundwasserleitern vorgestellt. Hierbei werden geometrische und hydraulische Parameter von Karstnetzwerken quantitativ aus der Schüttungscharakteristik von Quellen ermittelt. Die hier vorgestellte Untersuchungsmethode besteht aus der Erstellung einfacher Modellkonzepte zu Karstsystemen und der Ableitung analytischer Gleichungen zur Beschreibung eines Zusammenhanges zwischen Aquiferparametern und dem Auslaufkoeffizienten aus Schüttungsganglinien der Karstquellen. Mittels dieser analytischen Formeln werden die Eingabeparameter für die numerische Modellierung des "Bure-Aquifers" (Kanton Jura, Schweiz) berechnet. Der Vergleich der numerischen Simulationsergebnisse mit in-situ Daten der hydraulischen Parameter erlaubte die Validierung der Anwendbarkeit des Modells. Weiterhin diente das Bure-Testgebiet zur Bestimmung einiger genereller Eigenschaften von Karstsystemen mittels numerischer Modelle für ein stationäres hydraulisches Regime.

Die analytischen Berechnungen liefern zwei signifikant unterschiedliche Fließkomponenten, die von der Wahl der Grundkonfiguration der Aquiferparameter abhängen. Es zeigt sich, dass im Bereich des Basisabflusses von gut entwickelten Karstsystemen die hydraulische Leitfähigkeit der Karströhren keinen Einfluss auf die Entwässerung der hydraulisch gering leitfähigen Gesteinsmatrix hat. In diesem Fall wird der Abfluss allein vom Ausmaß der gering durchlässigen Blöcke und deren hydraulischen Parametern beeinflusst. Dieses Verhalten wird hier als "Matrix-kontrolliertes Fließregime" ("matrix-restrained flow regime", MRFR) definiert. Dagegen ist der Basisabfluss von Systemen im frühen Verkarstungsstadium sowie der Hochwasserrückgang von gut entwickelten Systemen nicht nur vom Ausmaß und den hydraulischen Parametern der gering leitfähigen Blöcke, sondern auch von der Leitfähigkeit der Karströhren und der Gesamtausdehnung des Aquifers abhängig. Demzufolge wird dieses Verhalten hier als "Röhren-kontrolliertes Fließregime" ("conduit-influenced flow regime", CIFR) bezeichnet.

Die numerischen Modellierungen für ein stationäres Fließregime haben gezeigt, dass vorhandene Geländedaten zur Bestimmung der räumlichen Verteilung von diskreten Karstwasserwegsamkeiten im allgemeinen unzureichend sind. Für das numerische Modell erwies es sich nämlich als notwendig, die vor Ort gewonnenen Informationen bezüglich des Karstnetzwerkes auf das gesamte Einzugsgebiet zu extrapolieren, um ein hydraulisches Ansprechen korrekt widerzugeben.

Weiterhin konnten mit Hilfe der analytischen Gleichungen die Schwächen von Äquivalenzmodellen aufgezeigt werden. Während diskret-kontinuum-Äquivalenzmodelle das hydraulische Ansprechen von nicht voll entwickelten Karstsystemen gut darstellen können, existiert für gut entwickelte Karstsysteme nur eine einzige entsprechende Parameterkonfiguration. Somit sind diskret-kontinuum-Äquivalenzmodelle für die Simulation des generellen Ansprechens eines entwickelten Karstsystems inadäquat. Dagegen entspricht die simulierte Schüttungscharakteristik im porös-Äquivalenzmodell dem Übergang von einem "Matrix-kontrollierten" zu einem "Röhren-kontrollierten" Fließregime. Somit kann auch dieser Ansatz nicht direkt zur numerischen Modellierung eines Karstgrundwasserleiters herangezogen werden.

Numerische Modelle, welche die Besonderheiten eines Epikarst miteinbeziehen, haben gezeigt, dass eine verzögerte Grundwasserneubildung – bedingt durch signifikante Wasserspeicherung in dieser Zone – den Auslaufkoeffizienten des Basisabflusses für den gesamten Aquifers merklich verkleinern kann. In solchen Fällen werden zusätzliche Daten

über die spezifischen Eigenschaften des Epikarst benötigt, um die Aquiferparameter mittels analytischer Berechnungen aus der Schüttungscharakteristik von Quellen zu bestimmen.

Eine umfassende hydrogeologische Neubewertung und numerische Modellierung des "Bure-Aquifers" hat gezeigt, dass die dortigen Astarte-Mergel des Malm nicht als hydraulischer Stauer fungieren. GIS-gestützte Berechnungen weisen zudem Bereiche von seichtem Karst in den Gebieten Buix und Croix aus. Die verschiedenen aktiven Fließsysteme, welche die einzelnen Karstquellen speisen, sind somit weit ausgedehnter als Geländebeobachtungen annehmen ließen. Die Höhle Milandrine ist Teil eines voll entwickelten Karstsystems, bei dem eine beträchtliche Wassermenge im Epikarst gespeichert wird.

TABLE OF CONTENTS

1. INTRODUCTION

Approximately 12 % of the Earth's surface is underlain by carbonate rocks, and 25 % of the planet's human population is supplied by karst waters (Ford & Williams, 1989). Although the proportion supplied vary from one region to another. In Europe, where 35 % of the land surface is occupied by carbonates, certain countries such as Slovenia and Austria obtain over 50 % of the total water supply from karst aquifers. The exploitation, maintenance of water quality, and the protection of karst aquifers are of a vital importance in these regions.

Besides conventional survey techniques, such as speleological surveys, geological mapping, borehole analysis, hydrograph analysis, chemical and isotopic analyses, tracing experiments, etc., the quantitative characterization of karst hydrogeological systems is increasingly important. Although numerical modeling techniques have been widely used for characterizing groundwater flow in porous media since the 1960s, the numerical modeling of groundwater flow in karst aquifers still represents a particular challenge, due to their strong heterogeneity and erratic hydraulic behavior.

1.1. CHARACTERISTIC FEATURES OF KARST AQUIFERS

The most important feature of karst aquifers from a hydrogeological perspective, that makes them different from any other kind of hydrogeological systems, is the high solubility of the flow medium in water. The solution process results in a positive feed-back loop, and thus a dynamic evolution of karst systems (Bedinger, 1966; Kiraly et *al*., 1971). Flowing groundwater dissolves the limestone around preexisting interconnected voids, thus enlarging their aperture and the hydraulic conductivity of the flow medium. The amount of dissolved carbonate depends on the chemical composition of the rock and of the water, but the relative karstification degree of the various fracture families depends mainly on the direction and the magnitude of the groundwater flux density vector (Király et *al.*, 1971, 2002). Consequently, the present hydraulic conductivity field and the void distribution result not only from the geological history of the rocks, but also from the overall evolution of the groundwater flow system. The geographical position of the recharge and discharge areas represent boundary conditions for the flow field, and their temporal evolution also influences karstification and hydraulic conductivity field (**Figure 1-1**).

The most significant consequence of limestone dissolution associated with karst evolution is increasing hydrogeological heterogeneity. Strong heterogeneity manifests in duality of fundamental hydraulic processes occurring in the aquifer (Király, 1994):

- Duality of the infiltration processes ("diffuse" or slow infiltration into the low permeability volumes contrasts with "concentrated" or rapid infiltration into the channel network). Apart from surface streams that disappear in sinkholes, concentrated infiltration can be enhanced by rapid drainage taking place in a shallow high conductivity zone termed epikarst (Mangin, 1975).
- Duality of the groundwater flow field (low flow velocities in the fractured volumes contrasts with high flow velocities in the channel network).
- Duality of the discharge conditions (diffuse seepage from the low permeability volumes compared to concentrated discharge from the channel network at the karst springs).

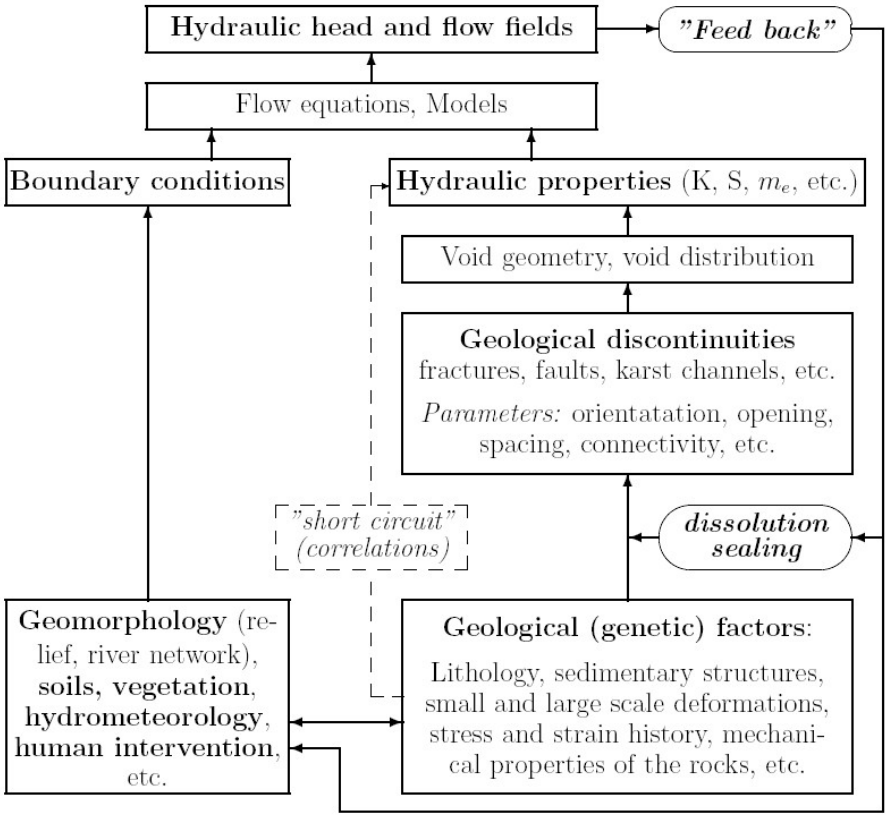

Figure 1-1: Schematic representation of the relations between groundwater flow field, hydraulic properties and geological factors in karst aquifers (after Király, 1975, modified).

1.2. CONCEPTUAL MODELS OF KARSTIC GROUNDWATER FLOW

Every reasonable conceptual model of karst systems incorporates heterogeneity and accordingly the duality phenomenon cited above. Moreover, most of the conceptual models distinguish three main zones (sub-systems) in the vertical direction. These are: soil with epikarst, unsaturated zone, and phreatic zone. Although many conceptual models include similar structural features, the role assigned to these features in the conductive and storage processes varies. Similarly, the geometric configuration of the high-conductivity conduit system also shows considerable differences.

According to the conceptual model of Mangin (1975), active conduit systems develop along one, well defined horizon (**Fig. 1-2**). Although deep phreatic conduits may exist, the majority of the conduit flow takes place near the saturated and unsaturated zone interface. This main conduit system transmits infiltration waters towards the karst spring but is poorly connected to large voids in the adjacent rocks, referred to as the 'annex-to-drain system'. The particularity of Mangin's conceptual model is that it associates the storage function of karst aquifers to the 'annex-to-drain system'.

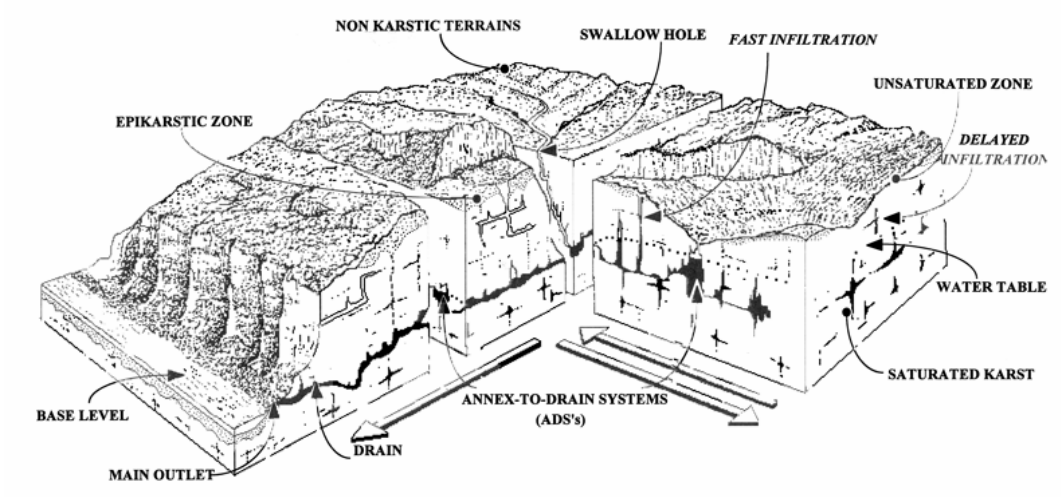

Figure 1-2. Conceptual model of a karst aquifer according to Mangin (1975).

Mangin (1975) introduced the concept of the *epikarst*. This being a shallow, high-permeability karstified zone below the aquifer surface (**Fig. 1-3**). This zone is assumed to hinder the surface runoff by absorbing and temporarily storing rainfall water. Moreover, it rapidly drains infiltrating waters toward enlarged vertical shafts, thus enhancing concentrated infiltration; the remaining stored water constitutes a perched saturated zone, and may contribute to diffuse recharge.

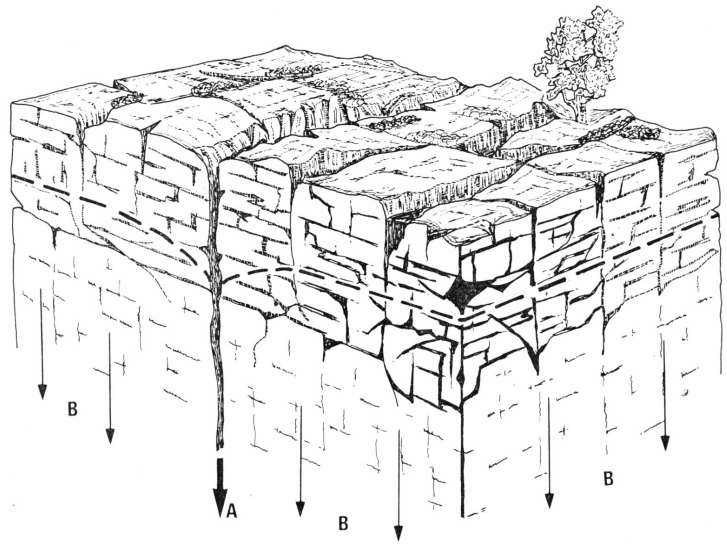

Figure 1-3. Schematic representation of the epikarst zone after Mangin (1975).
This zone rapidly drains infiltrating waters toward enlarged vertical shafts thus enhancing concentrated infiltration (A). Remaining stored water contributes to diffuse recharge (B).

The conceptual model of Drogue (1974, 1980) assumes, that the geometric configuration of karst conduit networks follow original rock fracture pattern; the hydraulic conductivity of certain fractures increase during the karstification process. Joints constitute a double-fissured porosity system (**Fig. 1-4**). This network consists of fissured blocks of hectometric size, separated by high-permeability conduits, which give rise to rapid flow. Every block is dissected by low-permeability fractures, in which slow groundwater flow takes place. The uppermost part of the aquifer is more intensely fissured than subjacent rock because of decompression phenomena. This increased permeability zone is responsible for enhanced infiltration of rainwater.

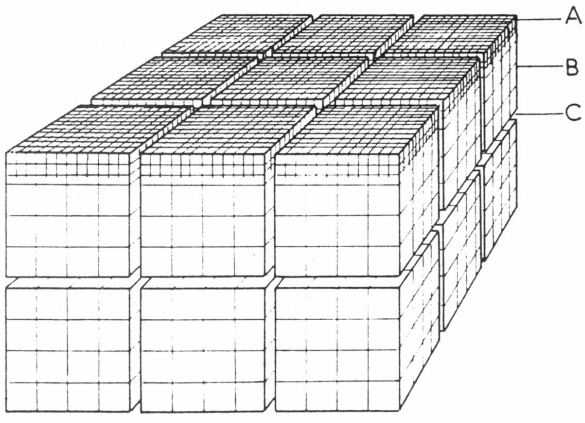

Figure 1-4. Conceptual model of a karst aquifer according to Drogue (1980). A: highly permeable upper zone, B: blocks with low-permeability cracks with slow flow, C: high-permeability karst conduits with rapid flow.

The conceptual model proposed by Király (1975, 2002) and Király et al. (1995) combine the two models discussed above. Although Királys (1975) model employs a hierarchical conduit network similar to the model of Mangin (1975) and takes the effect of the epikarst into account, it also comprises the hydraulic effect of nested discontinuity groups similar to those involved in the model of Drogue (1980). Király (1975) demonstrated the scale effect to be a consequence of coexisting discontinuity groups of different scale (**Fig. 1-5**). The term 'scale effect' denotes that the hydraulic conductivity of limestone rocks changes with the sample volume at every scale. Consequently, the definition of reference hydraulic parameters is not evident.

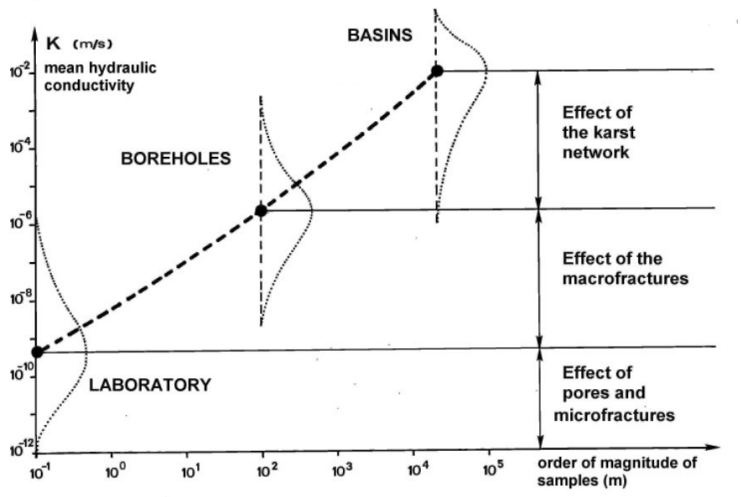

Figure 1-5. Scale effect on the hydraulic conductivity in fractured and karstified limestone aquifers (after Kiraly 1975, modified).

Királys (1975) solution for the problem was to combine the "fracture model" with the "intersection model". In other words the aquifer permeability was determined by the fracture intersections, and the effective porosity was determined by the fractures plains. According to the conceptual model of Király & Morel (1976a), two classes of hydraulic parameters can adequately reflect the hydraulic behaviour of karst systems. Carbonate aquifers can be

considered as interactive units of a high-conductivity hierarchically organized karst channel network with a low-permeability fissured rock matrix. The most significant difference between the model of Mangin (1975) and the models of both Drogue (1980) and Király (1975) is that while Mangin (1975) associates the storage function of karst aquifers with the 'annex-to-drain system', the later two authors associate it to the low-permeability matrix. The principal strength of Király's (1975) conceptual model is that it has been quantitatively tested and verified by numerical modeling (Király & Morel, 1976ab; Király et *al*., 1995). The main characteristics of this model have been synthesized in a conceptual model by Doerfliger & Zwahlen (1995) for the purpose of vulnerability mapping. A schematic representation of this concept is provided in **Figure 1-6**.

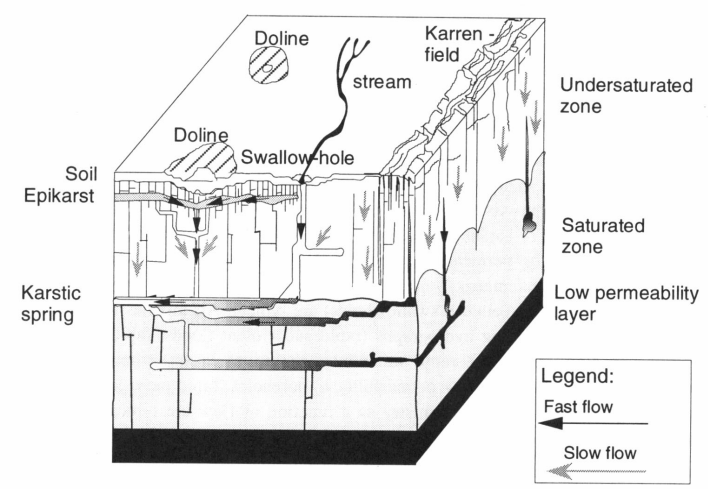

Figure 1-6. Conceptual model of karst aquifers. Doerfliger & Zwahlen (1995).

Two, fundamentally different approaches exist for studying and characterizing natural systems, including karst hydrogeological systems involving different survey techniques. The *functional approach* first applied to karst systems by Mangin (1975) focuses on analyzing the global temporal behavior of karst aquifers, and it does not account for spatially distributed parameters. However, the interpretation of results often involves hypotheses concerning the structural characteristics of the system, expressed in a qualitative form. This method has the advantage of having a relatively low data demand, and its suitability for making predictions. The disadvantage of this approach is that it does not provide a direct link between a spatially distributed hydraulic parameter field and the aquifers global response.

The *structural approach* first applied to karst systems by Király (1975) is based on physical phenomena, and it aims to deduce the temporal behavior of the system as the hydraulic response of a fully defined flow medium (representing the aquifer) given to the input signal. The principal advantage of this approach is that it synthesizes spatially distributed aquifer properties, recharge and discharge characteristics, and flow field in a strict and coherent form. Secondary advantage is that it allows for testing hypotheses involved in the functional approach. The disadvantage of the structural method is that it has high data demand especially for accurate hydraulic parameter distribution; this is difficult to obtain because of the strong heterogeneity of karst systems.

1.3. DIFFICULTIES IN MODELING OF KARST SYSTEMS

Mathematical models of groundwater flow have been developed since the late 1800s, and have evolved rapidly during the second half of the 20th century. However, analytical models developed over this period contain strong simplifications of real systems. The rapid development of computer science and technology since the 1960s facilitated the discretization of flow field and mathematical equations, and made the solution of more complex hydrogeological problems possible. In the meantime the utilization of numerical groundwater flow models in porous media has become an every-day practice. The reconstruction of a regional groundwater flow field, which is consistent with a given hydraulic conductivity field and with given boundary conditions, nearly always requires the use of numerical models (Király, 2002). However, the application of numerical methods in karst hydrogeology still remains very limited, and is mainly used for verifying general conceptional models of karst systems. This is because of several difficulties arising during almost every step of the modeling process. A general schema of groundwater flow modeling (**Fig. 1-7**) and the description of difficulties related to modeling karst systems were provided by Király (1994).

The first step of any modeling study is the schematic representation of the real system. This schema is also called conceptual model, and consists of the appropriate differential equations that describe flow within the geologic medium to be modeled, the geometry of the aquifer, a set of flow parameters, boundary conditions and initial conditions for every point of the model domain. The hydraulic parameter fields applied in groundwater flow models are usually obtained by interpolation between discrete observations. Because of the strong local heterogeneity of karst aquifers, the interpolation technique yields unacceptable results. Probably the most difficult task in karst modeling is to characterize the heterogeneity of the flow parameters, in other words to determine the geometry and hydraulic parameters of the high-conductivity conduit network.

The second problem is related to the development of a computer code based on numerical methods which allows the equations defined in the abstract scheme to be solved. The problem is not straightforward and in most cases the numerical model is only an imperfect realization of the abstract scheme. Strong heterogeneity of the flow medium and different flow regimes in high-conductivity channels and in the low-permeability matrix make the development of appropriate computer modeling codes particularly challenging.

The third problem in deterministic groundwater flow modeling is the transfer of the simulated results to a real system. These results are only valid in the numerical model, and their meaningful transfer into the real system requires that simplifying assumptions made in the conceptual and numerical models appear as uncertainties in the simulation results. Because of the higher degree of heterogeneity, these uncertainties are much higher for karst systems than for most porous aquifers.

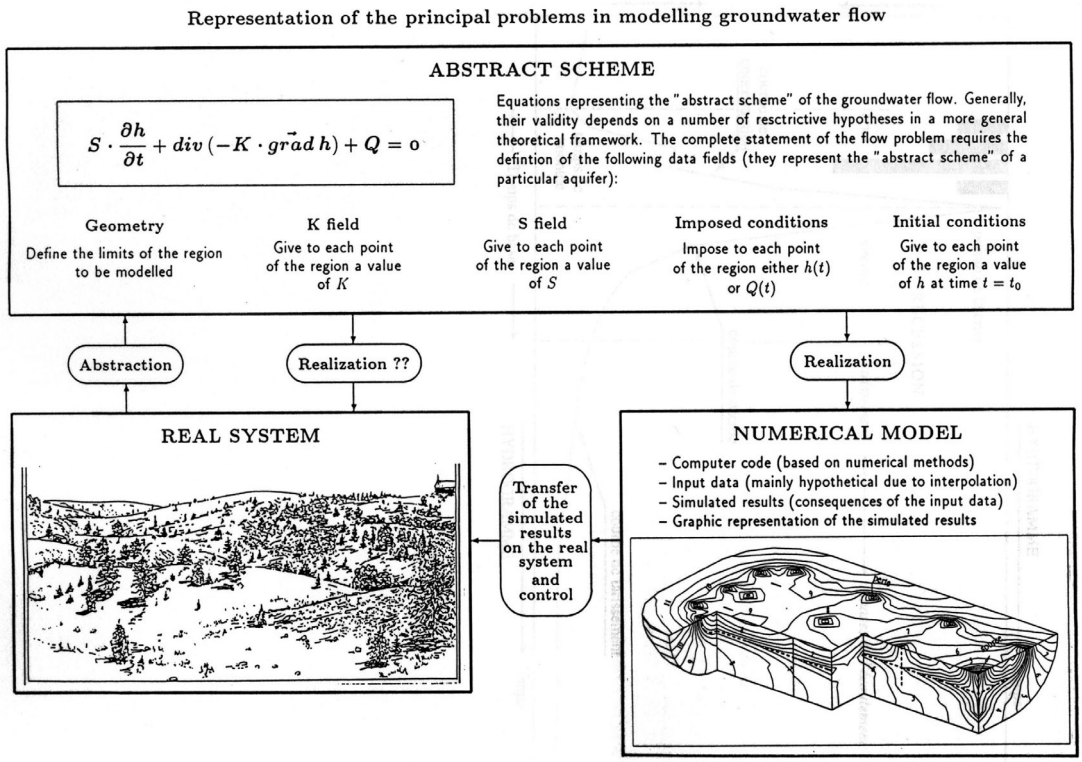

Figure 1-7: Principal tasks and related problems in modeling groundwater flow (after Kiraly 1994, modified).

1.4. OBJECTIVES AND THESIS STRUCTURE

As mentioned in Chapter 1.3., the principal obstacle in deterministic distributive modeling of karst hydrodynamics is the lack of sufficient field observations of the karst conduit system geometry and hydraulic parameters. Speleological exploration is limited to a minimum conduit diameter corresponding to the size of the human body, and in the case of phreatic conduits, to a maximum residence time of some hours attainable by underground scuba diving techniques. The reasonable high-resolution information that can be recovered by surface geophysical methods is limited to a penetration depth of some tens of meters, and these methods can rarely differentiate between active water-filled features, ancestral dry conduits, and fractures. Furthermore, they are often limited to easily accessible locations. Tracing techniques can provide information on travel time and conduit network interconnectivity, but not on exact conduit geometry. Similarly, boreholes are difficult to drill into karst conduits, and pumping tests do not always provide reliable information.

The principal aim of this thesis is to characterize flow systems in karst aquifers by acquiring quantitative information concerning the geometric and hydraulic parameters of the karst conduit network from the global hydraulic response of karst systems. This has been done with the secondary aim of facilitating hydraulic parameter estimation for groundwater flow modeling of karst hydrogeological systems using distributive models.

These goals have been achieved by applying two different investigation strategies (**Fig. 1-8**). A numerical approach consisted of the development of several conceptual models that are consistent with field observations. Field observations and measured hydraulic parameters were introduced into deterministic numerical models, used to simulate the global (spring hydrograph), and the spatial (groundwater flow field) behavior of the aquifer. Simulation results were compared with field measurements, and respective conceptional models were rejected, modified or accepted according to the validity of results. An analytical approach for

investigating more fundamental phenomena consisted of setting up conceptual models with simple geometries and deducing analytical solutions for the global hydraulic response of these model configurations. The analytical formulae were then tested by numerical models and simulation results were compared to generally accepted ideas about the hydraulic functioning of karst aquifers, deduced from field observations. A real-world application is also provided in order to test the limits of applicability of these analytical formulae.

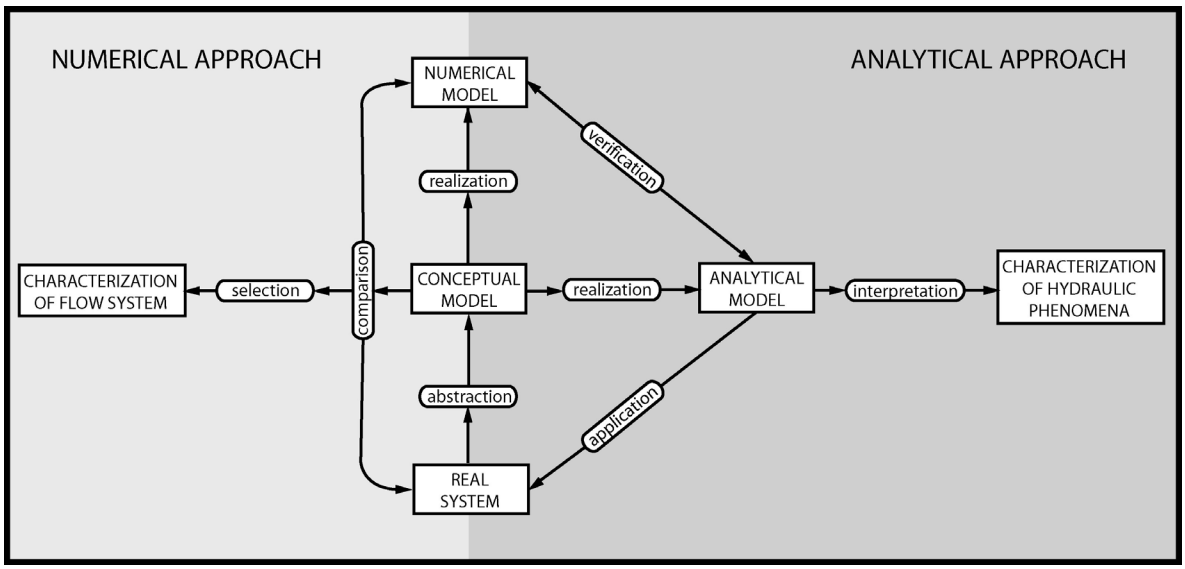

Figure 1-8. Investigation strategies applied for characterizing geometric and hydraulic parameters of karst conduit networks.

The construction of detailed and precisely calibrated groundwater flow models of particular aquifers is not of our interest in the present study. Contrary, this thesis aims to describe the general geometric and hydraulic characteristics of karst systems. Consequently, several simplifications of real systems have been applied, in order to keep models simple and controllable. This permitted to focus on the investigated phenomena, to decrease simulation time, and to exclude poorly defined phenomena, which can unnecessarily complicate the modeling process and lead to misinterpretations. Bearing these points in mind, only saturated flow in a two-dimensional flow medium was considered. Moreover, the low-permeability fissured medium was assumed to be homogeneous and isotropic. Finally, darcian flow and only water compression-related storage was assumed in karst conduits. As is demonstrated in the following chapters, these simplifications allowed the conduit network to be characterized in a general manner, and facilitated the quantitative characterization of the connection between aquifer properties and aquifer global hydraulic response.

Although several distributive modeling approaches have been applied for modeling karst hydrogeological systems, most of them are inadequate for simulating both temporal and spatial hydraulic behavior. Indeed, most of these approaches can be used when certain restrictions apply (Chapter 2). The nested model concept of geological discontinuities presented in Section 1.1. nearly always requires the combination of the continuum and the discrete approaches. The combined discrete-continuum approach proposed by Király & Morel (1976a) and Király (1979, 1985, 1988) facilitates the implementation of one- and two-dimensional discrete features into two- or three-dimensional continua. This is achieved by applying the finite element discretization method, which allows for the combination of one-,

two-, and three-dimensional finite elements. As representing a direct link between imposed hydraulic properties and simulation results, this approach is very suitable for testing conceptual models of karst hydrogeological systems, and serves as the basic investigation tool for this thesis.

The test site which provides a basis for verifying the validity of conceptual models is the Bure aquifer, located in the Jura Mountains, Ajoie, Switzerland. It underlies a sparsely populated area, and is relatively pristine. Consequently it represents almost natural conditions. For that reason it has been the target of several hydrogeological studies since the early nineties (Grasso & Jeannin, 1994ab; Jeannin, 1995ab; Jeannin & Grasso, 1995ab; Jeannin & Maréchal, 1995; Gretillat, 1996). These studies have included discharge measurements and hydrograph analyses, tracing experiments and water balance calculations, hydrochemical measurements and surface geophysical surveys, and yielded a considerable quantity of data, which allow numerical models to be verified. However, the revaluation of the most recent geological and hydrogeological data has not yet been done, and the synthesis of these hydrogeological observations into a coherent conceptual model constitutes an important goal of this thesis.

This thesis includes five separate studies focusing on different subjects. However, these studies follow a logical succession, and approach the principal goal step-by-step:

Chapter 2 provides a classification and critical review of the most frequently used global and distributive modeling methods in karst hydrogeology. This chapter provides the basics for further applications, and represents a link between conceptions behind global and distributive approaches. Furthermore, it provides a detailed description of the investigation tools applied in this thesis.

Chapter 3 provides an adequate real-world reference for further numerical modeling surveys. This chapter synthesizes most recent hydrogeological information from the Bure Plateau into a coherent conceptual model. This database can be then used as a basis for testing general conceptional models of karst systems.

Chapter 4 aims to identify the general geometric (extent and organization) and hydraulic characteristics of karst conduit networks. This is achieved by constructing steady-state numerical models of the Bure aquifer, and comparing simulation results with field observations. This chapter also aims to investigate the applicability of field observations for constructing reasonable numerical models.

Chapter 5 provides a quantitative link between aquifer's global response and spatially distributed hydraulic parameters, thus facilitating the estimation of conduit network characteristics from spring hydrograph recession coefficients. This is achieved by analytical survey and sensitivity analyses performed on synthetic models. Furthermore, this chapter exposes some fundamental characteristics of the hydraulic behavior of karst hydrogeological systems, which substantially determine the outcome of any numerical model configurations, and suggest the classification of karst systems based on physical phenomena. The domain of validity of equivalent parameter models is also evaluated here; this is an important issue, as equivalent parameter models are often used for modeling karst systems.

The aim of Chapter 6 is to demonstrate an application of the analytical formulae discussed in Chapter 5 for constructing transient flow models of real systems. This chapter gives an example for the parameter estimation and a possible methodology for modeling karst aquifers using the combined discrete-continuum approach. The effect of the epikarst on the global response of karst systems is also demonstrated here. This was achieved by simulating

the global response of a real karst system given to precipitation events, using distributive models.

Appendix 1 contains a list of symbols applied in this theis.

Appendix 2 provides a methodology for integrating Geographical Information Systems (GIS) into the groundwater flow modeling process of karst aquifers.

Appendix 3 contains parameter configurations and simulation results of two-dimensional square synthetic models applied for verifying analytical formulae deduced in Chapter 5.

2. MODELING KARST HYDRODYNAMICS (REVIEW)

ABSTRACT

This study presents a critical review and systematic classification of global and distributive methods for modeling karst hydrodynamics. Global methods are based on the analysis of spring discharge time series. These data are believed to reflect the overall hydraulic characteristics of karst hydrogeological systems. Single event methods deal with the global response of karst systems given to a single rainfall event. Although these methods are considered to reflect the physical functioning of karst hydrogeological systems, they neglect spatial heterogeneity, and their interpretation is only qualitative. Time Series Analyses involve the mathematical analysis of the response of karst systems given to a succession of rainfall events. As these methods are based on pure mathematical operations, they cannot be directly related to physical phenomena. The drawback of time series analytical techniques lies in their failure to consider temporal and spatial distributions of the rainfall, which may significantly influence uni- and bivariate statistical parameters. Distributed parameter models incorporate two concepts. Discrete approaches describe flow within networks of fractures or conduits. Continuum approaches treat heterogeneities in terms of effective model parameters and their spatial distribution. The Combined Discrete-Continuum approach (CDC) permits these methods to be combined. The Discrete Fracture Network Approach (DFN) simplifies a real system into a fracture network, and can be applied to fractured aquifers. The Discrete Channel Network Approach (DCN) considers groundwater flow in pipes as representing karst conduits or fracture intersections. DCN models can be applied to local scale modeling. The Equivalent Porous Medium Approach (EPM) neglects strong heterogeneity of the hydraulic parameter fields, and is inadequate for modeling groundwater flow in karst aquifers. In the Double Continuum (DC) concept, the conduit network and the fissured medium are represented as different continua. The low data demand of DC models makes this method a useful tool for modeling water resources or water budget problems. The CDC approach can handle discontinuities at all scales in karst systems. This approach is the only modeling concept that facilitates the direct realization of real parameter fields and geometry of karst aquifers. However, the practical application of this approach is limited by its high data demands.

Keywords: Karst, Modeling, Global methods, Distributive methods, Reservoir models, Hydrograph analysis, Black-box models, Discrete approach, Continuum approach, Classification of karst aquifers

2.1. INTRODUCTION

Mathematical models are exact tools for quantitatively characterizing the hydraulic behavior of karst hydrogeological systems. There are two fundamentally different types of models for the description of karst hydrodynamics.

As a consequence of the hierarchical structure of karst systems, the temporal variations of spring discharge reflect the overall (global) hydrogeological configuration of karst aquifers. *Global models* consist of the mathematical analysis of spring discharge time series (hydrographs). According to this approach, karst systems can be considered as transducers that transform input signals (recharge) into output signals (discharge). As the acquisition of spring discharge data is relatively simple, these models have been already used since the beginning of the last century. However, global models do not take into account the spatial variations within the aquifer. Consequently, they cannot provide direct information concerning aquifer hydraulic parameter fields.

For the quantitative characterization of the spatial variations of hydrogeological phenomena, the application of *distributive models* becomes necessary. Distributive methods consist of subdividing the model domain into homogeneous sub-units, and calculating groundwater flow by applying flow equations derived from basic physical laws. As they may consider both spatial and temporal variations of the recharge, the hydraulic parameters, and the discharge, distributive models can represent the complete quantitative characterization of flow systems in karst aquifers. However, distributive methods require sufficient information on aquifer geometry, hydraulic parameter fields, and recharge conditions. These parameters are often difficult to obtain.

Although several global and distributive methods exist, most of them are only suitable for specific hydrogeological problems, and may be applied under certain conditions. The aim of this study is to provide a critical review and systematic classification of modeling methods used for karst hydrogeological problems, in order to facilitate the selection of the appropriate method and the interpretation of model results.

2.2. GLOBAL METHODS

The measurement of discharge with time at the outlet of a karst aquifer makes the integral characterization of the hydraulic behavior of the entire system possible. The following two types of spring hydrograph analytical methods can be distinguished (Jeannin & Sauter, 1998):

Single Event Methods deal with the global hydraulic response of the aquifer to a single rainfall event. It is widely accepted, that three basic attributes manifest in the global response of a karst aquifer: Recharge, storage and transmission. Existing spring hydrograph analytical techniques make the characterization of these properties possible in a qualitative sense, but not quantitatively. However, most of these methods are based on simple, or sometimes more complex cascades of reservoirs, and involve physical phenomena. Consequently, it is more appropriate to call them *"grey-box models"* instead of *"black-box models"*.

Time Series Analyses deal with the global hydraulic response of karst systems to a succession of rainfall events. Univariate time series analytical methods are capable of identifying cyclic variations. Bivariate time series analyses are very suitable for analyzing the relation between the input (recharge) and output (discharge) parameters of different karst systems. These methods are based on pure mathematical operations, and they cannot be directly related to physical phenomena. Time-series analyses provide limited information

concerning the physical properties of the system itself. Consequently, they are "*black-box models*". On the other hand, the interpretation of the results of such models sometimes refers to some aspects of the hydraulic behavior of karst systems.

2.2.1. SINGLE EVENT METHODS (GREY-BOX MODELS)

Responding to a single rainfall event, spring hydrographs manifest a discharge peak having a delay, relative to the storm event. This peak can be generally decomposed into three main components: rising limb, flood recession and baseflow recession. During the last century many approaches have been developed to quantitatively characterize the recession limb of discharge peaks.

2.2.1.1. THE EXPONENTIAL RESERVOIR MODEL

This classical expression provided by Maillet (1905) is based on the emptying of a reservoir, and supposes that the spring discharge is a function of the volume of water held in storage. This behavior is described by an exponential equation as follows:

$$Q_{(t)} = Q_0 e^{-\alpha t} \tag{2-1}$$

where Q is the discharge [L^3T^{-1}] at time t, and Q_0 is the initial discharge [L^3T^{-1}] at an earlier time, α is the recession coefficient [T^{-1}] usually expressed in days. If this curve is plotted on a semi-logarithmic graph, it is represented as a straight line with the slope -α. This equation is usually adequate for describing karst systems at low water stages.

2.2.1.2. COMPOSITE EXPONENTIAL RESERVOIR MODEL

Decreasing limb of hydrograph peaks can usually be decomposed into several exponential segments. Forkasiewitz & Paloc (1967) assumed, that different segments of a spring hydrograph peak represent different parallel reservoirs, all contributing to the discharge of the spring (**Fig. 2-1**). They argued that such behavior reflects the existence of three reservoirs, representing the conduit network, an intermediate system of well integrated karstified fissures, and a low permeability network of pores and narrow fissures. According to this model, spring discharge can be described by the following formula:

$$Q_{(t)} = Q_1 e^{-\alpha_1 t} + Q_2 e^{-\alpha_2 t} + Q_3 e^{-\alpha_3 t} \tag{2-2}$$

Despite the simplicity of this approach, the analysis of spring hydrographs simulated by numerical models performed by (Kiraly & Morel, 1976b), and later by Eisenlohr et *al.* (1997a) have disproved its validity. According to Kiraly & Morel (1976b), different exponential hydrograph segments do not necessarily correspond to aquifer volumes with different hydraulic conductivities. Three exponential reservoirs can be fitted on the hydrograph of a system consisting of only two classes of hydraulic conductivities. In this case, the intermediate exponential could simply be the result of transient phenomena in the vicinity of the high hydraulic conductivity channel network. The baseflow recession coefficient component depends on the global configuration of the entire aquifer, not only on the hydraulic properties of the low-permeability matrix.

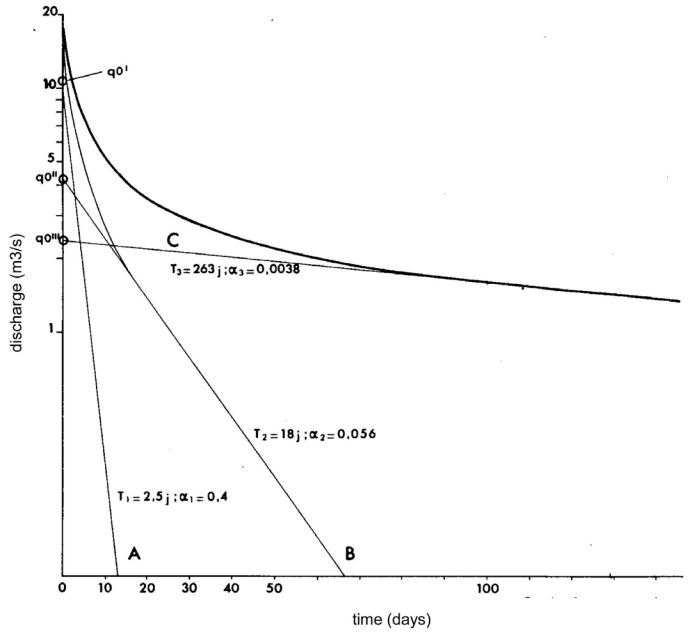

Figure 2-1. Decomposition of recession curves according to Forkasiewicz & Paloc (1967).

2.2.1.3. HYPERBOLIC FUNCTION MODEL

Drogue (1972) attempted to describe the whole recession process by using one single hyperbolic formula of the following form:

$$Q_{(t)} = Q_0 /(1+\alpha t)^n \tag{2-3}$$

where Q_0 is the discharge at an initial time, and α is called recession coefficient. This coefficient used by Drogue (1972) is not equivalent to the recession coefficient used by Maillet (1905). Although it is dependent on the slow recession process, it also depends on the fast recession process; these being two distinct physical phenomena. The exponent n is a calibration parameter usually having the values of 1/2, 3/2 and 2 (**Fig. 2-2**). Drogue describes the entire discharge process with a single, two-variable hyperbolic formula, and introduces a new parameter β, which depends on α and n.

$$\beta = \frac{\alpha}{\sqrt[n]{Q_0}} \tag{2-4}$$

Based on experimental relations the author proposed the dependence of the recession parameter β on the aquifer characteristics as follows:

$$\beta = f\left(\frac{K}{E \cdot R \cdot S_s}\right) \tag{2-5}$$

where K is hydraulic conductivity, S_s is specific storage coefficient, R is the surface area of the aquifer and E is the moisture condition of the aquifer and of the soil prior to the discharge process. Consequently, β may be regarded as a global parameter, while K and S are equivalent parameters, which can hardly be correctly measured in reality.

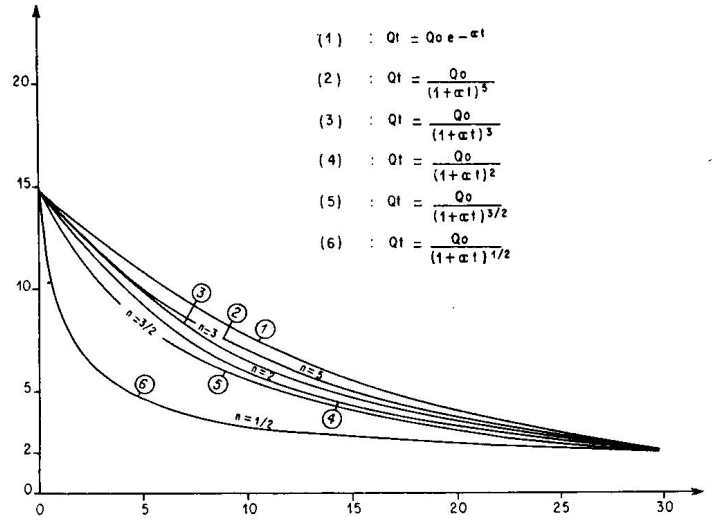

Figure 2-2: Hyperbolic fitting curves with different exponents suggested by Drogue (1972). This model describes two distinct phenomena (fast and slow recession) using a single formula. The exponent n=3/2 is the most representative, since it agrees with almost 60 % of the cases investigated.

This method provides a very good fit of the recession curves. However, it only provides qualitative information on the overall hydraulic parameters of the system itself. Using this approach the entire recession curve may be reproduced using one single recession parameter representing the physical properties of the entire karst system.

2.2.1.4. MANGIN'S HOMOGRAPH FORMULA

Mangin (1975) distinguished two processes that influence recession curves. The discharge from the non-saturated zone with a non-linear flood recession, as represented by the function $\Psi_{(t)}$, while the discharge from the saturated zone with a linear baseflow recession is represented by the function, $\Theta_{(t)}$. The recession curve can thus be expressed as follows:

$$Q_{(t)} = \Psi_{(t)} + \Theta_{(t)} \tag{2-6}$$

$\Theta_{(t)}$ is described by the classical Maillet formula (**Eq. 2-1**). Mangin provides the following empirical formula to express $\Psi_{(t)}$:

$$\Psi_{(t)} = q_0 \frac{1-\eta' \cdot t}{1+\varepsilon \cdot t'} \tag{2-7}$$

where q_0 is the difference between the peak discharge (Q_0), and discharge at the beginning of the slow recession (Q_{R0}). $\eta = 1/t_i$ [T^{-1}], where t_i is the duration of the fast recession and ε is the *coefficient of heterogeneity*, characterizing the concavity of the fast recession limb (the higher the value of ε is, the higher the concavity) (**Fig. 2-3**).

The volume of water in storage in the saturated zone above the level of the outflow spring is termed *dynamic volume.* Under baseflow conditions this may be found by integrating the Maillet equation:

$$V_d = \int_{t=0}^{\infty} Q_0 e^{-\alpha t} = \frac{Q_0}{\alpha} \tag{2-8}$$

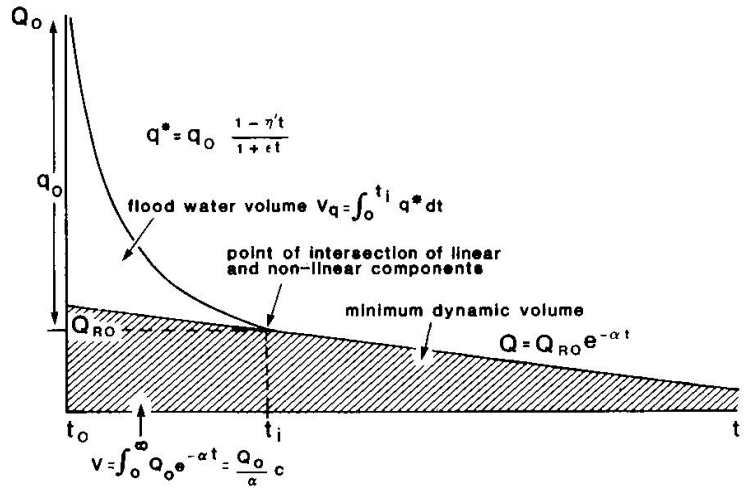

Figure 2-3: Recession curve analysis following Mangin`s approach (Ford &Williams 1989).

The approach of Mangin (1975) allows for good curve fitting. Furthermore, the technique characterizes the fast and slow recession processes separately, referring to physical characteristics in both cases. Based on this method, Mangin (1975) proposed a classification of karst systems. The author introduced the *regulation power* parameter (K_r), and defined as follows:

$$K_r = \frac{V_d}{V_t} \tag{2-9}$$

where V_d is the dynamic volume **(Eq. 2-8),** and V_t is the total discharge volume over an annual hydrological cycle. Mangin (1975) also introduced the parameter *i*, and defined it as the value of the function $\Psi_{(t)}$, picked two days after a flood peak, divided by the initial discharge (Q_0). Parameter *i* is assumed to represent the retardation between infiltration and discharge. Based on the plot of *i* against *K,* the author classifies karst aquifers according to **Figure 2-4.**

A critical study performed by Grasso & Jeannin (1994a) pointed out, that although *K* seems to be quite stable, parameter *i* shows a large variation for different recharge events for the same spring.

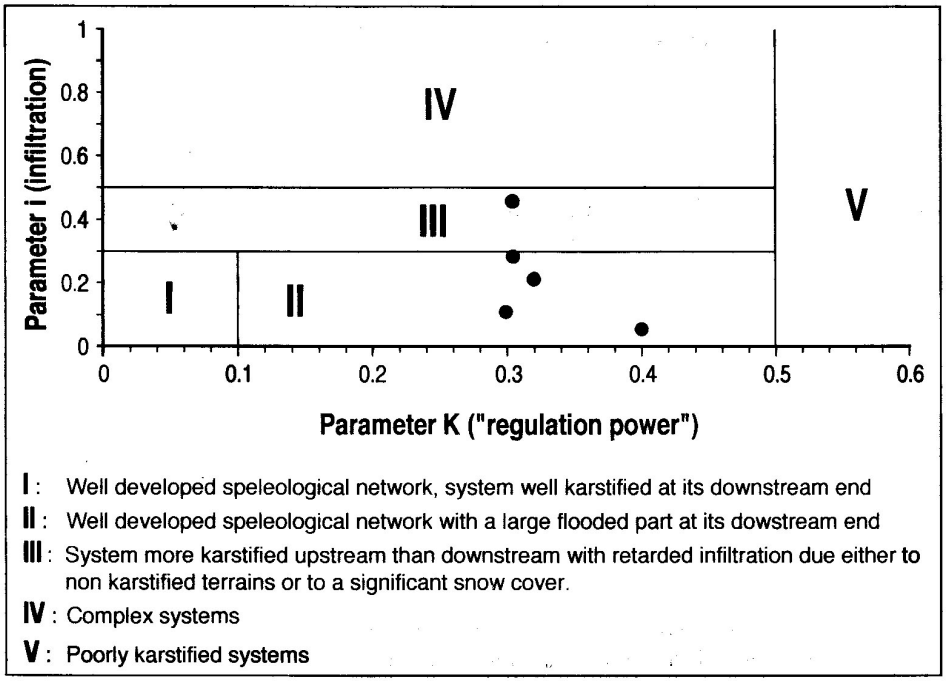

Figure 2-4. Classification of karst aquifers according to Mangin (1975), from Jeannin & Sauter (1998). Points represent various flood events from the same karst system (Milandrine, Jura, Switzerland). Although the parameter K seems to be stable, parameter i shows a large variation.

2.2.1.5. CASCADING RESERVOIR MODELS

Cascading reservoir models (also called lumped parameter models) consider a hydrogeological system as a union of different sub-domains, all having specific hydraulic parameters that interact with each other. This method was first proposed by Mero (1963, 1969), Mero & Gilboa (1974) and was later widely used by Guilbot (1975), Bezes (1976) and others.

Meros original equation considers the sum of the continuity equation for each distinct element of the medium:

$$\sum_{j=1}^{n} \frac{dV}{dt} = \sum_{j=1}^{n} S_{sj} A_j \frac{d\bar{H}_j}{dt} = \sum_{j=1}^{n} Q_{i,j} \tag{2-10}$$

where S_s is the storage coefficient [L^{-1}], $\bar{H}$ is the weighted average hydraulic head [L] in unit j and A_j is the recharge area [L^2] of unit j. Every sub-domain can be modeled as an individual reservoir, each having specific recharge and discharge conditions, conductive properties and storative properties. The different number of individual reservoirs applied, and the different interconnections introduced between them results in a variety of configurations. The complexity of these models make the use of computer codes necessary. One possible configuration developed by Bezes (1976) is presented in **Figure 2-5.**

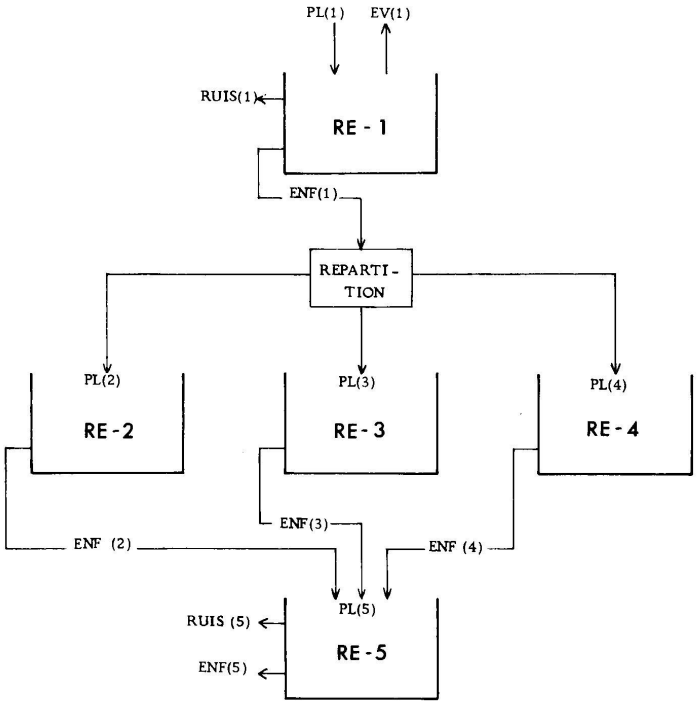

Figure 2-5. The structure of the BEMER model developed by Bezes (1976). PL=precipitation, EV=evapotranspiration, ENF=baseflow, RUIS=Surface runoff, RE=reservoirs (subsystems).

Lumped parameter models are based on physical phenomena. Consequently, they can supply significant information on the global functioning of a karst system. However, these models lack spatial predictive power since they do not consider spatial heterogeneity of the aquifers.

2.2.2. TIME SERIES ANALYSIS

Most of the methods used in time series analysis were principally developed by Jenkins and Watts (1968), and some later works. These investigations mainly focused on forecasting and data completion. The application of time series analyses to the description of the functioning of karst aquifers first appeared in Mangin (1971, 1975, 1981, 1984).

Conventional time series analysis uses both univariate (auto-correlation, spectral analysis) and bivariate (cross-correlation, cross-spectral analysis) methods. Univariate methods characterize the individual structure of the time series, while bivariate methods characterize the transformation of an input function into an output function.

2.2.2.1. UNIVARIATE METHODS

The *Auto-correlation* method is a tool for identifying some overall characteristics of a discharge time series, particularly cyclic variations. These variations may be related to some structural characteristics of karst aquifers. The auto-correlation method compares the discharge time series with itself. The time series is analysed with a systematically increased shift relative to itself, and the sample correlation coefficient is calculated for each shift. The auto-correlation coefficient is calculated using the following equations:

$$c_k = \frac{1}{N}\sum_{i=1}^{N-k}(z_t - \bar{z})(z_{t+k} - \bar{z}) \tag{2-11}$$

$$r_k = \frac{c_k}{c_0} \tag{2-12}$$

where c_k is auto-covariance, c_0 is variance, r_k is auto-correlation coefficient, k is the relative shift, and N is the number of the observations. The plot of r_k against k yields the correlogram.

The time required for the correlogram to drop below $r_k = 0.2$ is called memory effect (Mangin 1982). According to this author, the high "memory" of a system indicates a poorly developed karst network with large groundwater flow reserves (storage). In contrast, a low memory is believed to reflect a low storage in a highly karstified aquifer.

Grasso & Jeannin (1994) analyzed the correlograms of a synthetic, regular discharge time series. They demonstrated that the increase in the frequency of flood events resulted in a steeper decreasing limb in the associated correlogram. They also pointed out, that the sharper the peak of the flood event is, the steeper the decreasing limb of the correlogram becomes. Similarly, the decrease of the recession coefficient entails a steeper decreasing limb of the correlogram (**Fig. 2-6**).

The analysis of spring hydrographs simulated by numerical models, performed by Eisenlohr et al. (1997b) confirmed that the shape of the correlogram is strongly dependent on the frequency of precipitation events. These authors also demonstrated, that the spatial and temporal distribution of rainfall, and the ratio between diffuse and concentrated infiltration had a strong influence on the shape of the hydrograph, and subsequently on the correlogram. Consequently the shape of the correlogram and the memory effect derived from it depend not only on the maturity of the karst system, but also on the frequency and distribution of the precipitation events under consideration.

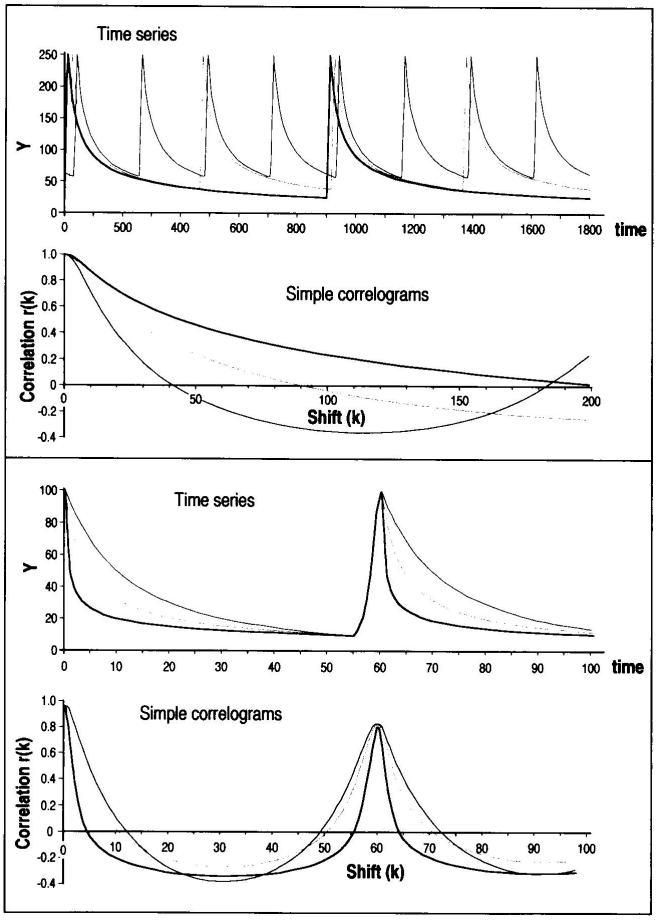

Figure 2-6. Synthetic hydrographs and corresponding correlograms presented by Grasso & Jeannin (1994). The shape of the correlogram and thus the memory effect are strongly dependent on the frequency of the flood events (above), and the speed of the recession process (below).

Spectral analysis offers considerable potential as a powerful tool for demonstrating periodicities within the time series (Box & Jenkins, 1976). A simple spectrum function (**Fig. 2-7**) may be given by the Fourier transform of the auto-covariance function (Mangin, 1984) as follows:

$$S(f) = 2\left\{1 + 2\sum_{k=1}^{m} W_k r_k \cos(2\pi \cdot f \cdot k)\right\} \tag{2-13}$$

where k is the relative shift between the same two time series, f is the frequency (f = days/2m for daily timestep), r_k is auto-correlation coefficient, m is the maximum shift and W_k is the Tukey-Hanning weighting function (Jenkins & Watts, 1968). W_k is defined as:

$$\mathrm{W_k} = \frac{1}{2}\left[1 + \cos(\pi \mathrm{k/m})\right] \tag{2-14}$$

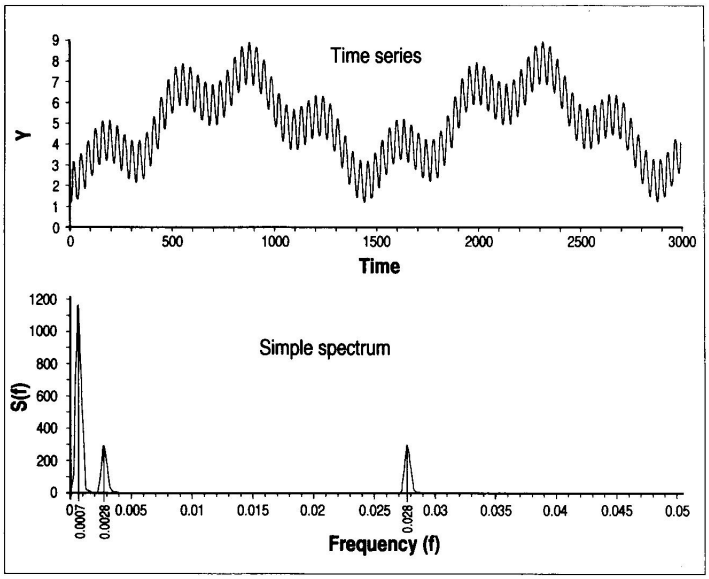

Figure 2-7. Synthetic time series consisting of three successive harmonics, and the corresponding sample spectrum function. Grasso & Jeannin (1994a).

This method provides a useful means for identifying periodicities in discharge time series. By comparing the spectrum of discharge time series to that of the rainfall events, some filtering effects of the karst system can be demonstrated.

2.2.2.2. BIVARIATE METHODS

The *cross-correlation* method was first presented by Jenkins & Watts (1968), and Box & Jenkins (1976). Mangin (1981, 1982, 1984) applied this technique to karst systems. Some further applications of this method were presented by Padilla & Pulido-Bosch (1995) (**Fig. 2-8**), Larocque et *al.* (1998), Grasso (1998) and Grasso & Jeannin (1998).

Cross correlation method permits the comparison of rainfall with spring discharge time series. This in turn allows positions of pronounced correspondence to be determined. This technique provides two kinds of information: The strength of the relationship between the two series and the lag between them. As these two series are not identical, the cross-correlogram is not symmetric about its middle. The cross correlation coefficients r_k and r_{-k} are defined as:

$$r_{+k} = r_{xy}(k) = \frac{c_{xy}(k)}{s_x s_y} \qquad \text{and} \qquad r_{-k} = r_{yx}(k) = \frac{c_{yx}(k)}{s_x s_y} \tag{2-15}$$

where k is the relative shift between the two time series,

$$c_{xy}(k) = \frac{1}{N}\sum_{i=1}^{N-k}(x_i - \bar{x})(y_{i+k} - \bar{y}) \text{ and } c_{yx}(k) = \frac{1}{N}\sum_{i=1}^{N-k}(y_i - \bar{y})(x_{i+k} - \bar{x}) \tag{2-16}$$

are the cross covariogram functions, and

$$s_x^2 = \frac{1}{N}\sum_{i=1}^{N}(x_i - \bar{x})^2 \qquad \text{and} \qquad s_y^2 = \frac{1}{N}\sum_{i=1}^{N}(y_i - \bar{y})^2 \tag{2-17}$$

are the variances.

In the case of linear and stationary systems, a transfer function can be defined, which is a characteristic function of the system, that reflects the processes taking place within it. The method of identifying the transfer function of an unknown system is known as deconvolution. Assuming the input function to be random, cross-correlogram can be considered as the transfer function of the system (Neuman & De Marsily, 1976; Dreiss, 1989; Mangin, 1984).

Mangin (1982) suggests that the shape of the transfer function is characteristic of the flow system structure. According to this author, the peak of the transfer function and the base section refer to the karst conduit system and to the storage respectively. While a short time lag and a sharp peak indicate high degree of karstification and a low storage capacity, a high lag value and a retarded peak indicate poorly drained systems.

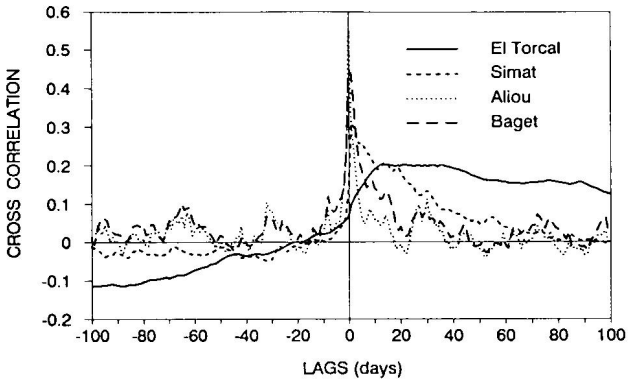

Figure 2-8. Cross-correlograms of rainfall and discharge for different karst systems (Padilla & Pulido-Bosch, 1995). El Torcal and Simat springs are located in SE Spain, Aliou and Badget springs are located in the French Pyrenees. The Aliou system displays very short response time, indicating a high degree of karstification, and the dominance of conduit flow (Mangin, 1982). In contrast, El Torcal system reflects long response time and slow decrease of the correlation values; these indicate a saturated, homogeneously karstified zone and a high system inertia. The two other systems manifest intermediate characteristics.

It is possible to define a *cross-spectrum*, which is the Fourier transform of the cross-correlation function. Due to the asymmetry of the cross-correlation function, the spectral-density function is expressed by a complex number (Padilla & Pulido-Bosch 1995):

$$\Gamma_{xy}(f) = \left|\alpha_{xy}(f)\right| e^{(-i\phi_{xy}(f))} \tag{2-18}$$

in which case i represents $\sqrt{-1}$, $\alpha_{xy}(f)$ and $\Phi_{xy}(f)$ are the values of the cross amplitude and the phase functions for the frequency f, the expressions of which are:

$$\alpha_{xy}(f) = \sqrt{\Psi_{xy}^2(f) + \Lambda_{xy}^2(f)} \tag{2-19}$$

$$\phi_{xy}(f) = \arctan\frac{\Lambda_{xy}(f)}{\Psi_{xy}(f)} \tag{2-20}$$

where the co-spectrum, $\Psi_{xy}(f)$, and quadrature spectrum, $\Lambda_{xy}(f)$ are expressed as follows:

$$\Psi_{xy}(f) = 2\left\{r_{xy}(0) + \sum_{k=1}^{m}\left[r_{xy}(k) + r_{yx}(k)\right]W_k \cos(2\pi f k)\right\} \tag{2-21}$$

$$\Lambda_{xy}(f) = 2\left\{\sum_{k=1}^{m}\left[r_{xy}(k) - r_{yx}(k)\right]W_k \sin(2\pi f k)\right\} \tag{2-22}$$

in which W_k is the Tukey-Hanning weighting function (**Eq. 2-14**).

The *cross-amplitude function ($A_{xy}(f)$)* can be associated with the duration of the impulse response function, and indicates the filtering of the periodic components of the rainfall data (**Fig. 2-9**). The *phase function ($\theta_{xy}(f)$)* shows the delay between the precipitation and the flow for different frequencies (**Fig. 2-10**).

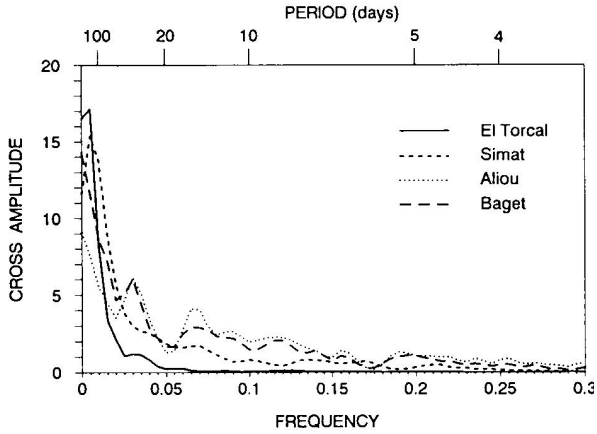

Figure 2-9. Cross amplitude function for different aquifers (Padilla & Pulido-Bosch, 1995). The cross-amplitude tends to zero in El Torcal for frequencies higher then 0.05. The other three aquifers show a decrease in the function values in intermediate and high frequencies.

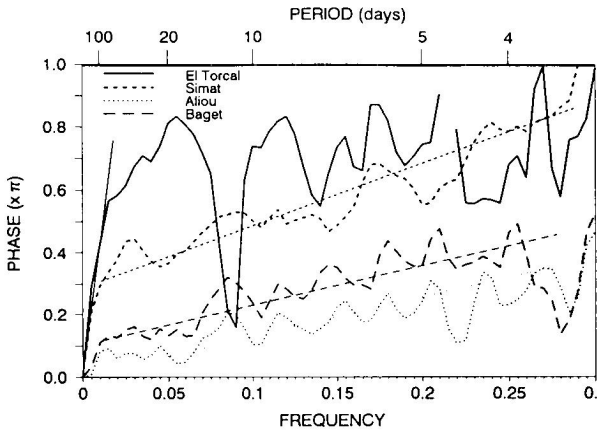

Figure 2-10. Phase functions for different aquifers (Padilla & Pulido-Bosch, 1995). The value of 1 coincides with the duration of the impulse response of the baseflow, the value of 0.4 corresponds to the duration of the quickflow. Intermediate values correspond to intermediate flow.

By the combination of the cross-amplitude function and the simple-density spectrum, new functions can be defined, such as the *coherence function ($\kappa_{xy}(f)$),* and the *gain function ($g_{xy}(f)$),* which are expressed as:

$$\kappa_{xy}(f) = \frac{\alpha_{xy}(f)}{\sqrt{\Gamma_x(f) + \Gamma_y(f)}} \tag{2-23}$$

$$G_{xy}(f) = \frac{\alpha_{xy}(f)}{\sqrt{\Gamma_x(f)}} \tag{2-24}$$

where $\Gamma_x(f)$ and $\Gamma_y(f)$ are the spectral-density functions of the x_t and y_t series.

The coherence function shows whether variations in the input series respond to the same type of variations in the output series, ie. it indicates the changes of the correlation with respect to frequency. It can be used for assessing the linearity of the system.

The gain function shows the amplification ($g_{xy}(f)>1$) or attenuation ($g_{xy}(f)<1$) of the input data (precipitation) through the intervening karst system. This function facilitates the differentiation of quickflow, intermediate and baseflow.

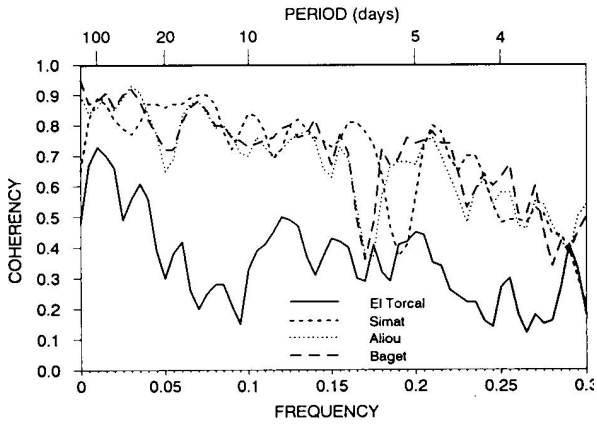

Figure 2-11. Coherence functions for different aquifers (Padilla & Pulido-Bosch, 1995).

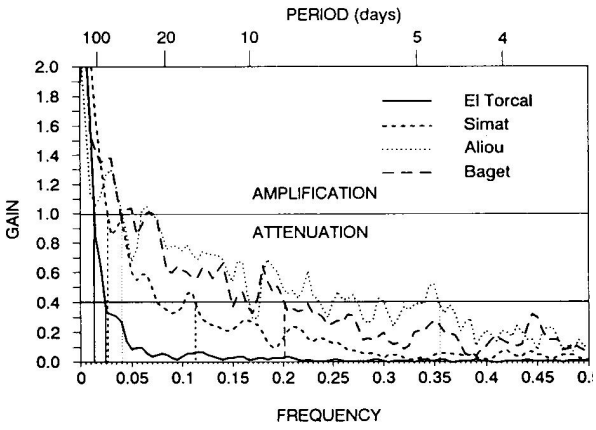

Figure 2-12. Gain functions for different aquifers (Padilla & Pulido-Bosch, 1995).

2.2.3. CLASSIFICATION OF KARST SYSTEMS BASED ON TIME SERIES ANALYSIS

Mangin (1982, 1984) provided a classification of karst systems based on time-series analysis. This author defined four characteristic parameters: memory effect, spectral band breadth, regulation time, and transfer function (**Fig. 2-13**).

Memory effect has been discussed in Section 2.2.2.1. Spectral band breadth is the frequency domain for which the system does not completely filter the input signals. Beyond this frequency domain, spectral density function takes zero value or follows random variations. Regulation time is obtained by dividing the maximum value of a simple spectrum function by the integral of this function between 0 and infinity. This parameter provides information about the duration of the influence of a unitary input signal. It characterizes the overall configuration of the karst conduit system. As explained earlier, the cross correlation function can be a good approximation of a transfer function, if the input time series can be considered as random.

Types	Memory effect (R_k=0.2)	Spectral band breadth	Regulation time	Transfer function
Aliou	very low (5 days)	very high (0.30)	10 to 15 days	
Baget	low (10-15 days)	high (0.20)	20 to 30 days	
Fontestorbes	high (50-60 days)	low (0.10)	50 days	
Torcal	very high (70 days)	very low (0.05)	70 days	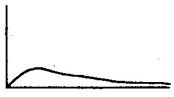

Figure 2-13. Classification of karst systems based on time series analysis (Mangin 1982).

In accordance with **Figure 2-13**, the low memory effect, short regulation time, high spectral band breadth and peaked transfer function indicate a high degree of karstification and the dominance of conduit flow (Mangin, 1982). High memory effects, long regulation times, low spectral band breadths and retarded transfer functions indicate saturated, homogeneously karstified zones and a high system inertia.

2.3. DISTRIBUTIVE METHODS

The spatial heterogeneity of karst aquifers may require the discretization of the hydrogeological media into homogeneous sub-units, each having its own flow parameters. The discretization of real systems involves the discretization of the differential equations describing groundwater flow as well. The principal formula describing transient groundwater flow in saturated media is the classical diffusivity equation derived from Darcy's flow law (momentum conservation) and the continuity equation (mass conservation):

$$S\frac{\partial H}{\partial t} = \nabla(K\nabla H) + i \tag{2-25}$$

where S is the storage coefficient [L^{-1}], K is hydraulic conductivity [LT^{-1}], H is hydraulic head [L], t is time [T], and i is the source term [T^{-1}].

Two types of discretization methods are widely used in hydrogeology. Finite Difference Method (FDM) consists of subdividing the model domain into rectangular cells. Partial derivatives are then approximated by simple differences between a given number of adjacent nodes located at the corners or in the center of each cell. According to the Finite Element Method (FEM), the model domain is subdivided into an irregular network of triangular and/or quadrangular finite elements. The approximation of differential operators is analytical, and it involves integral quantities elementwise. The advantage of the FDM method seems to lie in its simplicity. However, FDM discretization entails an artificial orthogonal anisotropy parallel to cell sides. As the FEM method is far more complex than the FDM method, it requires not only longer simulation time but also more sophisticated computational tools. However, the FEM method provides more accurate solutions than the FDM method. Furthermore, the FEM method allows the combination of one-, two- and three-dimensional elements of various shapes, thus facilitating proper discretization, the introduction of strong heterogeneity into the model and the implementation of realistic boundary conditions. A detailed explanation of the FDM and FEM discretization methods can be found in Kinzelbach (1986), Wang & Anderson (1982) and Huyakorn & Pinder (1983).

As a consequence of discretization, a matrix equation is obtained, and the numerical solution requires matrix inversion. As matrix inversion calculations can be easily computerized, distributive models represent efficient tools for modeling groundwater flow in complex hydrogeological systems.

In order to solve the equation system, *initial conditions* (for transient problems) and *boundary conditions* are needed. The initial conditions consist of the spatial distribution of the unknown function. The boundary conditions consist of the definition of either the *hydraulic potential* (head boundary) or *flux* (flux boundary) values along the domain boundaries.

The duality of karst systems may require the use of different kinds of differential equations describing flow in the low permeability matrix and in the karst conduits (Király, 1975). Moreover, the introduction of finite elements of different dimensions becomes necessary too. Depending on the flow media considered, several methods exist, all of which

have advantages and limitations. The selection of the appropriate modeling approach may be crucial with respect to the outcome of the simulation.

A systematic classification and a critical review of distributive methods developed for modeling groundwater flow in karst aquifers is provided below. In order to facilitate the selection of the appropriate approach, representative case studies are briefly presented too.

2.3.1. CLASSIFICATION OF DISTRIBUTIVE MODELING APPROACHES

Distributed parameter groundwater models include two principle concepts. The *discrete concept* considers the flow within individual fractures or conduits. In contrast, *continuum approach* treats heterogeneities in terms of effective model parameters and their spatial distribution. The physical parameters of the flow medium can be directly or indirectly derived from real field observations (*deterministic models*) or can be determined as random variables (*stochastic models*).

Several alternative model representations are available, that apply either the discrete or the continuum approach. These methods may be also combined (Király, 1985, 1988; Király & Morel, 1976a). Based on the classification of Teutsch & Sauter (1991, 1998) (**Fig. 2-14**), the following five distributive approaches applied for modeling karst hydrodynamics are distinguished (contrary to the classification of the above authors, discrete approaches are distinguished according to the dimensionality of the discrete features applied):

- Discrete Fracture Network Approach (DFN)
- Discrete Channel Network Approach (DCN)
- Equivalent Porous Medium Approach (EPM)
- Double Continuum Approach (DC)
- Combined Discrete-Continuum Approach (CDC)

Description and discussion of these methods is provided in the following sections.

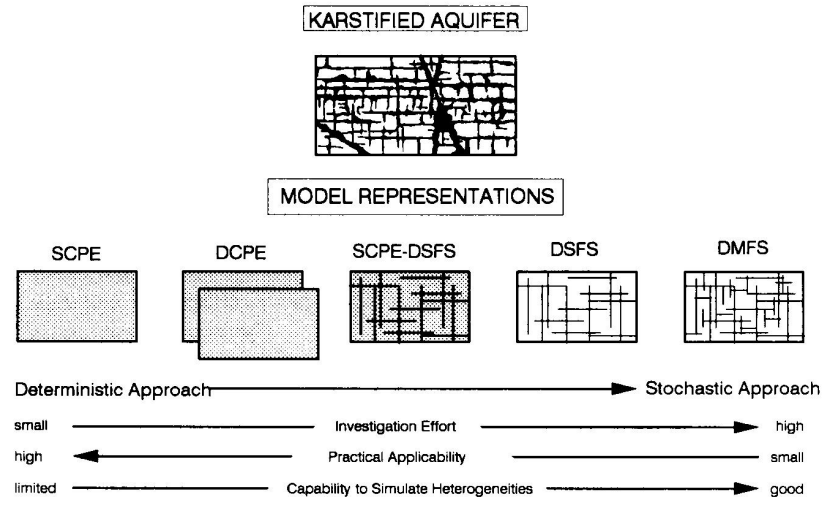

Figure 2-14. Classification of distributive methods applied to modeling karst hydrodynamics (Teutsch & Sauter, 1998). SCPE: Single Continuum Porous Equivalent Approach, DCPE: Double Continuum Porous Equivalent Approach, SCPE-DSFS: Combined Single Continuum - Discrete Fracture Set Approach, DSFS: Discrete Singular Fracture Set Approach, DMFS: Discrete Multiple Fracture Set Approach.

2.3.2. DISCUSSION OF MODELING APPROACHES

2.3.2.1. DISCRETE FRACTURE NETWORK APPROACH (DFN)

According to this approach, only certain sets of fractures are considered as permeable. The matrix medium is considered to have zero permeability. This concept simplifies the real system into a network of two-dimensional fracture planes. It is mainly applicable for fractured aquifers. The location, length, direction and aperture of fractures are usually generated statistically.

The mathematical formulation of the average velocity of groundwater flow in discrete 2D fractures is given by the "cubic law" (Kiraly 1969, Snow 1969):

$$\vec{v} = -\frac{a^2}{12}\frac{\rho g}{\mu}\vec{I} \tag{2-26}$$

where a is fracture aperture [L], μ is dynamic viscosity of water [$ML^{-1}T^{-1}$], ρ is fluid density [ML^{-3}], g is acceleration due to gravity [LT^{-2}], and $\vec{I}$ is hydraulic gradient vector [-].

The discharge Q [L^3T^{-1}] of a single fracture can be expressed as follows:

$$Q = \vec{v}A_f = \frac{a^3 w}{12}\frac{\rho g}{\mu}I \tag{2-27}$$

where w is the fracture width [L]. The transmissivity T [L^2T^{-1}] of a single fracture can be expressed as follows:

$$T = \frac{a^3}{12}\frac{\rho g}{\mu} \tag{2-28}$$

The "cubic law" is valid for laminar flow in open or closed fractures (Witherspoon et *al.* 1980). The storativity of a single fracture assuming water compression only, can be expressed as follows:

$$S_f = \frac{\rho g}{E_w}a \tag{2-29}$$

where $E_w = 1/\beta_w$ is the bulk modulus of water compression [$ML^{-1}T^{-2}$] .

Long et *al.* (1982) constructed a two-dimensional finite element model, where the geometry and the location of fractures were generated in a random way, and the fractures were represented by one-dimensional elements. They investigated the effect of the fracture geometry on the equivalent permeability tensor, and examined the possibility of modeling a fissured aquifer as an equivalent porous medium.

The authors found two basic criteria for replacing the discrete fracture system with an equivalent porous continuum. On the one hand, any changes of the test volume must result in an insignificant change in the value of the equivalent permeability. On the other hand, an equivalent symmetric permeability tensor must exist. (This permeability cannot exist, if the size of the REV exceeds the real rock volume, or if the fracture density is low). They also found that fracture systems behave more like porous media, if fracture density is increased, apertures are constant rather than distributed, orientations are distributed rather than constant, or larger sample sizes are considered.

Fractures, which are connected to the discrete network in three dimensions, may loose their connectivity in the plane of the analysis, when simplifying the aquifer into two dimensions. Thus two-dimensional analysis tends to underestimate the permeability of a domain.

Kraemer & Haitjema (1989) investigated the possibility of applying the continuum approach to fractured aquifers. They constructed a two-dimensional discrete fracture model, where fractures were generated stochastically. They found, that preferred flowpaths exist even in random fracture networks. On the one hand, higher fracture density results in more distributed flow. In this case it is more likely the continuum representation can be fitted. On the other hand, a reduction of fracture length results in weaker fracture connectivity, and promotes the formation of discrete pathways.

Long et *al.* (1985) constructed a three-dimensional DFN model, and simulated steady-state flow for simple theoretical configurations of orthogonal fractures. These authors used a combined analytical-numerical technique, where the flow within fracture planes was calculated analytically, and the flux through the entire system was determined numerically.

In order to enable the application of analytical formulae inside the fracture planes, Long et *al.* (1985) proposed to apply circular fractures (**Fig. 2-15**). According to this method, fractures act as permeable discs having impermeable boundaries (parallel plate model), while the intersection of fractures act as sources or sinks. Along the intersections constant average hydraulic head is imposed (no flow takes place within the intersections).

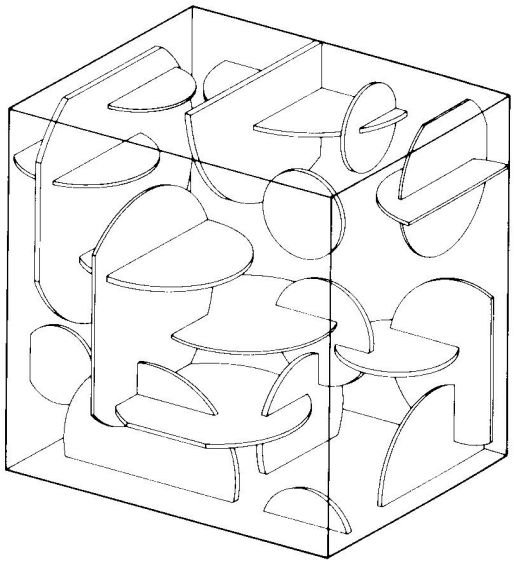

Figure 2-15. Three-dimensional discrete fracture network of disc-shaped orthogonal features applied by Long et al. (1985).

Although the study of Long et *al.* (1985) exposed some general characteristics of DFN models, it involved some unrealistic assumptions. Orthogonal networks of disc shaped fractures differ significantly from the conjugate systems of elongated faults, those present in nature. Consequently, the applicability of this approach to modeling real systems is strongly limited.

Andersson & Dverstorp (1987) presented a method of conditioning the statistical generation of fracture sets using field data. These authors developed a computer code, which generates three dimensional, non-orthogonal sets of circular fractures (**Fig. 2-16**). Andersson & Dverstorp (1987) applied field measurements for conditioning the radii, orientation, and center position of fractures and found, that large fractures and high fracture density results in a good connectivity in the networks. Moreover, high fracture density implies a small variance in the flow rate through the network. Trace conditioning decreases estimation variance only if the fracture network consists of large fractures.

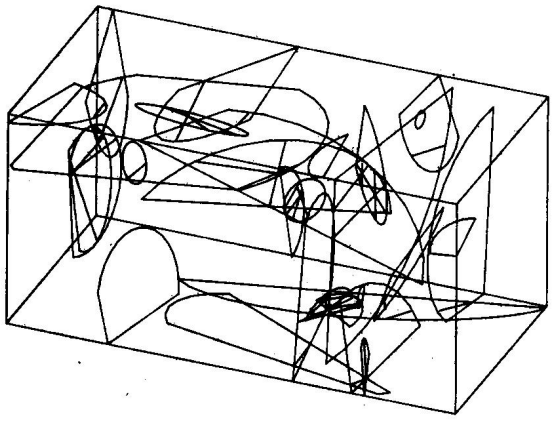

Figure 2-16. A network of 3D, non-orthogonal, disc-shaped fractures as applied by Anderson & Dverstorp (1987)

Although the study of Andersson & Dverstorp (1987) still considers natural fracture systems as a network of two-dimensional discs, it represents a nexus with reasonable real-case applications of DFN models. The conditioning of the fracture geometric parameters by field observations, and the elimination of artificial orthogonality provides a tool for constructing realistic geometry of the flow medium.

Dverstorp & Andersson (1989) attempted to calibrate their three-dimensional discrete fracture model by measuring flow distribution and fracture-trace geometry in the roof of an experimental drift and in vertical boreholes in the Stripa mine, Sweden. This study concluded, that the specific length and number of wet fractures represent reasonable information concerning the density of conductive fractures. Although the network of discrete fractures obtained in this manner may describe uneven flow observed during their tracing experiments, the authors argued that different realizations of fracture networks based on the same conditioning parameters yield different results.

Despite strong simplifications concerning the shape of fractures, DFN method is applicable to groundwater flow modeling in fissured aquifers. Several sensitivity analyses of the DFN approach have been performed so far. These analyses illustrate that simulation results are strongly dependent on the shape, size, density and orientation of the fractures. Moreover, these studies demonstrated that preferential flow paths exist in any discrete networks, and the simplification of a fissured aquifer into an equivalent porous medium model is possible only under certain conditions. Two-dimensional DFN models involve significant discrepancies and can hardly be used for modeling real aquifers.

2.3.2.2. DISCRETE CHANNEL NETWORK APPROACH (DCN)

The DCN approach aims to model the flow in a network of one-dimensional pipes representing karst conduits or fracture intersections. Conduit network geometry can be generated statistically, or it may represent a real field situation

The mathematical formulation of the average velocity of laminar flow in one-dimensional conduits may be expressed by the Hagen-Poiseuille law:

$$\vec{v} = -\frac{r^2}{8}\frac{\rho g}{\mu}\vec{I} \tag{2-30}$$

where r is the conduit radius [L]. The discharge of a single conduit can be expressed as follows:

$$Q = A_c \vec{v} = \pi r^2 \frac{r^2}{8} \frac{\rho g}{\mu} I = \frac{\pi r^4}{8} \frac{\rho g}{\mu} I \tag{2-31}$$

where $r^2/8$ is conduit permeability, and $r^2\pi$ is conduit cross-section.

Because in numerical modeling the elements representing conduits are one-dimensional, and thus no cross-sectional area can be assigned to them, the conduit conductivity is expressed as follows:

$$K_c = A_c K = \pi r^2 \frac{r^2}{8} \frac{\rho g}{\mu} = \frac{\pi r^4}{8} \frac{\rho g}{\mu} \tag{2-32}$$

The mathematical formulation of turbulent flow in one-dimensional conduits is given by the Darcy-Weissbach friction law:

$$Q = -K' A_c \sqrt{I} \tag{2-33}$$

where K' is the turbulent flow effective hydraulic conductivity [LT^{-1}], A_c is the cross sectional area [L^2], and I is hydraulic gradient [-]. Louis (1968) expressed the effective hydraulic conductivity for fully constricted (phreatic) pipe flow as follows:

$$K' = 2\log\left(1.9 \frac{D_h}{\varepsilon}\right)\sqrt{2gD_h} \tag{2-34}$$

where $D_h=4R_h$ is the hydraulic diameter [L], and ε is the absolute size of irregularities along conduit wall [L]. Similarly, Strickler (1923) expressed the effective hydraulic conductivity for non-constricted (vadose) pipe flow as follows:

$$K' = K_s R_h^{2/3} \tag{2-35}$$

where K_s is the Strickler-coefficient [$L^{1/3}T^{-1}$] depending on roughness, R_h is the hydraulic radius (cross section divided by wet perimeter) [L].

The storage coefficient of a conduit assuming water compression only, can be formulated as follows (Cornaton & Perrochet, 2002):

$$S_c = \frac{\rho g}{E_w} r^2 \pi \tag{2-36}$$

A summary and comparison of these formulae, along with case studies for their application is provided by Jeannin & Maréchal (1995), and Jeannin (2001). These authors constructed a two-dimensional fully constricted pipe-flow model of the Hölloch Cave, Muotathal, Switzerland, in order to simulate groundwater flow under various discharge conditions (**Fig. 2-17**). The geometric properties of the conduits were derived from field observations. The model was calibrated on the base of several head and discharge measurements in conduits. The study concluded that the storage capacity of epiphreatic karst conduits and nearby fissured limestone is negligible at the local scale over short simulation time of the model. However, the presence of overflow conduits modifies the aquifer conductivity, when they become active. This results in the strong non-linearity of the system. The typical effective hydraulic conductivity of karst conduits ranges between 1 and 10 m/s and the Louis formula is adequate for calculating head-losses under such circumstances.

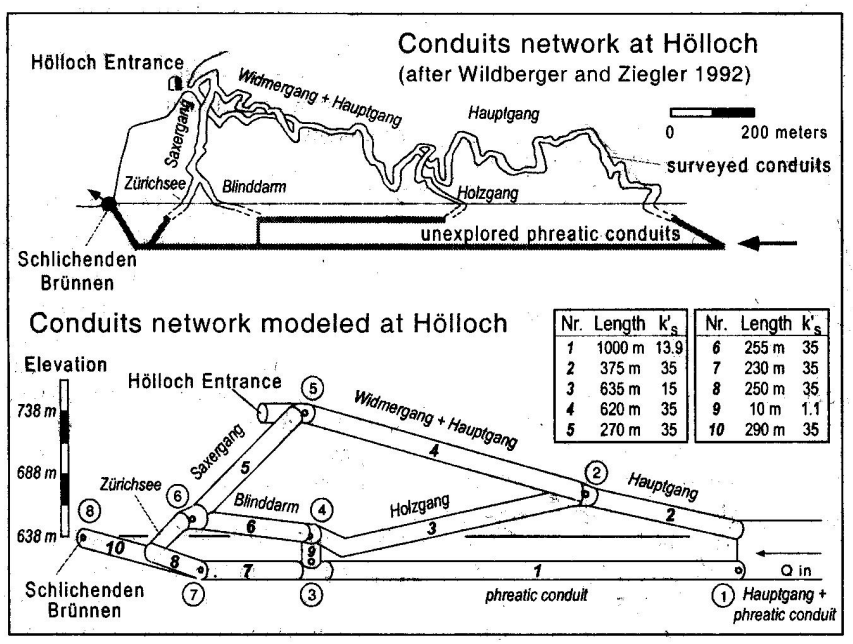

Figure 2-17. The DCN model of the downstream part of the Hölloch cave, Muotatal, Switzerland (Jeannin 2001). The paramter k'_S is equal to K'A.

Thrailkill et *al.* (1991) constructed a two-dimensional open-channel flow model of the Inner Bluegrass Karst region, Kentucky, USA. This study provided data on the conduit network geometry by comparing the stage-discharge relationships with dye-dilution measurement methods. The results suggest that dye-dilution method provides a significant insight into the geometry of the conduit system, but is unsatisfactory for determining discharges at a spring, as diversion of flow between the input point and the spring results in unequal dye fluxes.

Similarly, Jeannin & Marechal (1995) constructed an open-channel model of the Milandrine cave, Ajoie, Switzerland. They discretized the underground river into segments separated by nodes that correspond to different points of confluence. By applying the Strickler-formula, the values of the Strickler-coefficient (K_S) were estimated for each section by the empirical formula of Cowan. Velocity and stage values were calculated by the FED method. An inverse calculation of the Strikler-coefficient was also carried out, by determining flow velocities using tracer tests. The Strickler-coefficients calculated from tracer-velocities showed considerable differences from the values calculated by the Cowan formula. These deviations may be the consequence of cascades, which significantly modify hydraulic head-losses.

2.3.2.3. EQUIVALENT POROUS MEDIUM APPROACH (EPM)

The EPM approach assumes an insignificant change of aquifer hydraulic parameters between adjacent units of discretization (no abrupt contrasts are supposed). As karst systems are typically strongly heterogeneous, EPM approach is applicable under limited conditions only, and model results have to be interpreted with caution.

One of the verified case studies is presented by Teutsch (1988), who constructed a three-dimensional finite difference model of a moderately karstified part of the Swabian Alb aquifer (S. Germany). The author assumed that this approach was adequate based on borehole tests that showed homogeneous underground conditions. The calculated flow velocities were in a

good agreement with the results of short distance tracer tests, and also with average residence times, determined from tritium measurements. Nevertheless, the possibility cannot be eliminated, that groundwater flow took place through high permeability zones too.

The EPM approach is essentially inadequate for modeling groundwater flow in karst aquifers, as it fails to reflect strong heterogeneity. However, it may be applied to poorly karstified or fissured aquifers with certain restrictions, already discussed in Section 2.3.2.1.

2.3.2.4. DOUBLE CONTINUUM APPROACH (DC)

The difficulties of obtaining data for constructing DCN or CDC models, and the inability of the EPM approach of involving strong heterogeneity of karst aquifers, have motivated the development of the DC method, which can simulate specific karstic features without requiring detailed knowledge of the conduit network geometry.

The first numerical solution using the DC approach was provided by Teutsch (1988), who used the original concept of Barenblatt et *al.* (1960). In a double continuum model the conduit network and the fissured medium are both represented by continuum formulations. The exchange of water and solute between the two continua is calculated based on the hydraulic head difference between them, using a linear exchange term. Flow equations may be formulated as follows:

$$\nabla(K_1 \nabla H_1) = S_s^1 \frac{\partial H_1}{\partial t} + Q_1 + \alpha_{ex}(H_1 - H_2) \tag{2-37}$$

$$\nabla(K_2 \nabla H_2) = S_s^2 \frac{\partial H_2}{\partial t} + Q_2 - \alpha_{ex}(H_1 - H_2) \tag{2-38}$$

where the last term is the exchange flux between the two continua, calculated from the hydraulic head difference, multiplied by an empirical steady-state exchange coefficient (α_{ex}) as follows:

$$q_{ex} = \alpha_{ex}(H_1 - H_2) \tag{2-39}$$

The α_{ex} parameter [$L^{-1}T^{-1}$] characterizes the rate of the fluid transfer between the two media. This parameter is believed to depend on the permeability of the porous medium, and the degree of fissuring:

$$\alpha_{ex} \sim k_2 \sigma^2 \tag{2-40}$$

where σ [L^{-1}] is the surface of fissures per unit volume (Barenblatt et *al.* 1960). The flux value of a node (e.g. spring discharge) can be then evaluated as the sum of the fluxes from the two different media, while head values are observed separately in the two media.

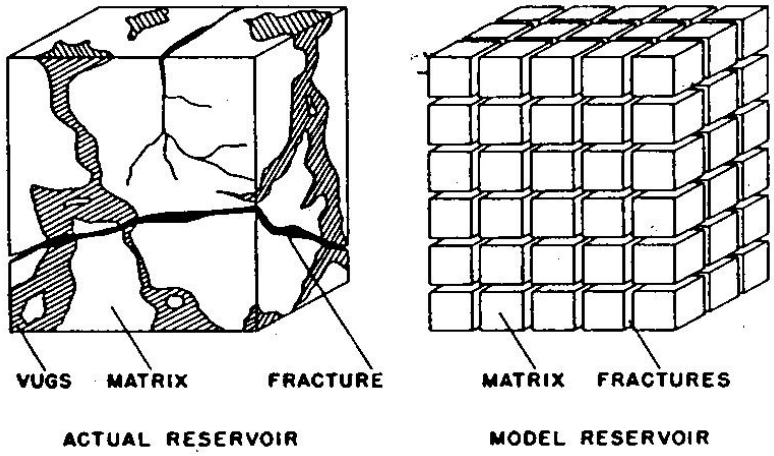

Figure 2-18. Conceptual model of karstified medium according to Warren & Root (1963). The natural irregular network of fractures and karst channels is replaced by a regular fracture network.

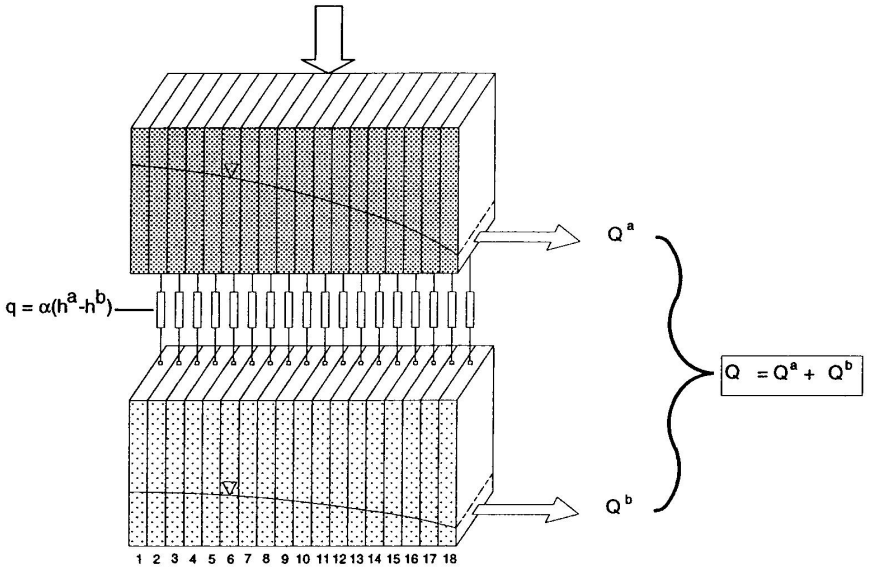

Figure 2-19: Schematic representation of a one-dimensional DC model (Teutsch, 1988).

Although the DC concept is the simplest distributive approach, which can describe dual hydraulic behavior of karst aquifers, hydraulic parameters can be obtained only by calibration (inverse modeling)(Sauter, 1992; Mohrlok, 1996). This implies that the applied parameter distributions have no direct physical relation to the real system. As the calibration of the parameters is basically a "trial- and-error" method based on the available head data series, the quality of the model results strongly depend on the density and the location of the observation points. **Figure 2-20** shows calibrated weight factor fields for different measurement point configurations of the same aquifer (Mohrlok,1996).

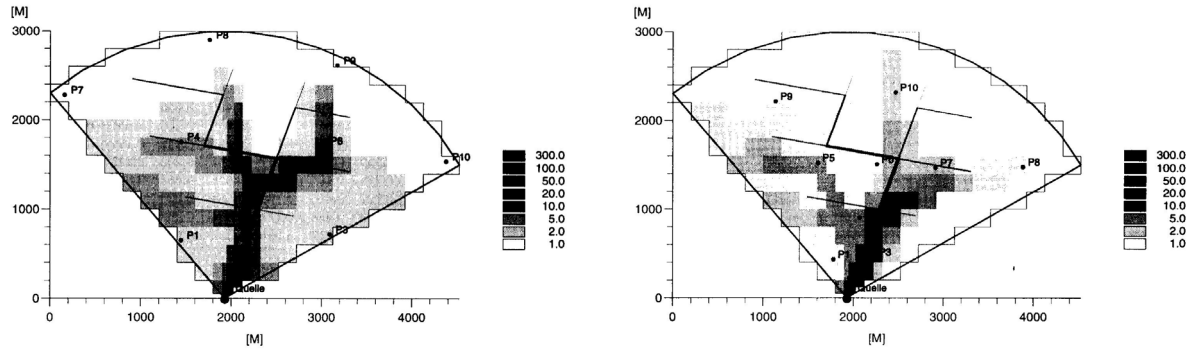

Figure 2-20. Calibrated weight parameter fields for two different observation point configurations in the same aquifer (Mohrlok, 1996).

The adequacy of DC model results and calibrated parameter fields has been tested by several authors. Mohrlok & Teutsch (1997) demonstrated that simulated spring discharges obtained from calibrated DC models show a good correspondence to observations *(***Fig. 2-21a***)*. The adequacy of calculated hydraulic heads is strongly dependent on the spatial location of the observation point considered. When it is located exactly in a karst conduit, the simulated hydraulic head in the continuum representing conduit network, provides a good approximation of the real values (**Fig. 2-21b***)*. If an observation point is located near to a conduit, real head values range between the simulated head values obtained from the two continua (**Fig. 2-21c***)*. And finally, if an observation point is located far from the conduit system, the head values in the continuum representing the low permeability matrix provide a good approximation of the real hydraulic heads (**Fig. 2-21d***)*.

Cornaton (1999) constructed three-dimensional DC models and tested the physical meaning of the calibration parameters. The author applied discrete-continuum models as references, representing the real system. The study demonstrated a strong dependence of the exchange coefficient on matrix storage coefficient and on conduit network density. This relationship was verified by a one-dimensional analytical solution for the problem.

Another critical aspect of the DC concept is that it cannot handle the temporal delay of diffuse infiltration, since both subsystems are coupled directly at every node. In order to involve retarded diffuse infiltration in a DC model, a retention function is necessary (Sauter, 1992). While Kiraly & Morel (1976a) suggest that more than 40% of concentrated recharge should be applied, Sauter (1992) argued that 5-10 % of the total recharge should be applied to the medium representing the karst channel network. Two-dimensional real-world applications of the DC concept were performed by Teutsch (1998), Sauter (1992) and Lang (1995).

Since the calibration of a DC model in three dimensions seems to be extremely difficult, and it requires three-dimensional head data, three-dimensional real-world applications have not yet been performed.

As is apparent from the above studies, the DC approach can be used for modeling the global response of karst systems. In order to obtain simulated hydraulic head information, the proper knowledge of the spatial relation between the observation points and the conduit network is essential. However, spatial distribution of calibration parameters can supply approximate information on the real conduit system configuration.

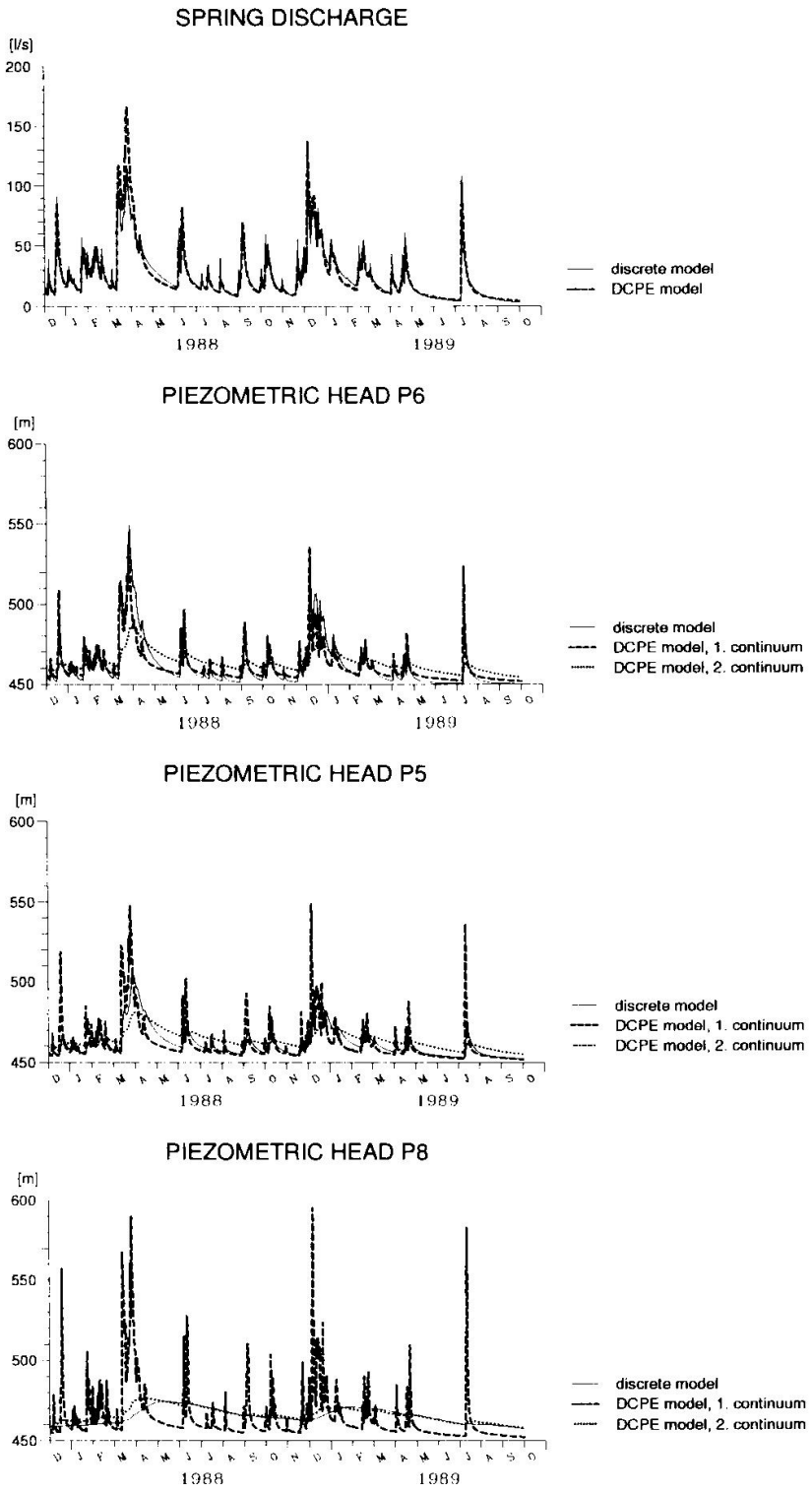

Figure 2-21. The effect of the spatial location of the observation points on the simulation results (Mohrlok & Teutsch, 1997).

2.3.2.5. COMBINED DISCRETE-CONTINUUM APPROACH (CDC)

The CDC approach is capable of handling the discontinuities that exist at all scales in a karst system (fractures, fault zones, karst channels, etc.), by representing them as networks of different orders of magnitude embedded in each other. This nested model explains the duality of karst (duality of the infiltration process, the flow field and the discharge conditions), and the scale effect on hydraulic conductivities (Kiraly, 1975).

The CDC approach uses the FEM discretization method, as it allows the combination of one-, two-, and three-dimensional elements (Király, 1979, 1985, 1988; Király et *al.*, 1995; Király & Morel 1976a). According to the CDC method, high conductivity karst channels can be simulated by one-dimensional finite elements, which are set in the low permeability matrix represented by three-dimensional elements. Similarly, the application of two-dimensional elements makes the simulation of fractures and fault zones possible.

The CDC method was first applied by Király & Morel (1976a). This study modeled the effect of an artificial channel, draining karst water between two adjacent synclines during low water periods, as a means of regulating spring discharges (**Fig. 2-22**). In this two-dimensional model a synthetic network of one-dimensional finite elements represented the conduit system, while low-permeability fissured matrix was represented by two-dimensional finite elements. The aim of the model was to simulate the discharge evolution of the spring and of the artificial channel. This was the first time that typical behavior of a karst spring was adequately simulated by a distributive model. Although this model was an oversimplified version of reality, it incorporated all the important properties of karst aquifers.

These initial studies led to some basic conclusions on the behavior of karst systems (Kiraly, 1998a). The application of equivalent porous medium models (EPM) requires artificial hydraulic conductivities that are higher than their true values, in order to simulate realistic hydraulic heads. However, these discrepancies disappear with the introduction of the high conductivity channel network into the FEM model. Typical spring hydrographs cannot be simulated without applying concentrated infiltration. The rate of this concentrated input should be more than 40% of the total infiltration. Apart from surface waters entering swallow-holes, a thin high conductivity layer called epikarst (Mangin, 1975) may play an important role in draining infiltrating water, and driving it towards the karst channel network (Király et *al*. 1995). The models constructed by Király & Morel (1976b) showed that during recharge periods, the hydraulic heads take higher values in karst channels than in the low permeability volume. In other words, karst channels do not drain, but inject water into the low-permeability matrix. In contrast, hydraulic heads take lower values in the channel network draining the low permeability matrix, during recession periods.

This phenomenon is called *gradient inversion*, and is caused by concentrated infiltration (**Fig. 2-23**). This strongly variable behavior of karst systems in time and space queries the validity of the "karst water table" concept. Another consequence of the gradient inversion is the negative baseflow during recharge periods. This phenomenon requires the revision of the hydrograph decomposition methods .

The CDC approach is the only distributive modeling concept that facilitates the direct application of observed aquifer geometry and measured hydraulic parameters. The CDC approach facilitates to test conceptual models of karst systems. However, the practical application of this concept is mainly limited by its high data demands.

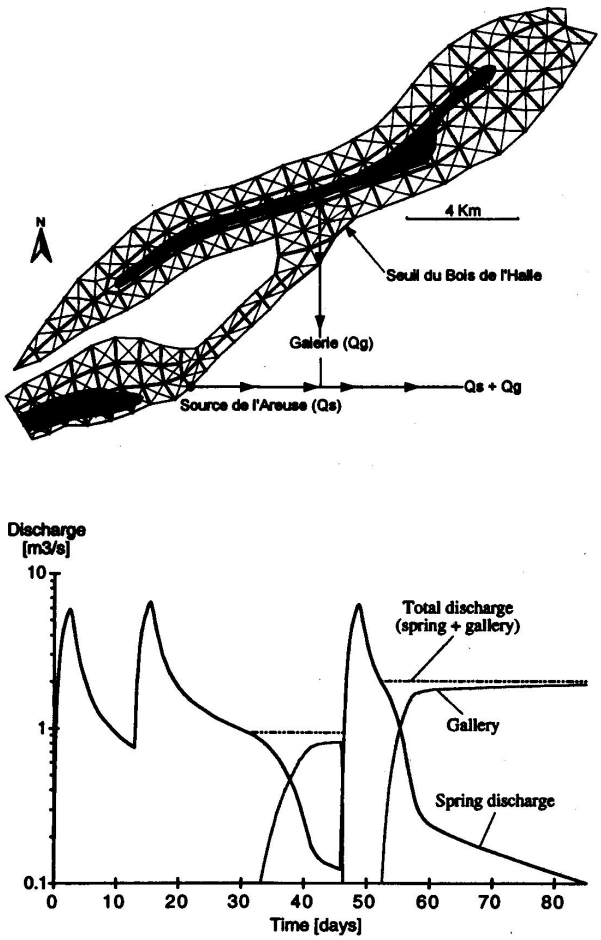

Figure 2-22. Finite element mesh and simulated spring hydrographs of the first CDC model (Areuse Basin, Switzerland), Kiraly & Morel (1976a).

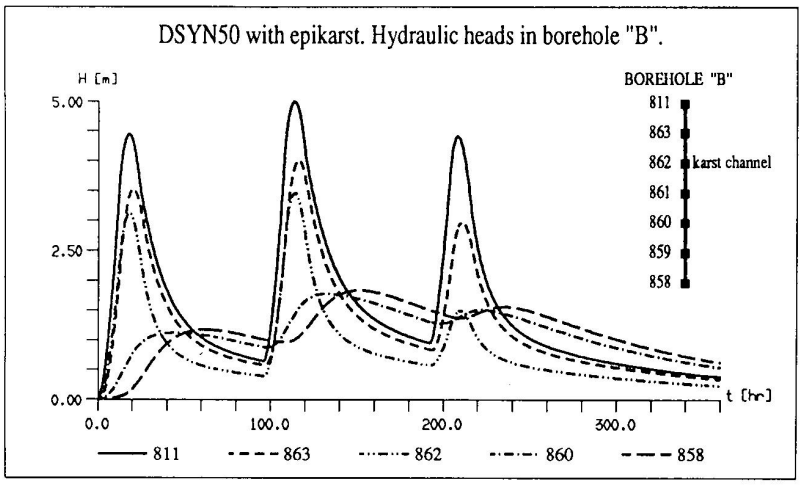

Figure 2-23: Simulated variations of hydraulic head in a borehole crossing a karst conduit, Király (1995).

2.4. CONCLUSIONS

This chapter presented a critical review and systematic classification of hydrodynamic modeling methods applicable to karst hydrogeological systems. While global methods represent an overall characterization of aquifers hydraulic response, distributive methods may provide a complete quantitative characterization of spatio-temporal hydrogeological phenomena.

Global methods include two fundamentally different approaches: Single event methods deal with the global response of karst systems given to one particular rainfall event. These methods are based on physical laws derived from reservoir models. Consequently, they can provide information on the hydrogeological properties of karst systems. Although the mathematical description and the interpretation of the fast recession are varying, the baseflow recession is generally described by the classical Maillet formula. Recession coefficient, which is a characteristic parameter of the baseflow recession process, is believed to depend on the spatial configuration of the karst conduit network and on the hydraulic parameters of the aquifer. However, the interpretation of this parameter is only qualitative.

Time series analytical models consist of the mathematical analysis of the long-term response of karst systems given to recurrent rainfall events. As these methods are based on pure mathematical operations, they cannot be directly related to any physical phenomena. Consequently, they provide only indirect information on the physical functioning of karst hydrogeological systems. Univariate methods deal with discharge time series analysis. These methods are suitable for identifying cyclic variations of spring hydrographs. Bivariate statistical methods consist of comparing rainfall and discharge time series, and analyzing their relationship in a systematic way. The drawback of time series analytical methods lies in their failure to consider temporal and spatial distributions of rainfall, which may significantly influence statistical parameters.

Distributive groundwater flow models include two principle concepts: Whereas discrete approaches describe flow within networks of fractures or conduits, continuum approaches treat the heterogeneities in terms of effective model parameters and their spatial distribution. The CDC approach represents a combination of these methods.

The DFN approach simplifies the real system into a network of fractures and fails to consider flow through the low permeability matrix. This method is mainly applicable for certain fractured aquifers. Fractures can be generated stochastically. Simulation results are strongly dependent on the shape, size, density and orientation of fractures. Preferential flow paths exist in every discrete network. Two-dimensional DFN models involve significant discrepancies and are not appropriate for modeling real aquifers.

The DCN approach aims to model the flow in the network of one-dimensional pipes representing karst conduits or fracture intersections. The geometry of the conduit network can be generated statistically, or it may represent a real field situation. Real-case DCN models require a detailed knowledge of the conduit network geometry and the discharge conditions in every conduit. Such an approach can be applied to local scale modeling. DCN models can permit complex global response of karst aquifers to be better understood, but hardly can be applied for modeling regional groundwater flow.

The EPM approach assumes an insignificant change of aquifer parameters. As karst systems typically highly heterogeneous, the EPM approach is inadequate for modeling groundwater flow in karst aquifers. Nonetheless, it may be applied to poorly karstified or fissured systems with certain restrictions.

In the DC concept, the conduit network and the fissured medium are represented as different continua. The exchange of water is calculated based on the hydraulic potential difference between the two continua. Although this method does not incorporate conduit network characteristics, the low data demand makes it a useful tool for several applications. The DC approach can be used for modeling the global response of karst systems. In order to simulate hydraulic head information, the spatial relation between the observation points and the conduit network must be appropriately determined. The spatial distribution of calibration parameters can provide approximate information on the real conduit system configuration. This method can be applied for water resources or water budget problems.

The CDC approach can handle discontinuities, which exist at all scales in a karst system, as it allows the combination of one-, two-, and three-dimensional elements. These elements represent karst conduits, fractures and low permeability matrix respectively. The CDC approach is the only distributive modeling concept, which facilitates the direct application of real aquifer parameters. Furthermore, the CDC approach facilitates to test conceptual models of karst systems. However, the practical application of this concept is mainly limited by its high data requirements.

3. HYDROGEOLOGICAL OVERVIEW OF THE BURE PLATEAU, AJOIE, SWITZERLAND

ABSTRACT

This study presents a hydrogeological synthesis of the most recent data from the Bure plateau in Ajoie, canton Jura, NW Switzerland. Included is a complete reappraisal of aquifer geometry and aquifer boundaries, the delineation of catchment areas based on tracing experiments, and the evaluation of the hydraulic role of different hydrostratigraphic units. Furthermore, it presents GIS-based calculations on the mean piezometric surface, the thickness of the unsaturated zone and the thickness of the minimum and mean saturated zones. The spatial extension of the shallow karst zone is also evaluated. The research site is 83 km^2 in area and is underlain by slightly folded layers of Mesozoic limestones and marls. The Bure plateau is dissected by normal faults, which form a succession of elongated horst and graben structures. The main aquifer consists of Malm limestones, with thicknesses varying between some meters (eastern border) and 320 m (south-eastern regions). The aquifer is bounded from below by the Oxfordian Marls. The underlying sediments of Middle Jurassic age are considered to be hydraulically independent. The surface topography of the Oxfordian Marls shows the presence of the periclinal termination of a wide anticline over the plateau and a syncline in the southern parts. The aquifer contains three marl intercalations. Tracing experiments prove that marl layers do not act as regional aquicludes. These experiments also allowed for the division of the aquifer surface into several water catchments. Based on tracing tests and piezometric data a NW-SE oriented groundwater divide seems to extend in the regions of Porrentruy – Bure – Croix. Calculations of the average and minimum water tables indicate an extended shallow karst zone in the region of Boncourt – Buix - St-Dizier. The thickness of the saturated zone increases towards the edges of the research site, being thickest in the South. The thickness of the unsaturated zone shows a large variation, reaching its maximum in the central areas.

Keywords: Karst aquifer, Flow modeling, Conceptual model, Bure plateau, Milandrine, Shallow karst, GIS

3.1. INTRODUCTION AND AIMS

The Bure plateau is a sparsely populated area, underlain by a karst aquifer. As it is relatively pristine, conclusions drawn from field observations refer to the general natural behavior of such karst hydrogeological systems. For that reason it has been the target of several hydrogeological studies since the early nineties (Grasso & Jeannin, 1994ab; Jeannin, 1995ab; Jeannin & Grasso, 1995ab; Jeannin & Maréchal, 1995). These studies have included discharge measurements, hydrograph analyses, tracing experiments, water balance calculations, hydrochemical measurements and surface geophysical experiments, mainly focused on the Milandrine cave system, which is the largest explored karst system in the area.

So far, the only overview of the Bure plateau hydrogeology has been made by Gretillat (1996). However, this work was based on a limited data subset.

A large number of experiments and observations have been carried out for academic research (Karst Research Group at CHYN, University of Neuchâtel), as well as for the construction of the A16-Transjura highway, which will cross the Bure plateau.

The aim of the present paper is to summarize and analyze available geological and hydrogeological information in the area, in order to provide a better understanding of the regional hydrogeology.

3.2. GENERAL CONTEXT

3.2.1. GEOGRAPHICAL SITUATION AND HYDROGRAPHY

The *Bure plateau* is located along the Swiss-French border in *Ajoie, canton Jura*, NW Switzerland at the southern margin of the *Plateau Jura*, to the west of the southern end of the *Rhine Graben* (**Fig. 3-1**).

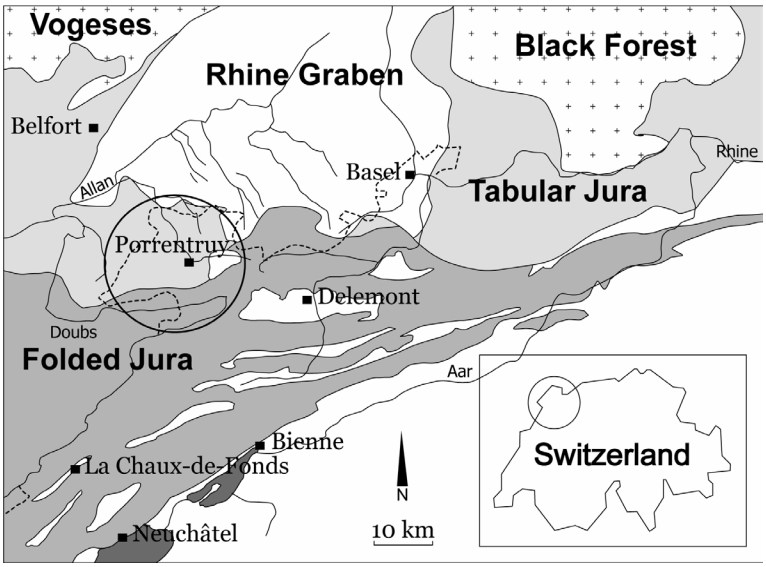

Figure 3-1. Regional geographical and geological settings of the study area.
Circle indicates the Bure plateau. Solid lines indicate rivers;
dashed line marks the Swiss-French boundary.

The Bure plateau is drained by the *River Allaine* (**Fig. 3-2**), which is a tributary of the *River Doubs*. The average discharge of the Allaine river is about 3 m^3/s. Minimum discharge measured in the eighties was 370 l/s, while the maximum discharge estimated during the flood of 1983 reached 90 m^3/s. The gradient of the riverbed is about 5 m/km.

The plateau is bordered by the Allaine river to the West and by the *Porrentruy – Chevenez – Grandfontaine dry valley* to the South (**Fig. 3-2**). This valley is often flooded after high precipitation events. A partly explored underground river, the *Ajoulotte* stream, underlies the valley bottom. Several springs are located along the *Delle – Lebétain valley*, delineating a hydrogeological boundary to the North-West of the Plateau. In the vicinity of *Fahy* the hydrological delimitation is uncertain, it is assumed to follow the topographic high.

The area of the Bure plateau, delineated as described, is 83 km^2. The highest topographic elevation is about 630 m above see level and the lowest point is 360 m above see level. The highest difference in elevation between the plateau and the Allaine outflow is about 270 m. Excepting some valley incisions, the topography of the plateau is rather smooth with a relief in the range of 60 m to 150 m. Between Porrentruy and Delle the plateau is dissected by five dry valleys (**Fig. 3-2**). These are *Le Varieu, Mormont, Les Echiouses, La Grande Vallée* and *Les Coires – Goulattes*. The largest of these valleys is "*La grande valle*".

From the Bâme spring upstream to the South a large karst system has been explored by speleologists. It extends directly from one end to the other over 3 km, between Boncourt and le Maira. Its total length is about 10 km. It contains an underground river called "Milandrine". In the South, the Creugenat and Creux-des-Prés systems have been explored over nearly two kilometers along the Porrentruy – Chevenez – Grandfontaine dry valley. Some other small caves (up to 30 m long) are known in the area of Rocourt, Porrentruy, Courchavon and Courtemaiche.

Surface morphology of the Bure Plateau is characterized by various types of karstic landforms (dolines, dry valleys and shafts). There are no significant surface streams over the site. 63% of the plateau is covered by pasture, 34% is covered by forests, the rest (3%) is used for tillage.

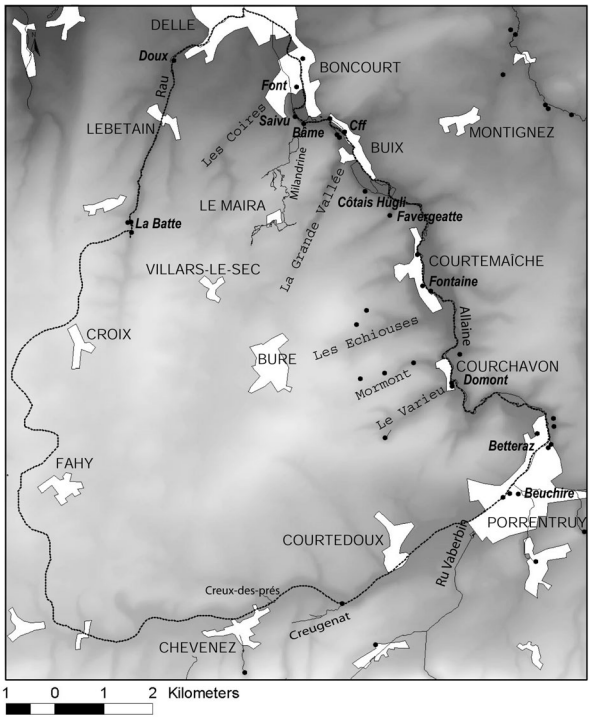

Figure 3-2. Research site topography. The Bure plateau is dissected by five NE-SW oriented dry valleys (Le Varieu, Mormont, Les Echiouses, La Grande Vallée, and Les Coires). Thin solid lines indicate explored cave systems, dashed lines indicate rivers, spring locations are marked by black dots.

3.2.2. GEOLOGICAL SETTINGS AND LITHOSTRATIGRAPHY

The Bure plateau is underlain by slightly folded layers of Triassic to Late Jurassic shallow marine limestones and marls. The total thickness of this mesozoic block is 1000 – 1500 m (Labhart & Decrouez, 1997).

The Malm limestones form the main aquifer. Older formations are not of interest in this study. The total thickness of the Malm sediments is about 300-400 m. These limestones are underlain by the Oxfordian Marls, which have a thickness of up to 100 meters (**Fig. 3-3**).

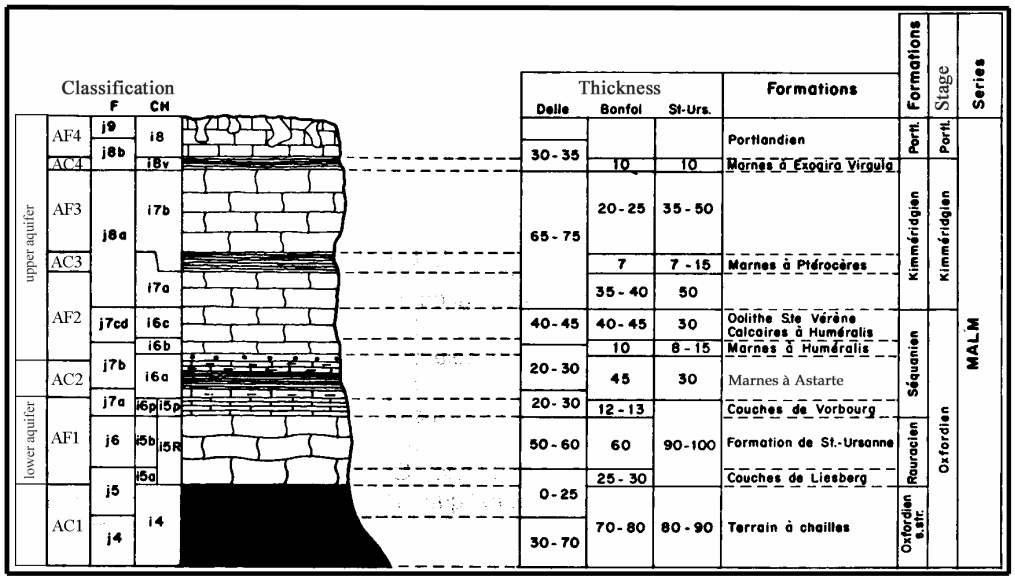

Figure 3-3. Research site lithostratigraphy and hydrostratigraphy (After Gretillat 1996). The Swiss (CH) stratigraphic codes are used in this paper. French (F) codes are shown for comparison. The thicknesses of different formations are shown for three different locations.

The *Oxfordian Marls Formation* (i_4) is subdivided into two different sedimentary units (Laubscher, 1963, Liniger 1970). In the lower part pyritous clay with pyritized ammonites (*Renggeri Marls)* occures. Overlying sediments are called "*Terrain à Chailles*", which reflects the presence of siliceous nodules. The upper part of the formation consists of marls or sandy marls, which alternate with beds bearing flints, corals or crinoids.

Rauracian reef limestones (i_{5r}) have a beige to gray color and are rich in corals. The thickness of these sediments can vary between 60-76 m. This unit is divided into two formations. The lowermost is called *Couches de Liesberg* (i_{5a}), and consist of dark-gray limestone banks alternating with lime and marly limestone at the bottom. These sediments often contain *Millericrinus* remnants and corals. The uppermost beds consist of coarse oolitic limestones in the north and fine grained limestones in the south. The overlying *St-Ursanne Formation* (i_{5b}) consist of pure, white chalky limestones containing coral reefs (patch-reefs) or coarse breccia layers. In the south, pelletal limestones indicate the proximity of a reef ridge facies.

The Milandrine cave itself is located within the Rauracian limestone layers. These limestones are directly underlain by the Oxfordian Marls.

The *Couches de Vorbourg* (i_{6p}) occur at the base of the Sequanian unit. These thick bedded light color and compact limestones often show a limnic influence with quartz grains and limestone breccias (*Cailloux Noirs*). They are usually morphologically well exposed.

Astarte Marls (also called *Natica Beds*) (i_{6a}) are the lowermost and thickest (30-40 m) of the three Malm marl layers in this area. Astarte Marls display a gradual transition from the underlying Rauracian limestones. Marl layers alternate with fine grained, gray, often oolitic or crinoidal limestones with Astarte coquinas, reef limestones or sandstone layers. The upper part of this formation is typically pure crinoidal marl.

Humeralis Marls (i_{6b}) are yellow chalky-marls, which contain coquinoid layers and echinoderm breccia. Fe-ooid bearing layers are also common, and rich of fossils. The *St-Vérène Oolite* (i_{6c}) consist of oolith bearing sediments whereas the concentric structure of the oolith grains is not visible.

Lower-Kimmeridgian limestones (i_{7a}) are light, well stratified, with intercalations of fine breccia and pseudoolitic layers. They have a thickness of 35-50 m.

The *Pteroceras Marls* (i_{7b}) are 10 m thick, limy and sandy marls bearing bivalves and *Pteroceras.*

The Upper-Kimmeridgian limestones (i_{7b}) are well stratified, sometimes even thin layered, light colored sediments which often contain marl intercalations. They have a thickness of 30-50 m. More than 500 dinosaurs tracks have been found in this formation in the vicinity of *Courtedoux*.

Virgula Marls (i_{8v}) show a sharp transition from the underlying limestones. These marls have bluish-gray or dark brown color, bearing the masses of *Exogyra Virgula*. The top of this unit contains the intercalations of laminated crinoid limestones, or greenish glauconitic limy marls. Their thickness is approximately 10 m.

Portlandian limestones (i_8) are similar to the Kimmeridgian sediments, but generally contain more fossils. These limestones are sometimes white, fine bedded, chalk-like fine grained sediments with a maximal thickness of 20 m in this area.

Tertiary sediments are very rare in the area. Some small sandy gravel bodies are situated over the Bure plateau in the area of Porrentruy and Courchavon. The thickness of these sediments does not exceed a few meters.

Quaternary loess sediments cover about the 30% of the Mesozoic rocks in the area. Quaternary alluvial sediments are present along the Allaine river, and along the Rocourt-Porrentruy valley. The thickness of the alluvium is about 10-20 meters. These alluvial bodies form separate aquifers, which have hydraulic connection either to the river or to the Malm aquifer at many locations.

The Malm plateau is dissected by NS (0°-180°), NW-SE (150°-330°) and NE-SW (60°-240°) oriented faults (Kiraly et al. 1971), resulting in a succession of long horst and graben structures. The first system is related to the formation of the Rhine Graben, while the others are realated to the Jura folding.

3.2.3. HYDROGEOLOGICAL SETTING

Bure Plateau Aquifer consists 300-400 m of Malm limestones. The aquifer is underlain by the Oxfordian Marls (100 m thick). Deeper underlying sediments of Dogger age can be considered to be hydraulically independent (Gretillat 1996). These two aquifers can only communicate in strongly tectonised zones, such as at the contact of the tabular and folded Jura (south of research area).

The Malm aquifer contains three low-permeability marl intercalations (**Fig. 3-3**). The lowermost is the 40m thick Sequanian Astarte Marls Formation. Due to gradual change from the Rauracian sediments to Sequanian marls, and also because of large normal faults with displacements of 30 to 40 meters, the Astarte Marls can not be considered as aquiclude at the scale of the Bure plateau. As shown in the following sections tracing experiments confirm this assumption. The two succeeding Kimmeridgian marl layers, with a thickness of about 10 m each, play a very restricted role in the regional flow patterns.

Jeannin & Grasso (1995b) calculated the effective infiltration taking place over the upstream catchment of the Milandrine river (*Milandrine amont*) for the early nineties. According to their calculations based on potential evapotranspiration, about 50% of the average yearly precipitation (1000 mm) is effective infiltration (500 mm/y). From this quantity nearly 50% has to be considered as quick flow, feeding directly to karst conduits. The rest is retarded as storage in the epikarst and in the main aquifer. This is in agreement with the estimations of Kiraly (1998a) who pointed out that this division is a result of the water-capturing effect in the epikarst zone. Gretillat (1998) also made calculations on the effective recharge for the late eighties, and came to very similar conclusions (48% effective infiltration of precipitation of 1013 mm/y).

Tracing experiments have shown that several karstic drainage basins are present over the Bure Plateau (Gretillat 1996), each having its own outlet (karst spring).

The largest system ($Q_{average}$ = 800 l/s) discharges at the Beuchire spring. Its catchment covers one-third (37 km^2) of the Bure Plateau, and also extends to the south of the Porrentruy-Chevenez-Grandfontaine dry valley. Some sections of the karst conduit network have been explored by cavers, such as the Creugenat and the Creux-des-Prés caves. The Creugenat is a karst window at low flow conditions (large collapsed doline in contact with the water table at its bottom). At very high water stages, the doline floods and becomes a spring having a discharge of several cubic meters per second. One conduit can be dived upstream from the doline and leads to about 2 km of cave passage. It ends in further siphons. A significant discharge flows through the conduit. The Creux-des-Prés opens as a vertical shaft of about 20 meters reaching an underground stream at its bottom. The stream can be followed downstream for about 50 meters and upstream for about 300 meters. Siphons at both ends should be dived to further explore the cave.

The Milandrine catchment is the second largest in the region covering an area of 13 km^2. The combined average discharge of the Saivu, Bame and Font springs is in the range of 200 l/s. It encloses the Milandre cave which stretches over a total length of more than 10 km. The underground river of this catchment can be followed for some 4.6 km from the Bâme spring upstream. Flow is mainly free surface flow. Only the downstream part (500 m) is phreatic. River discharge ranges between 20 l/s – 1500 l/s.

The other smaller systems remain completely unexplored. They are related to the following springs: Côtais Hugli, Favergeatte, Fontaine, Domont, Trou de la Doux, La Batte (**Fig. 3-2**).

3.3. HYDROGEOLOGICAL DATA AND INTERPRETATION

With the exception of the synoptic work of Gretillat (1996), the only articles published focus on particular phenomena or methodology. These articles worked on data and observations concerning mainly the Milandrine cave system, its catchment area and its springs. In the following sections we attempt to summarize geological and hydrogeological data from the whole plateau into an integral conceptual model.

3.3.1. AQUIFER GEOMETRY

An understanding of the three dimensional aquifer geometry is essential for the comprehension of the hydraulic functioning of the aquifer. Based on the existing geological interpretations (Diebold et *al.*, 1963; Liniger, 1969) and recent borehole data obtained from the construction works of the Transjura Highway (MFR, 1993, 1996), a hydrostratigraphic map of the region at 1:25000 scale has been established. A reduced version of this map is shown on **Figure 3-4**. This interpretation also includes a set of geological cross sections (**Fig. 3-5**) and structural maps of the Oxfordian and Astarte Marl surfaces (**Fig. 3-6 & 3-7**) which provide an understanding of the geological structure in three dimensions.

Structural surfaces clearly show the presence of a wide WNW-ESE oriented syncline, which is marked out by the Porrentry-Chevenez valley. The periclinal termination of a wide anticline, parallel to the syncline, is present in the region of Bure, which corresponds to the Bure plateau. These structures are dissected by NS (0°-180°), NW-SE (150°-330°) and NE-SW (60°-240°) oriented faults (Király et *al*. 1971). The first system is related to the formation of the Rhine Graben, while others are a consequence of the tectonic activity during the Jura folding.

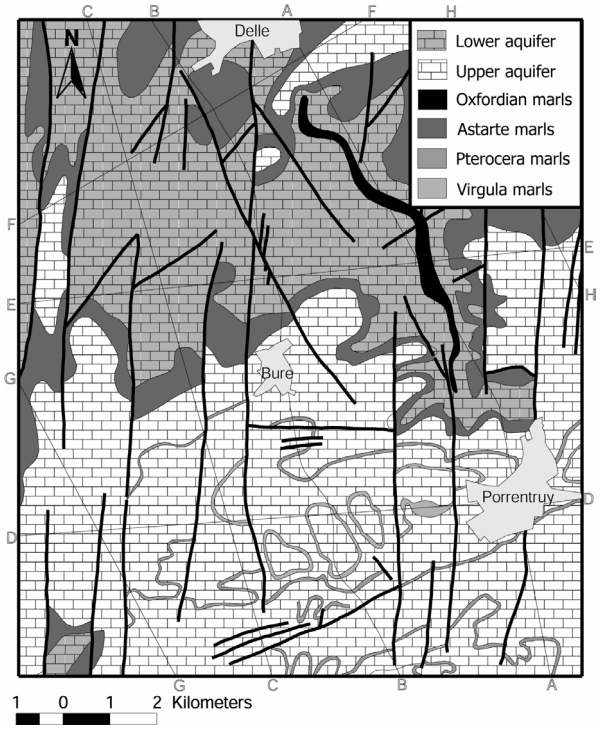

Figure 3-4. Hydrostratigraphic map. Tertiary and Quaternary sediments are omitted. Marl levels are indicated for orientation. Malm limestones are merged for simplicity. Thick lines mark tectonic features; cross sections are indicated by thin solid lines.

Since the Oxfordian Marls form a persistent hydraulic threshold, the thickness of the Malm calcareous aquifer is the difference between the aquifer surface topography and the top of the Oxfordian Marls. While the aquifer thickness exceeds 300 m to the north-west of Porrentruy, it decreases to some meters in thickness along the Allaine River in the area of Buix (**Fig. 3-8**). Here the Oxfordian Marls are covered only by Quaternary alluvial sediments.

The Astarte Marls are dissected by surface topography in the region of Bure and, because of the dry valleys mentioned above, they have a sinuous surface appearance in the area of Courchavon. To the north of Bure, no Sequanian or Kimmeridgian Limestones occur over the plateau, except for a small body located to the SW of Boncourt.

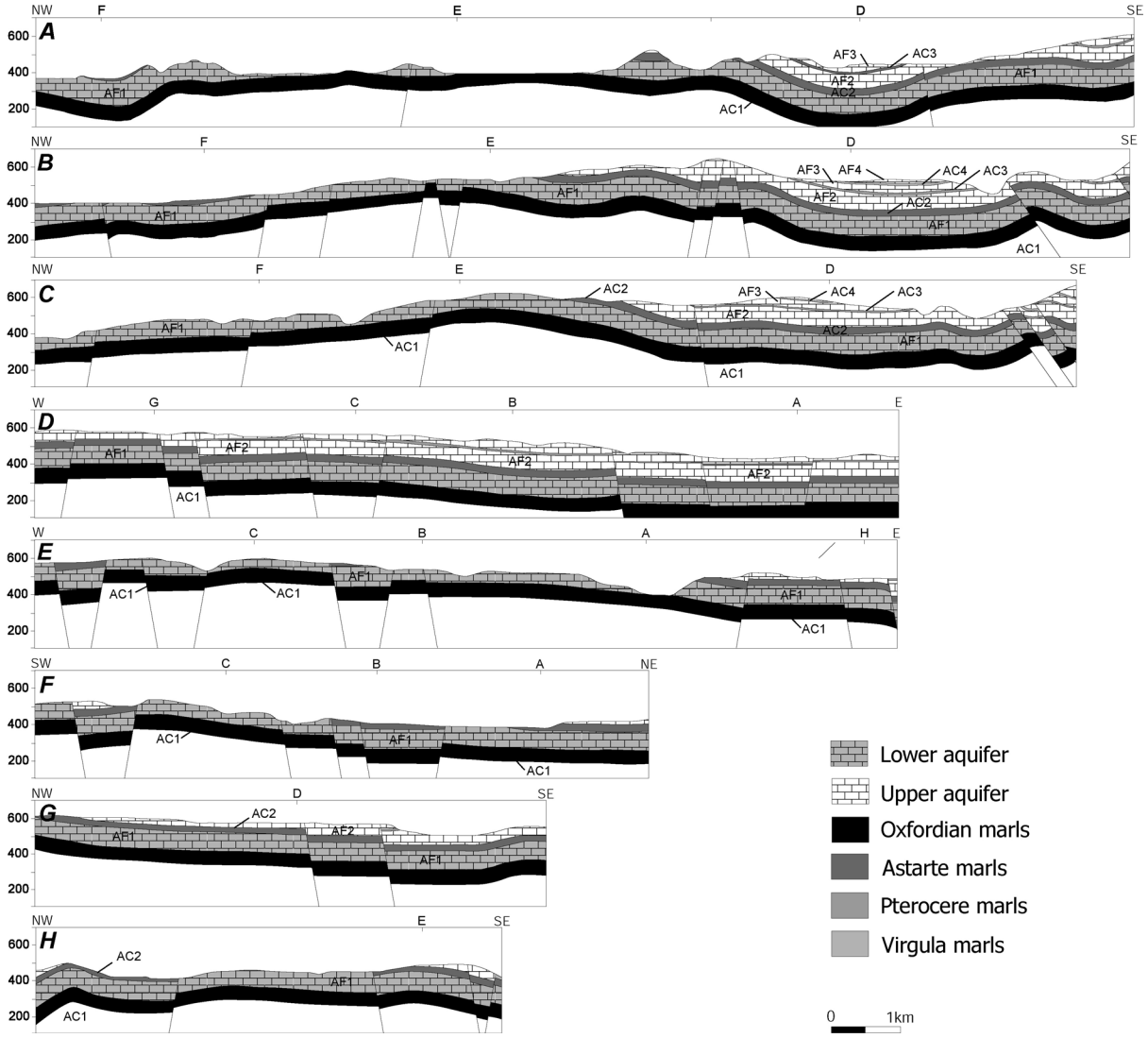

Figure 3-5. Hydrostratigraphic cross sections. Hydrostartigraphic units are labeled with their codes for orientation. Vertical exaggeration is 2.5.

3.3.2. HYDRAULIC PARAMETERS

Some borehole tests were made in the Malm aquifer both in the Maira region, and further to the east in the area of Delemont.

The hydraulic conductivity of the Rauracian limestones, measured from borehole tests, is in the range of 10^{-6} – 10^{-7} m/s (Fleury & Allemann, 1991; Jeannin, 1995b). Both lower and higher values were measured, but the mentioned values are typical. The hydraulic conductivities of Sequanian and Kimmeridgian limestones are similar (Fleury & Allemann, 1991).

As the displacement along faults (20-40 m) is generally more than the thickness of Kimmeridgian marls, and as these formations are relatively thin, they can probably be neglected as hydraulically continuous thresholds. Tracing tests confirm this assumption (see next section).

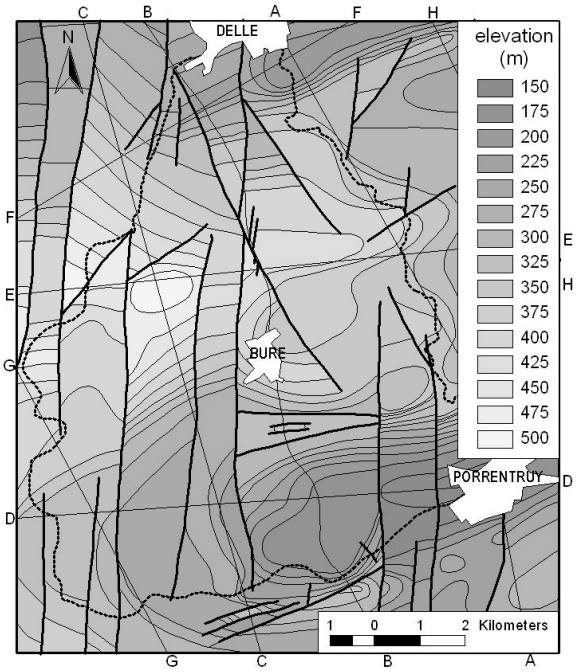

Figure 3-6. Structural surface of the Oxfordian Marls. Dashed line marks aquifer boundaries. Thick lines indicate tectonic features. Cross sections are marked by thin solid lines.

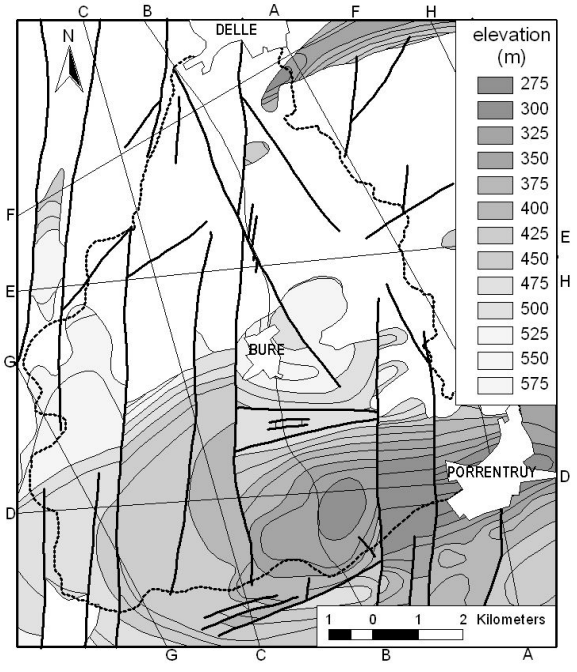

Figure 3-7. Structural surface of the Astarte Marls. Thick solid lines indicate faults. The aquifer boundary is marked by dashed line; thin solid lines indicate cross sections.

The hydraulic role of the Sequanian Astarte Marls is not evident. Tectonic displacement exceeds their thickness in some cases, but it is usually smaller. One of the aims of this study is to estimate whether this layer can be considered as a hydrogeological barrier or not. As we see in the following section, though marly sediments are usually of a low hydraulic conductivity, they do not strongly influence the flow field, probably because of karstification phenomena.

The estimation of the conductivity of fractured zones is very approximate, as there is a large variation of values even over the same formation (Jeannin 1995a). We assume that the conductivity values along fractured zones are one order of magnitude higher that the matrix conductivity. Numerical models discussed in the following chapter appears to support this assumption.

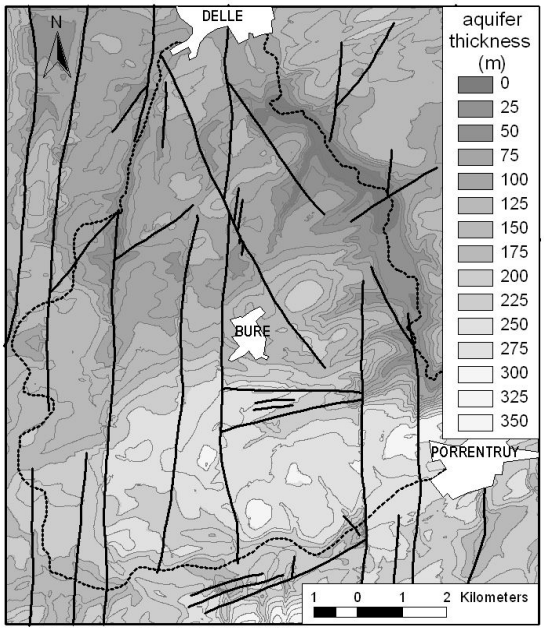

Figure 3-8. Aquifer thickness map.

Fleury & Allemann (1991) provides measured values for the storativity of confined Malm limestones in the area of Delémont. These values vary between $6 \cdot 10^{-5}$ and $3 \cdot 10^{-4}$ [-] in the 255 m thick confined aquifer. Jeannin & Grasso (1995b) estimated the effective porosity of the Bure aquifer to be in the range of 0.7 – 1 %.

3.3.3. AQUIFER DEFINITION AND CATCHMENT AREAS DELINEATION

Several tracing experiments (**Fig. 3-9**) have been carried out in the region since 1970 (Fleury, 1984; Gretillat, 1996; Favre 2001). The most frequently used tracers were fluorescent solutes (uranine, amidorhodamine, sulforhodamine and napthionate) and bacteriophages. Measured average velocities range between 1 and 700 m/h, but are usually in the range of 20-50 m/h.

The Bure plateau is hydraulically bordered by the Allaine river to the West and by the *Porrentruy – Chevenez – Grandfontaine dry valley* to the South. The southern border contains an underground river, the *Ajoulotte stream*, that underlies the valley bottom. These valleys act as the base levels of the plateau. Several springs are located along the *Delle – Lebétain valley*, delineating a hydrogeological boundary to the North-West of the Plateau. In the vicinity of *Fahy* the hydrological delimitation is uncertain, information obtained from tracing tests are very sporadic, and hydraulic boundary is assumed to follow the topographic high. Tracing experiments all confirmed the above mentioned delimitation, since no tracers passed these hydraulic boundaries.

Detection of artificial dyes in karst springs facilitated the delineation of several water catchments (Gretillat, 1996; Grasso & Jeannin, 1994b; Favre, 2001). Water budget calculations were also taken into account when delimiting water catchments. Based on these studies and numerical models, a detailed delineation of catchment areas is shown on **Figure 3-9.**

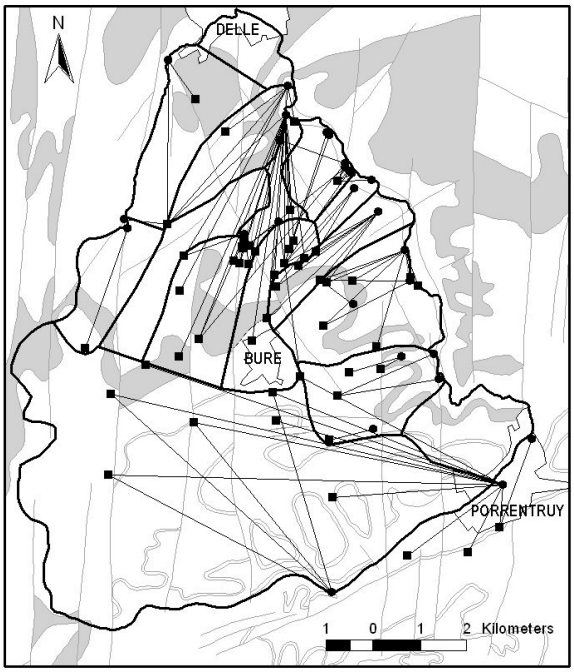

Figure 3-9. Delineation of water catchments based on tracing tests and water balance calculations. (Modified after Gretillat, 1996; Grasso & Jeannin, 1994 and Favre, 2001). Figure shows a selected set of dye tracer pathways, which link tracer injection points (quadrangles) and monitoring points (dots). Minor catchments at the northern and eastern extremities of the domain were determined by numerical models.

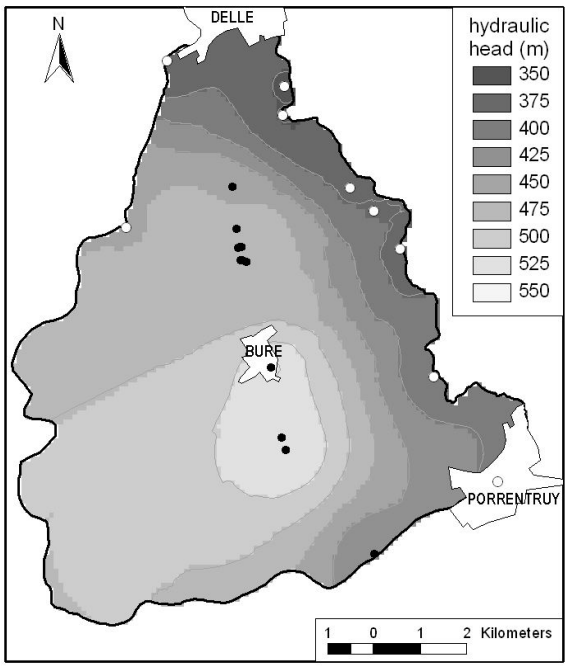

Figure 3-10. Water table map. It was obtained by Inverse Distance Weighted Interpolation between piezometric levels (black dots) and spring topographic elevations (white dots). Because of the sparse available piezometric data, this map provides only a loose approximation of the mean hydraulic heads throughout the low-permeability fissured matrix.

While the largest catchment area belongs to the Beuchire spring, tracing experiments supplied the most detailed information over the Milandrine catchment, where a greater number of experiments took place. Speleological exploration made the localization of tributaries confluences possible, and facilitated the measurement of their respective discharge rates.

Tracing experiments have another important consequence, which fundamentally influences our conception about the hydraulic functioning of the Malm aquifer. They clearly show that some tracers injected in certain zones into the aquifer above the Astarte Marls reappear in springs below the Astarte Marls. That means that Kimmeridgian Astarte Marls – according to our assumption based on structural properties - do not interrupt the aquifer hydraulic continuity in these zones. However the role of the Astarte Marls is not obvious at catchment scale, as there is no evidence whether infiltration waters penetrate the Astarte Marls all over the aquifer or not.

The zone where tracers could penetrate the Astarte Marls coincides with the zone where marls are located within the unsaturated zone. This zone also corresponds to the upstream part of the Milandrine catchment. Consequently any tracers injected south of this zone flow to the south and reappear in the Beuchire spring. However, there is no sufficient information to determine whether groundwater flow takes place above, or below the Astarte Marls.

By way of the most obvious approach, all of the Malm sediments superposed on the Oxfordian Marls are considered as an integral unit in this study.

3.3.4. PIEZOMETRIC SURFACE

Although water table in karst aquifers can be only poorly approximated by a few measurements obtained from piezometers or boreholes (Jeannin 1995a), these data can be used for roughly estimating regional head distribution and hydraulic gradients. A water table map has been established based on piezometric data obtained from a selected set of piezometers, and spring elevations. In the course of data selection, boreholes intruding deep into the saturated zone were considered exclusively and shallow penetration piezometric data were rejected, as they can be false and misleading.

The result of the Inverse Distance Weighted interpolation is presented in **Figure 3-10.** Since no piezometric observations are available in the western part (Fahy – Croix) of the domain, this map has to be considered as a very approximate one.

A piezometric dome extends to the south of Bure (Haut du Mont) with a maximum piezometric head at 580 m a.s.l. Confirmed by tracer flow directions, this dome designates a NW-SE oriented regional groundwater divide along the line connecting Porrentruy, Bure and Croix. To the north of this line, the general flow direction is NE. In the Southern regions the general flow direction is ESE.

The thickness of the saturated zone was calculated as the difference between the interpolated piezometric surface and the Oxfordian Marls surface (**Fig. 3-11)**. Saturated zone thickness reaches 300 m in the southern part of the site; it drops down to zero in the area of Boncourt – Buix and St-Dizier, indicating shallow karst conditions.

The maps presented here are based on incomplete and approximate data. Applied piezometric data indicate the mean water levels in the fissured matrix. Consequently, this approach maximizes the thickness of the saturated zone at low water levels.

3.3.5. REGIONAL HYDROGEOLOGICAL CONCEPTUAL MODEL

Field observations and measurements interpreted above from a regional perspective are now merged into a general conceptual model.

The Bure aquifer consists of karstified limestones varying in thickness between 0 and 320 meters. Malm sediments contain marl intercalations, which seem to be sufficiently karstified to allow groundwater flow. Thus the entire Malm sequence (above the Oxfordian Marls) is considered as a single heterogeneous aquifer.

Because of folding and subsequent erosion, the aquifer considerably thins over the anticline, while at the southern part of the aquifer it remains substantially thick.

The saturated zone also shows a large variation in thickness. According to available piezometric data over the anticline, the thickness of the saturated zone is negligible (**Fig. 3-11**). In this shallow karst zone, mainly unsaturated and channel flow takes place and the hydraulic gradient is determined by the topography of the Oxfordian Marls.

When assuming a zero hydraulic gradient upstream from the springs, we make a minimum estimate of the piezometric level in the karst conduits. This approach has been applied to the two main springs (Saivu and Beuchire) in the region (**Fig. 3-12**). While the former better characterises the low-water saturated thickness over the northern part of the domain, the latter relates to the southern part of the aquifer.

As piezometric data refers to the hydraulic heads in the fissured matrix and conduit flow also possesses some hydraulic gradient, which was not considered during the minimum piezometric level calculations, **Figure 3-11** shows thicker saturated zones than **Figure 3-12.**

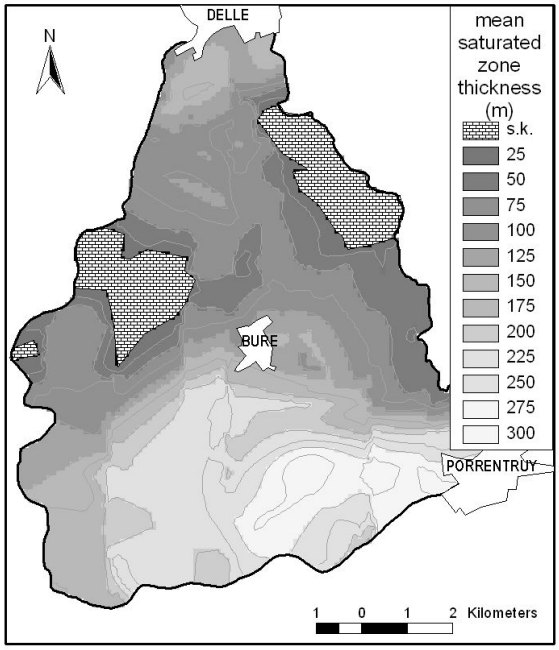

Figure 3-11. Mean saturated zone thickness map. It was calculated as the difference between interpolated water table and the top of the Oxfordian Marls, consequently it is very approximate. In the area of Boncourt – Buix and St-Dizier the thickness of the saturated zone decreases dramatically, indicating shallow karst conditions (s.k.).

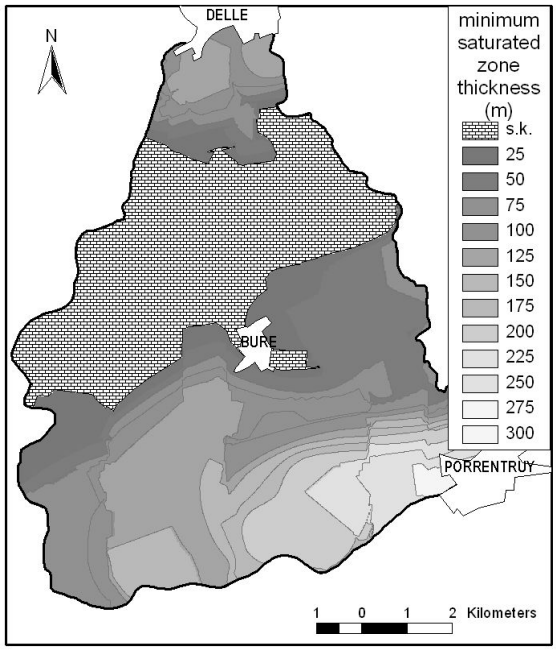

Figure 3-12. Minimum saturated zone thickness map. The minimum saturated zone thickness throughout the northern part of the aquifer was calculated as the difference between the elevation of the Saivu spring and the Oxfordian Marls surface. Similarly, over the southern part of the site it was calculated as the difference between the elevation of the Beuchire spring and the Oxfordian Marls surface.

Development of observed and minimum water tables is shown in **Figure 3-13.** Real hydraulic heads over the conduit network occur between these two surfaces. At high precipitation events conduit hydraulic heads can exceed average observed (matrix) piezometric levels.

Infiltration waters, after having been stored or distributed by the epikarst zone, descend through the unsaturated zone down to the saturated zone. Water from the fissured matrix flows through the conduit network towards the karst springs. The thickness of the unsaturated zone varies greatly; while it exceeds 150 meters in certain regions, in other parts of the aquifer it reaches only a few meters (**Fig. 3-14**).

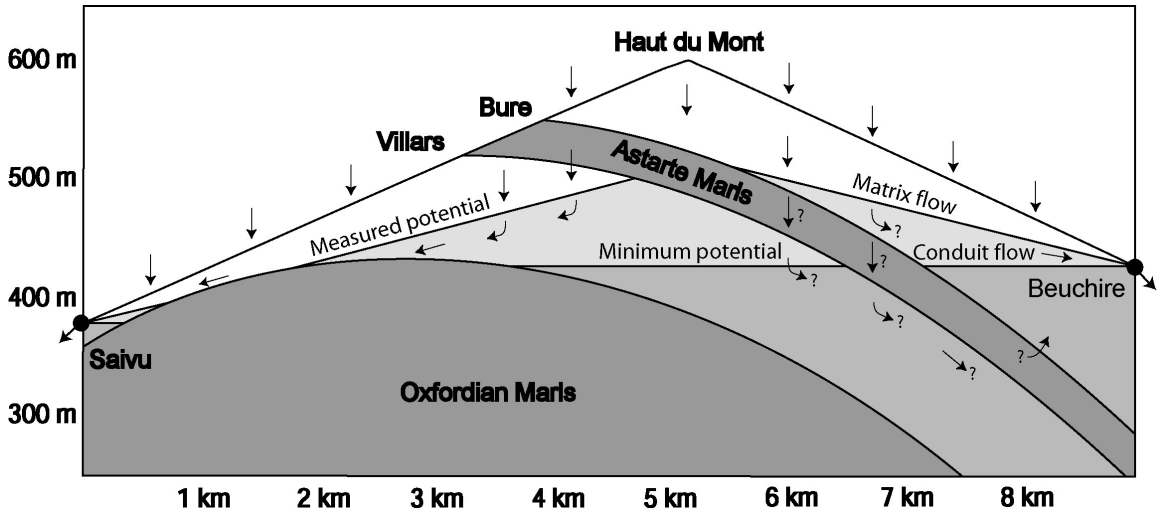

Figure 3-13. Conceptual model of the Bure aquifer. This N-S oriented theoretical cross section between Boncourt and Courtedoux shows the minimum estimate of the hydraulic heads in the karst conduits (assuming zero hydraulic gradient) and the mean water table (obtained from piezometers). Arrows indicate flow directions.

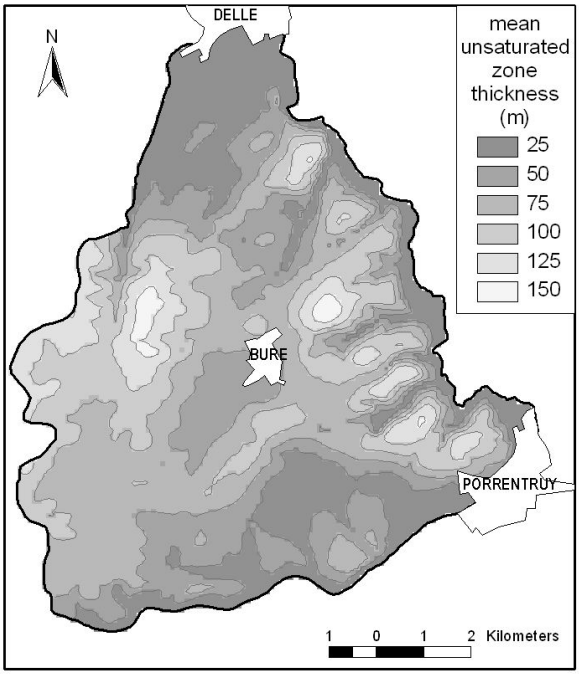

Figure 3-14. Mean unsaturated zone thickness.

3.4. CONCLUSIONS

This study presents a synthesis of hydrogeological data from the Bure plateau.

A detailed geometrical – hydrostratigraphic reconsideration of the research site was performed. A hydrostratigraphical map, cross-sections and structural surfaces have been constructed based on the most relevant data. Aquifer geometry and hydraulic boundaries were determined.

A summary of former tracing experiments was presented, the catchment boundaries were defined, and new subcatchments were established. One of the main achievements of this study was to clarify the hydraulic role of the Malm marl layers. Tracing experiments showed that the Sequanian and the two Kimmeridgian marl horizons do not act as aquicludes, and they do not significantly influence regional flow patterns.

Based on geometrical properties, piezometric observations, tracing tests and theoretical speculations, a coherent conceptual model of the Bure aquifer was constructed. On the basis of piezometric observations and aquifer geometry the maps of the average water table, saturated, and unsaturated zone thickness were constructed. Moreover, the possible extent of the shallow karst zone was estimated from the calculation of the minimum and average water tables. While the minimum water table calculated in this manner approximates the minimum hydraulic heads over the karst conduits, the average water table calculated from piezometric observations, approximates the average water levels over the fissured matrix.

These calculations located the regional groundwater divide along the Porrentruy – Bure – Croix axis, and designated extended shallow karst zones in the area of Buix and Croix.

4. ESTIMATION OF CONDUIT NETWORK GEOMETRY BY THE MEANS OF STEADY-STATE DISTRIBUTIVE GROUNDWATER FLOW MODELING

ABSTRACT

Steady-state two-dimensional and quasi three-dimensional groundwater flow models of the Bure aquifer (Ajoie, Switzerland) were developed using the combined discrete-continuum approach, in order to estimate the spatial configuration and hydraulic properties of the conduit system. Several conceptions of the conduit network geometry were tested using a range of configurations extending from pure equivalent porous medium to extended conduit network. Numerical simulations demonstrated that the equivalent porous medium approach is inadequate for simulating karst systems even under steady-state conditions. Furthermore, the implementation of observed karst channels into the model was still insufficient. Moreover, the simultaneous simulation of observed hydraulic heads and spring discharges following this approach was not possible without extending the observed conduit systems to catchment boundaries. The conduit conductivity of each extended conduit sub-system is roughly proportional to its spring discharge. The superposition of two-dimensional finite element layers interconnected by vertical discrete features facilitated the simulation of multi-layered karst aquifers. However, this approach considerably increases modeling effort and complicates the calibration process. Because of the lack of appropriate field data, a multi-layer model of the Bure aquifer cannot provide reliable information on the vertical organization of the conduit network. However, the introduction of phreatic karst conduits into the model does not significantly modify simulation results.

Keywords: Karst aquifers, Groundwater flow, Distributive models, Conduit network geometry, Bure Plateau, Milandrine cave

4.1. INTRODUCTION

One of the most significant characteristics of karst systems is strong heterogeneity due to the presence of high permeability voids created through dissolution. A karst aquifer can be considered as an interactive unit of a low permeabiliy matrix of fissured carbonate with an immersed hierarchical network of karst conduits. The spatial configuration of the conduit network and the hydraulic properties of either the low permeability matrix or the karst conduits have a strong influence on the hydraulic behavior of the aquifer and of the karst springs which discharges from it. The influence of conduit network geometric and hydraulic properties on the hydraulic head distribution and on spring discharge has been demonstrated by Király and Morel (1976b) and later by Eisenlohr (1996) and Eisenlohr et *al.* (1997a). All of these studies used numerical models to qualitatively demonstrate the effect of aquifer parameters alteration on a systems hydraulic behavior.

Speleological exploration may provide information on the extent, spatial geometry, and diameter of certain karst conduits. However, since the minimum diameter of conduits accessible by this method is limited to the size of the human body, and because of technical difficulties involved in subterranean exploration, this approach can only provide spatially restricted information on the geometry of conduit networks. Although this information can be further extended by the application of surface geophysical methods, tracing experiments, and borehole logging, knowledge of conduit geometry often remains limited and uncertain.

The aim of this study is to estimate the general geometric characteristics (extent and hierarchy) of the conduit network in karst aquifers, and the efficiency of field observations for constructing reasonable numerical groundwater flow models. This may be done by comparing model results with field observations. For this purpose, a set of two-dimensional and quasi three-dimensional groundwater flow models of the Bure Aquifer have been developed, using the combined discrete-continuum approach. Although a section of the conduit system of the Bure Aquifer over 10 km long has been explored by speleologists, most of the network remains uninvestigated. In order to estimate the spatial configuration and hydraulic properties of the entire conduit network, several conceptional models were tested from pure observed conduit network configuration to extended systems, as well as equivalent porous medium models.

A uniform average value of conductivities derived from borehole tests was assigned to the low permeability matrix. The preliminary value of conduit conductivity was obtained from field observations. The approximate density of the conduit network was estimated from cave maps. Measured average hydraulic potentials, average spring discharges and catchment boundaries designated from tracing experiments served as control parameters for the calibration process.

In order to facilitate the development of conceptual models using field data and the subsequent construction of numerical models and associated data exploitation, GIS tools (ArcView/ArcInfo) were used (Appendix 2). The Finite element mesh was generated by Feflow 4.8. Flow equations were solved making use of the groundwater modeling code FEN1 (Király, 1985).

4.2. CONCEPTIONAL MODELS

The development of a conceptual model of the study area required the application of several simplifications of the real system, necessary to achieve the goal of this study. A series of steady-state flow models was developed, in which model input and control parameters were temporally averaged, and in which simulation results correspond to a long-term generalization of hydrogeological processes.

In spite of the considerable thickness (40 m) of the Sequanian Astarte marls, tracing tests suggest that the underlying and overlying aquifer volumes are hydraulically connected (Chapter 4). However, it is uncertain whether Astarte Marls act as low-permeability percolation horizons, or whether vertical flow takes place exclusively through large-scale fractures or/and karstified zones. Therefore, two different conceptual models of the aquifer geometry have been tested. A two-dimensional approach substituted vertically heterogeneous material with a varying transmissivity homogeneous medium. In contrast, a quasi three-dimensional approach distinguishes upper and lower aquifer volumes, which are hydraulically independent, apart from communicating through vertical high-permeability zones. According to this approach, upper and lower aquifer volumes are also two-dimensional.

In both cases an average of the measured hydraulic conductivity was assigned as a uniform parameter to the fissured rock matrix over the entire model domain. Transmissivity values were proportional to the varying thickness of the saturated zone of the respective aquifer volumes. The initial conduit conductivities were estimated from mean spring discharge and hydraulic gradient of the Milandrine system. This value was later modified during the calibration process for each karst subsystem. Darcian flow was calculated in both low permeability blocks and conduits. As a result of the reduction of a three-dimensional system into two spatial dimensions, karst conduits represented by one-dimensional elements hydraulically behave as trenches in the model.

Observed hydraulic head distribution, average spring discharges, and drainage basin boundaries provided target values for the calibration process. A uniform effective recharge (500 mm/y) was distributed throughout the aquifer surface, as calculated by Jeannin & Grasso (1995).

Delimitation of the model domain and that of the karstic catchments is demonstrated in **Figure 4-1**. The eastern boundary of the model domain is delimited by the Allain river, and by karst springs which are located along the riverbank. In this zone, Dirichlet type boundary conditions have been imposed. Dirichlet boundary conditions were also defined along the northern part of the western boundary, which follows a surface stream. Along the rest of the western model boundary, Neumann (no flow) type boundary conditions were defined following the topographic high. The southern model boundary was delimited by a dry valley, below which an underground river flows. This river is represented by a high-conductivity channel along a no-flow type Neumann boundary.

In the course of the calibration of different flow models, two of the piezometric data points, borehole BUR-7 and FN-1 were used as reference points, as well as maximum simulated hydraulic head (**Fig. 4-2**). The aim of approximate model calibration was to demonstrate the limitations and suitability of a given concept, rather than to precisely reflect measured hydraulic data. Consequently, model results are not expected to exactly reproduce the observed hydraulic head distribution and spring discharges, and consequently they may differ from field measurements.

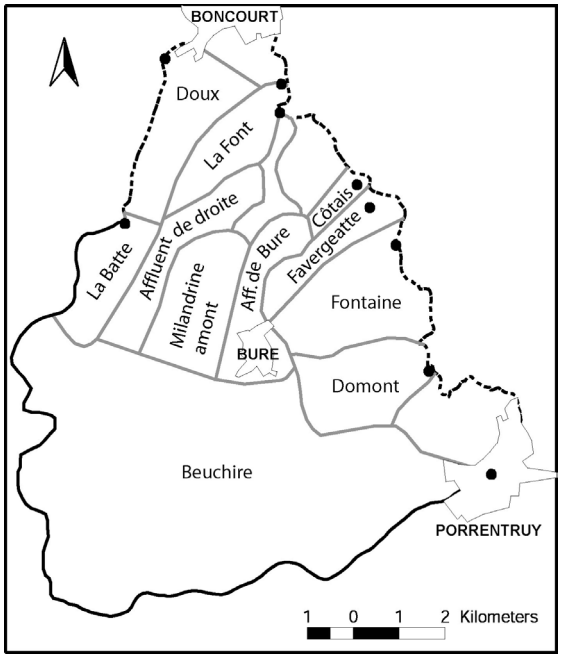

Figure 4-1. Delineation of model domain and catchment areas. Black solid line designates Neumann no-flow type boundary conditions; black dashed line indicates Dirichlet boundary conditions. Gray solid lines indicate catchment boundaries.

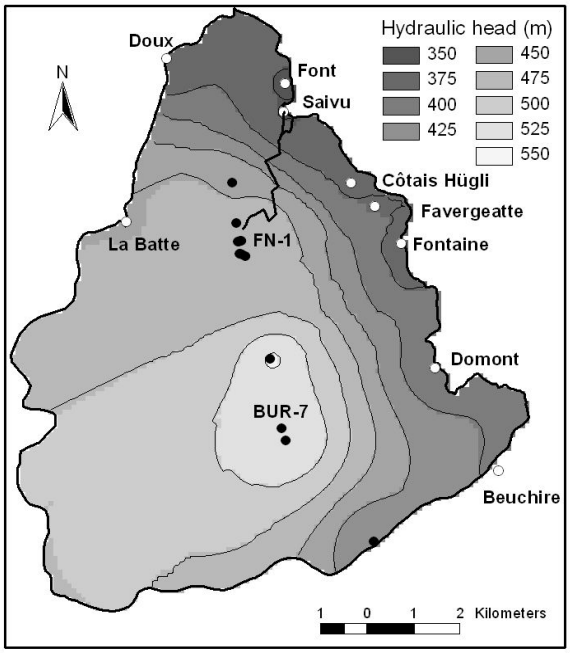

Figure 4-2. Piezometer (white dots) and spring (black dots) locations and average piezometric surface obtained by interpolation between these observation points. Solid line indicates the explored conduit system called Milandrine. The boreholes FN-1 and BUR-7 were used as reference points in the course of model calibration.

Groundwater flow simulations were based on the combined discrete-continuum approach (Király & Morel, 1976 ; Király, 1985, 1998a). This approach allows for the combination of 1-D, 2-D and 3-D linear or quadratic finite elements to be used. The code FEN1 facilitates the simulation of saturated, steady-state groundwater flow in two or three dimensions.

4.3. DISCUSSION OF TWO-DIMENSIONAL MODEL RESULTS

The two-dimensional representation of aquifer geometry neglects marl horizons, and simplifies the aquifer to a two-dimensional mesh of finite elements (**Fig. 4-3**). Transmissivity values are proportional to the thickness of the saturated zone obtained as a difference between the base of the aquifer (Oxfordian Marls) and the observed water table.

In the course of modeling process several conceptual models and realizations of conduit network geometry were tested. In order to obtain indirect information on the structure of karst conduit systems, two different parameter distributions were assigned to each model conception. One distribution is consistent with measured hydraulic conductivity, while the other is calibrated to observed piezometric data.

As an initial scenario, discrete features were omitted in order to investigate the applicability of the equivalent porous medium approach for modeling the Bure test site.

According to **Figure 4-4**, realistic parameter model (PMref) yields excessive hydraulic heads and unrealistically low spring discharges. This is the direct consequence of the lack of the drainage system which drains infiltrating waters and focuses them towards karst springs.

In order to roughly calibrate simulated head values to observed piezometric surface (**Fig. 4-5**), an increase in the measured matrix conductivity by more than one order of magnitude became necessary (**Tab. 4-1**). Although this equivalent porous model (EPMcal) of the aquifer is capable of revealing measured hydraulic heads in a steady-state, spring discharges could not be simulated by using this scenario even under steady-state conditions. As the simulation of transient phenomena taking place in strongly heterogeneous media is even a more challenging task, it can be concluded directly from this example that equivalent porous medium approach is unlikely to be suitable for modeling karst aquifers.

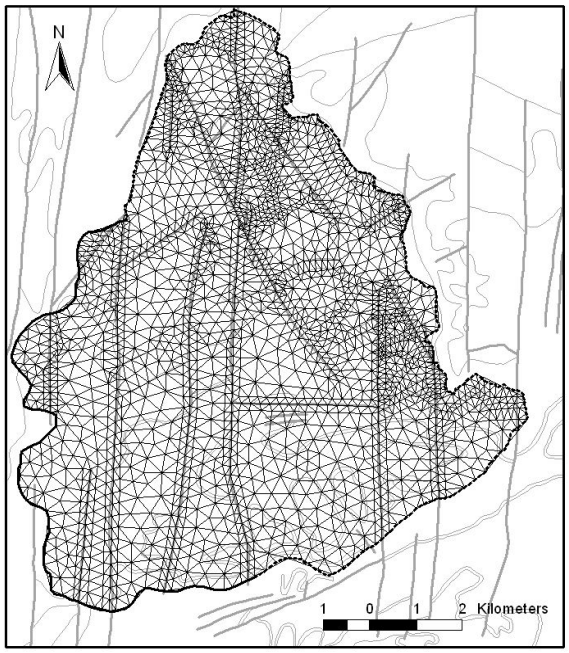

Figure 4-3. Two dimensional finite element mesh.

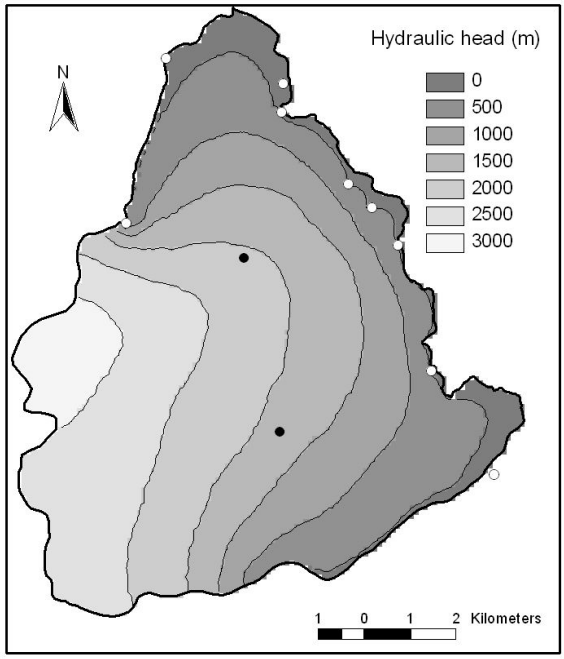

Figure 4-4. Porous medium reference model (PMref) simulation results.

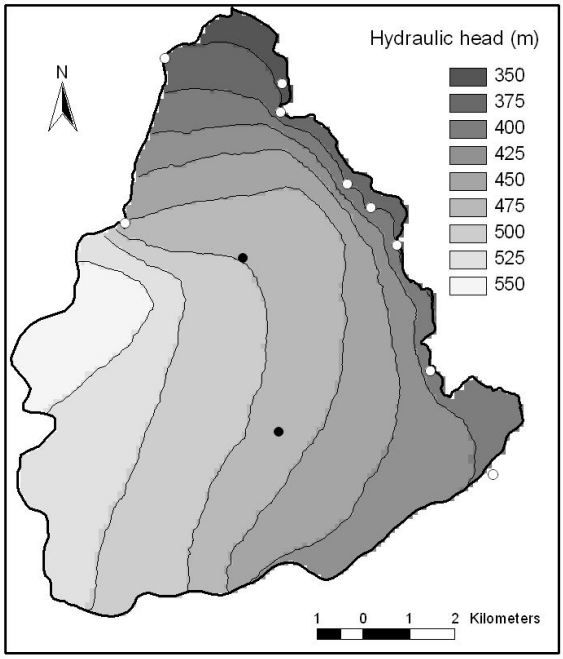

Figure 4-5. Equivalent porous medium model (EPMcal) simulation results.

MODEL	K_m (m/s)	K_c (m^3/s)	Conduit network	H (m) Bur-7	H (m) Fn-1	Q (m^3/s) Saivu	Q (m^3/s) Beuchire
reference	7.0E-07	8	observed	550	480	1.55E-01	8.00E-01
PMref	7.0E-07	-	omitted	1741	2102	9.02E-03	9.91E-03
EPMcal	1.8E-05	-	omitted	500	485	5.72E-03	9.91E-03
CDocnref	7.0E-07	8	observed	1715	1536	1.76E-01	9.87E-03
CDocncal	1.5E-05	8	observed	490	490	7.82E-02	9.26E-03
CDecn	7.0E-07	0.1-30	extended	526	508	2.05E-01	6.04E-01

Table 4-1. Comparative table of field measurements (reference), hydraulic parameters, and model results.

The Milandrine cave system was incorporated into the models CDocnref and CDocncal (**Fig. 4-6 & 4-7**), in order to check whether explored conduit network is sufficient for simulating hydraulic behavior of the entire system. Only field observations were integrated in model CDocnref. The resulting model contains the entire observed conduit system, having a uniform conductivity estimated from mean spring discharge (0.155 m^3/s) and hydraulic gradient (0.02) of the Milandrine underground river. The conduit conductivity estimated in this manner is K_c=8 m^3/s. Measured hydraulic conductivity was assigned to the low permeability fissured matrix. This model yielded greatly excessive hydraulic heads (**Fig. 4-6**) and low spring discharges for all springs, except that belonging to the explored conduit system. Consequently, pure field observations were concluded to be insufficient for modeling an aquifer containing unexplored conduit subsystems.

In order to adjust head distribution, the hydraulic conductivity of the fissured matrix had to be increased (**Tab. 4-1**). Although the calibrated matrix conductivity of model CDocncal (**Fig. 4-7**) is lower than that of the equivalent porous medium model (EPMcal), it is still more than one order of magnitude higher than measured values. Moreover, simulated spring discharges are far lower than that measured.

It is important to emphasize that exclusive increase of observed conduit conductivities can slightly decrease hydraulic heads and increase the discharge of the observed conduit system. However this alteration did not permit either remaining spring discharges or hydraulic heads to be calibrated.

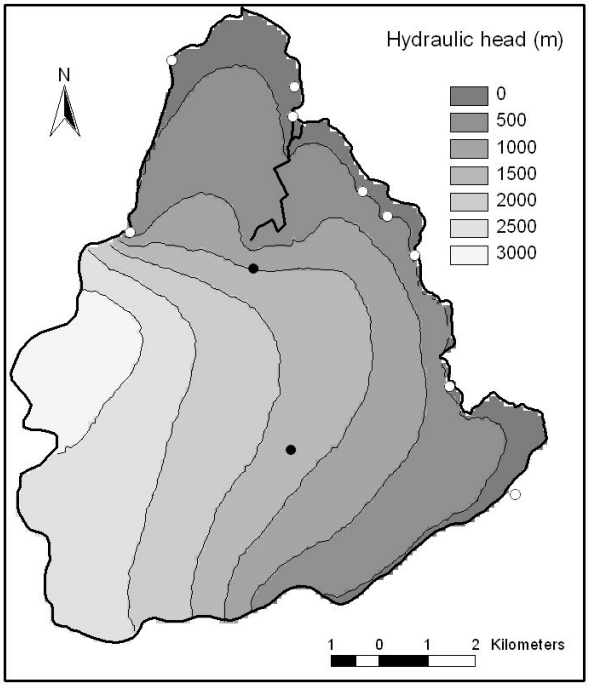

Figure 4-6. Reference model (CDocnref) results. This model is constructed on the base of pure field measurements and observations.

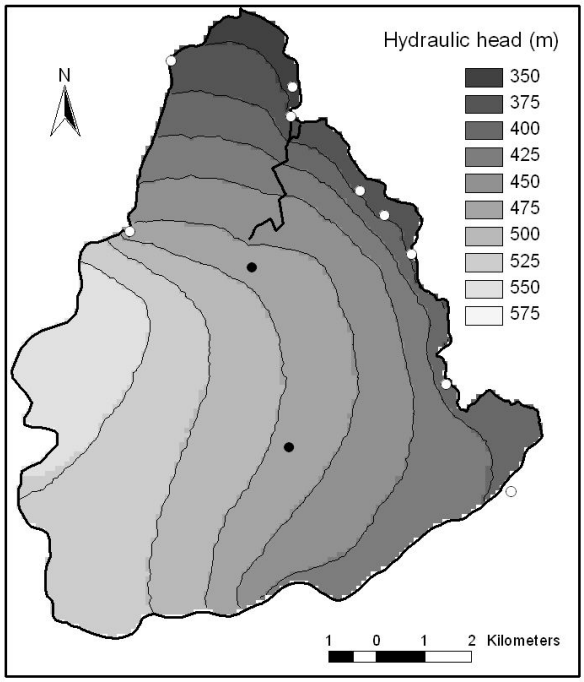

Figure 4-7. Calibrated observed conduit network model (CDocncal) simulation results.

As explained above, the simultaneous simulation of measured spring discharges and observed hydraulic heads was not possible by using only the explored karst conduits in the numerical model. An extension of observed conduit network was thus a logical necessity. Consequently, the observed conduit network was extended to the catchment boundaries, and further networks added to every single catchment in model CDecn. Manually constructed synthetic conduit networks followed a hierarchical structure, converging on karst springs. Initial conduit conductivity was estimated to be 8 m^3/s. Conduit network density was increased until excessive heads over low-permeability blocks disappeared. This state of calibration still involved steep gradients between adjacent karst systems as illustrated in **Figure 4-8**. These irregularities of the simulated water table were smoothed and hydraulic heads were calibrated by adjusting conduit network conductivities (**Fig. 4-9**); this also resulted in appropriate simulated spring discharges (**Tab. 4-2**).

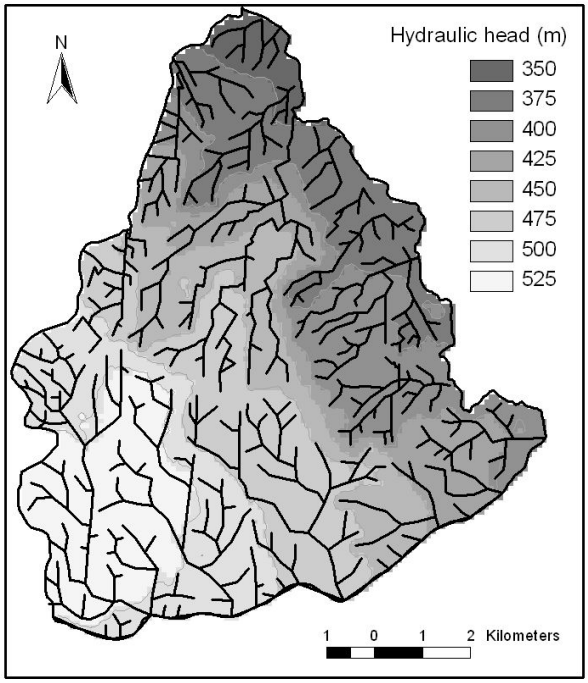

Figure 4-8. Hydraulic head distribution simulated by the extended conduit network model (CDecn), before the adjustment of conduit network hydraulic conductivities (K_c=8 m^3/s in every conduit).

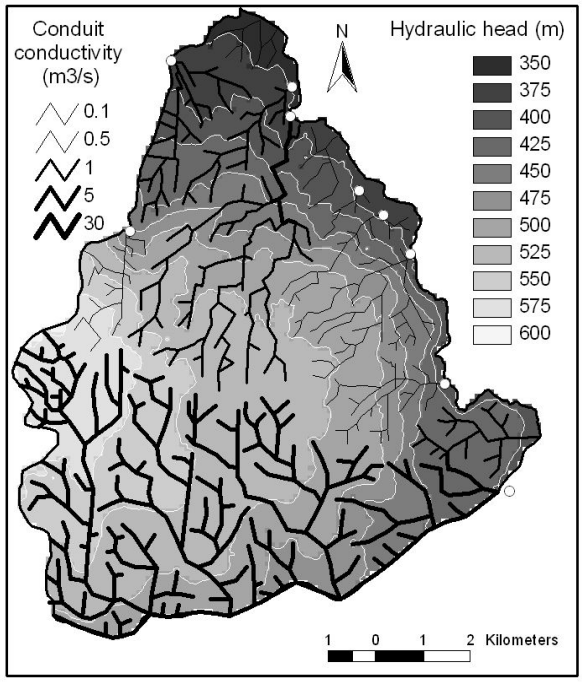

Figure 4-9. Extended conduit network model (CDecn) conduit geometry and calculated hydraulic heads. Calibrated conduit conductivities are numerical values and refer to darcian flow conditions.

Although the conduit system geometry implemented in model CDecn was only one realization of the infinite number of possibilities, the density of the conduit network and the corresponding conduit conductivities are particular characteristics of the model. According to the hydraulic parameters of the low-permeability matrix, only a restricted set of combinations of conduit network density and conduit conductivity can yield realistic results. The extended conduit network model clearly shows that simultaneous simulation of observed hydraulic heads and measured spring discharges is only possible by the extension of the observed conduit network.

spring	measured discharge (m^3/s)	calculated discharge (m^3/s)
SAIVU	0.155	0.205
COTAIS-HUGLI	0.010	0.019
FAVERGEATTE	0.030	0.025
FONTAINE	0.065	0.077
DOMONT	0.040	0.060
BEUCHIRE (*)	0.800	0.600
BATTE	0.020	0.053
DOUX	0.150	0.060
FONT	0.050	0.050

Table 4-2. Measured and calculated spring discharges. Calculated values originate from the extended conduit network model (CDecn). The catchment area of the Beuchire spring extends outside of the model domain.

The extended conduit network model provides an acceptable approximation of observed water table and yields spring discharges comparable to those measured (**Tab. 4-2**). Since the catchment area of the Beuchire spring extends outside of the model domain, simulated discharge of this spring is considerably less than that measured. The model CDecn clearly suggests the existence of extended conduit systems over the model domain, and shows that applied conduit network density and matrix transmissivity determine the possible range of conduit conductivity values that yield meaningful results.

4.4. DISCUSSION OF QUASI THREE-DIMENSIONAL MODEL RESULTS

In the quasi three-dimensional approach two horizontal sheets of two-dimensional linear finite elements portray aquifer geometry and represent aquifer volumes separated by the Astarte Marls Formation (Chapter 4). Aquifer volumes represented by horizontal finite element sheets are connected by vertical two-dimensional finite elements that represent conductive fault zones (**Fig. 4-10**). Otherwise no hydraulic connection exists. Chains of one-dimensional finite elements embedded in the two-dimensional element networks represent karst conduits. The upper two-dimensional network extends to the northern limit of the lower aquifers confined zone. Between this limit and the Astarte Marls outcrops, the potentiometric surface in the lower aquifer is lower than the Astarte Marls base, and unconfined flow takes place (**Fig. 3-13**). Consequently this zone is represented by one finite element layer.

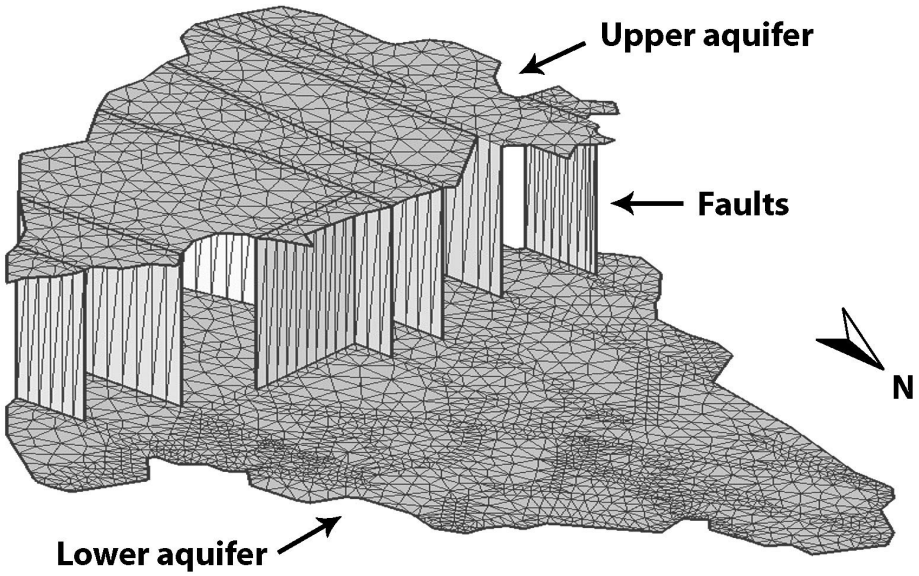

Figure 4-10. Quasi three-dimensional model geometry. Horizontal finite element sheets represent aquifer volumes; vertical finite elements represent faults.

The aim of the quasi-3D approach was to investigate the possible configuration of the conduit network in the Bure aquifer, assuming that aquifer volumes can communicate hydraulically only through discrete conductive zones. Two-dimensional models demonstrated the assumed horizontal configuration of the conduit system (Section 4.3). However, two-dimensional models can not provide information on the vertical position of conduit networks. Consequently, quasi-3D approach was expected to determine whether conduit systems are developed only in the upper aquifer volume, or in both the upper and lower aquifers.

Transmissivity values in the upper aquifer volume are proportional to the saturated zone thickness. This was obtained as a difference between Astarte Marls surface and the water table. The transmissivity of the lower aquifer volume is proportional to its thickness in the confined zone, and to the saturated zone thickness in the unconfined zone. The transmissivity of vertical faults was assumed to be 10^{-4} m^2/s. A uniform effective infiltration of 500 mm/year was distributed along the upper aquifer and the unconfined part of the lower aquifer.

As a first scenario (2layCDecn1), conduit network was extended in the upper aquifer volume, and in the unconfined zone of the lower aquifer. This approach involves that the confined zone is poorly karstified, and there are no karst conduits present in this zone.

As demonstrated in **Figure 4-11** and in **Table 4-3**, observed hydraulic heads can be closely reproduced following this approach. According to model simulations, in the central zones of the upper aquifer hydraulic heads are higher than in the underlying aquifer volume, indicating downward water filtration. However, along the southern model boundary, the simulated hydraulic heads in the upper aquifer are lower than those in the lower aquifer. This indicates an upward water movement in the discharge zone.

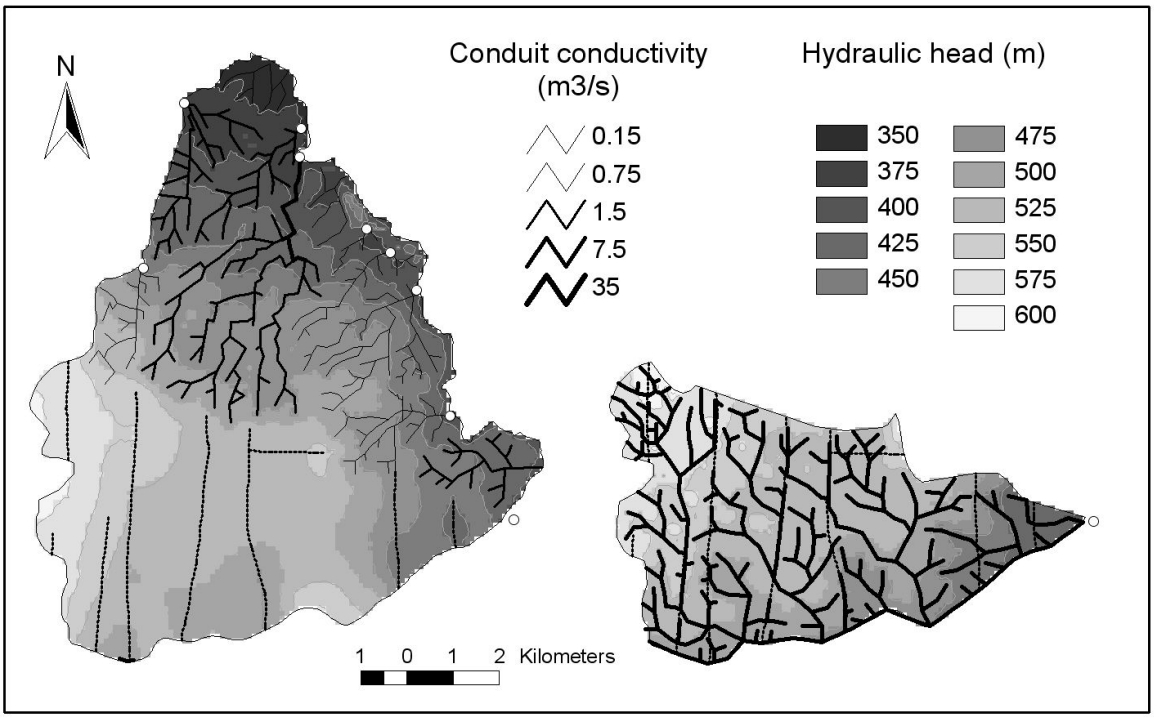

Figure 4-11. Two-layer model (2layCDecn1) conduit geometry and simulated hydraulic heads. Dashed lines mark vertical features connecting upper and lower aquifer volumes.

MODEL	K_m (m/s)	K_c (m^3/s)	Conduit network	H (m) Bur-7	H (m) Fn-1	Q (m^3/s) Saivu	Q (m^3/s) Beuchire
reference	7.0E-07	1	observed	550	480	1.55E-01	8.00E-01
2layCDecn1	7.0E-07	0.15-35	extended	550	478	2.28E-01	5.88E-01
2layCDecn2	7.0E-07	0.1-30	extended	522	502	1.97E-01	6.68E-01

Table 4-3. Comparative table of field measurements (reference), hydraulic parameters and two-layer model results.

The model 2layCDecn2 applied extended karst systems in the confined aquifer volume too. This conduit network has the same pattern as that in the upper aquifer, and both units discharge to the Beuchire spring. The conduit network geometry and simulated hydraulic heads of this model are summarized in **Figure 4-12**. Simulated hydraulic heads in the upper aquifer volume are higher than those in the lower aquifers covered zone, indicating downward water flow along vertical features.

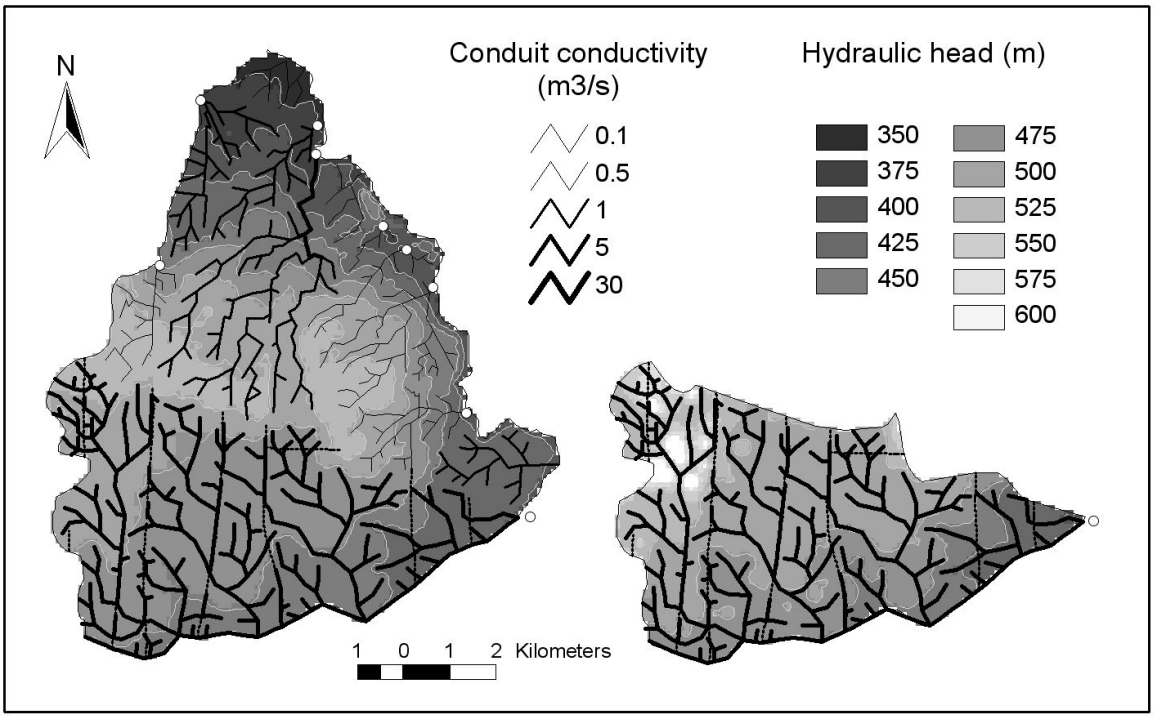

Figure 4-12. Two-layer model (2layCDecn2) conduit geometry and calculated hydraulic heads. Dashed lines mark vertical features connecting upper and lower aquifer volumes.

Table 4-4 indicates that simulated spring discharges approach measured values for both models. However, for the model 2layCDecn1, a portion of waters infiltrating throughout the upper aquifer also recharges the lower aquifer volume through vertical faults. Groundwater in this lower unit mainly flows to the north. Consequently, lower aquifer spring discharges are slightly higher than those of the one-layer model, and upper aquifer spring discharge of this model is slightly lower than that of the one-layer model. In contrast, spring discharge rates of the model 2layCDecn2 in the lower aquifer are lower than those of the one-layer model, and the simulated discharge of the Beuchire spring is higher than that of the one-layer model. This is the result of the increased number of high-conductivity channels that discharge at the Beuchire spring.

spring	measured discharge (m^3/s)	Model 2layCDecn1 discharge	Model 2layCDecn2 discharge
SAIVU	0.155	0.228	0.197
COTAIS-HUGLI	0.010	0.018	0.019
FAVERGEATTE	0.030	0.029	0.027
FONTAINE	0.065	0.089	0.082
DOMONT	0.040	0.073	0.059
BEUCHIRE (*)	0.800	0.588	0.668
BATTE	0.020	0.050	0.040
DOUX	0.150	0.076	0.060
FONT	0.050	0.054	0.050

Table 4-4. Measured and simulated spring discharges; (*) indicates that the Beuchire catchment extends outside of the model domain.

As there is no available information on the hydraulic heads in the confined zone, and both of the two-layer model scenarios yield realistic spring discharges, it is difficult to draw conclusions from the model simulations concerning the configuration of the conduit network in the confined zone. In order to verify the two-layer model scenarios, further piezometric data from the lower aquifer volume are necessary. Consequently, no conclusions concerning the vertical organization of the conduit network in multi-layered karst aquifers can be drawn from the numerical modeling of the Bure aquifer. However, the increased complexity of model geometry does not result in any significant improvement of the model results for this site. Furthermore, complex model geometry and the introduction of discrete vertical features into the model make model calibration more difficult, as well as requiring increased modeling effort and longer calculation time. Consequently, the one-layer approach is believed to be the most reasonable modeling scenario for simulating hydraulic phenomena in the Bure aquifer.

4.5. CONCLUSIONS

Indirect information on the spatial extent of the conduit network in the Bure Aquifer has been obtained by the means of numerical modeling. Steady-state two-dimensional and quasi three-dimensional finite-element models have been constructed making use of the combined discrete-continuum approach. This method facilitated testing different configurations of hydraulic parameters and the spatial geometry of the high-conductivity karst channel network, by allowing for the implementation of one-dimensional elements into the two-dimensional element network.

Simulation results showed that the equivalent porous medium approach is inappropriate for modeling karstified medium, since it yields systematically lower spring discharges than measured values, due to the lack of high-conductivity drainage networks.

The implementation of observed conduit systems into the model is insufficient for retrieving measured spring discharges. Simultaneous simulation of mean water levels and average spring discharges requires the extension of the observed conduit system across the entire model domain where effective infiltration takes place. Each karstic spring requires an extensive conduit network discharging to it, otherwise the simulation of spring discharges fails even under steady-state conditions. Flow simulations suggest that the hydraulic conductivities of extended conduit systems are roughly proportional to their respective spring discharges.

The superposition of two-dimensional finite element layers interconnected by vertical discrete features makes the simulation of flow fields in multi-layered karst aquifers possible. However, complicated model geometries do not necessarily yield more reliable simulation results than two-dimensional models. Furthermore, the multi-layer approach considerably increases modeling effort, and complicates the calibration process. Due to the lack of comparative field data, the multi-layer model of the Bure aquifer cannot provide reliable information on the vertical organization of the conduit network.

5. EVALUATION OF AQUIFER HYDRAULIC AND GEOMETRIC PARAMETERS FROM SPRING RECESSION COEFFICIENT

ABSTRACT

This paper presents a quantitative characterization of the dependence of a karst systems global response on aquifer hydraulic and geometric parameters. Analytical formulae identified two, significantly different flow domains, depending on the overall configuration of aquifer parameters. During the baseflow recession of mature karst systems, the hydraulic parameters of karst conduits does not influence the drainage of the low-permeability matrix. In this case the drainage process is influenced by the size and hydraulic parameters of the low-permeability blocks alone. This flow condition has been defined as matrix-restrained flow regime (MRFR). During the baseflow recession of premature karst systems and the flood recession of mature systems, the recession process is dependent not only on the hydraulic parameters and the size of the low-permeability blocks, but also on conduit conductivity, and the total extent of the aquifer. This flow condition has been defined as conduit-influenced flow regime (CIFR). Analytical formulae also demonstrated the limitations of equivalent models. While equivalent discrete-continuum models of premature karst systems may reflect their real hydraulic response, there is only one adequate parameter configuration for mature systems that yields appropriate recession coefficient. Consequently, equivalent discrete-continuum models are inadequate for simulating global response of mature karst systems. The global response of equivalent porous medium models corresponds to the transition between matrix-restrained and conduit-influenced flow regimes. Consequently, the equivalent porous medium approach cannot be directly applied for modeling karst aquifers.

Keywords: Karst aquifers, Global response, Conduit network geometry, Hydraulic parameters, Analytical formulae, Sensitivity analysis, Equivalent models

5.1. INTRODUCTION

In order to be able to construct informative distributive numerical groundwater flow models of karst systems, which reflect either the global or the spatial behavior of a real system, the definition of realistic hydraulic and geometric parameters is essential (Király & Morel, 1976a; Király, 1998). The lack of such data gives rise to significant difficulties in modeling karst hydrogeological systems.

A simple conceptual model of karst systems can be characterized by the hydraulic parameters of the low-permeability matrix and the conduit system, conduit spacing and the spatial extent of the aquifer (**Fig. 5-1**.).

Information on the hydraulic and geometric properties of karst systems can be obtained from classical geological and hydrogeological survey data, borehole tests, tracing experiments, speleological and geophysical observations, and discharge measurements.

Classical geological exploration methods such as geological mapping or borehole logging provide detailed information on the extension and spatial geometry of the aquifer.

While borehole tests usually provide reasonable information on the hydraulic properties of the low-permeability matrix (Király, 1975), the characterization of the conduit system requires information derived from additional exploration techniques, which are rarely accessible.

Tracing experiments may provide information on the interconnectivity of karst conduits, but not on their precise geometry.

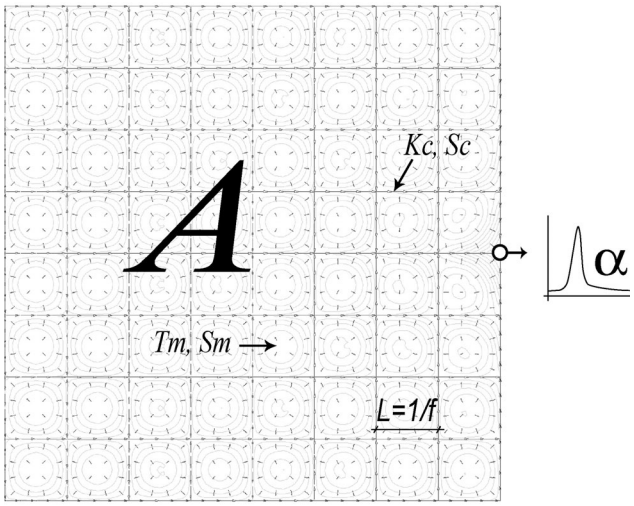

Figure 5-1. A simple conceptual model of karst aquifers. Characteristic hydraulic and geometric parameters are: Transmissivity of the low-permeability matrix T_m [L^2T^{-1}], storativity of low-permeability matrix S_m [-], conduit conductivity K_c [L^3T^{-1}], storage coefficient of karst conduits S_c [L], spatial extent of the aquifer A [L^2], and the frequency of karst conduits f [L^{-1}].

Although classical speleological exploration provides detailed information on the spatial configuration and hydraulic properties of certain conduits, data obtained using this approach is strongly limited to a minimum conduit diameter corresponding to the size of the human body. Furthermore, extensive parts of even the large scale conduits often remain unexplored because of physical obstacles, siphons, or simply because they are too deep in the phreatic zone.

Surface geophysical methods are relatively fast and cheap, and they provide detailed information on the spacing of the tectonically weakened zones (Militzer et *al.*, 1979; Müller 1982; Turberg & Müller, 1992; Guerin & Benderitter, 1995; Armadillio, 1998 Bosch & Müller, 2001; Gurk & Bosch, 2001). On the other hand these methods are not capable of differentiating either between fractures and conduits, or between dry and water-filled voids. Moreover, their application is often limited to easily accessible locations, and their penetration depth may be insufficient.

In most cases some spring discharge time series data, coupled with information on the hydraulic properties of the low-permeability rock matrix are available. Although the global response of karst aquifers has been analyzed by several authors for a long time (Maillet, 1905; Forkasiewicz & Paloc, 1967; Drogue, 1972; Mangin, 1975), the interpretation of this information has hitherto been mainly qualitative, and it has scarcely been used as a means of determining appropriate input data necessary for distributive modeling.

The aim of this paper is to demonstrate the connection between the hydraulic and geometric properties of karst aquifers and their global response, in order to provide a tool for characterizing flow field and for facilitating distributive groundwater flow modeling of karst systems. This has been achieved by deducing analytical solutions for the global hydraulic response of simple two-dimensional domains. The analytical formulae were then tested by numerical models. Resulting formulae express the connection between the hydraulic and geometric properties of a karst system and the spring hydrograph recession coefficient, which is believed to be a characteristic parameter of a systems global response.

5.2. PRECEDENTS

Every hydraulic process taking place in a karst aquifer manifests in the temporal variations in spring discharge. The plots of spring discharge versus time are called spring hydrographs (Chapter 2). Hydrographs consist of a succession of individual peaks, each of which represents the global response of the aquifer given to a precipitation event (**Fig. 5-2**). Hydrograph peaks consist of rising and falling limbs; the former comprises of a concave and a convex segment separated by an inflexion point. This inflexion point represents the maximum infiltration state (Király, 1998b). The falling or fast recession limb of the hydrograph peak is also divided into a convex segment and a concave segment by a second inflexion point, which represents the end of the infiltration event. The flat part of the hydrograph following the end of hydrograph peaks is called baseflow recession. This is the most stable section of any hydrograph, and also the most representative feature of the aquifers global response. This is because baseflow recession is supposed to be the less influenced of any segment of the hydrograph by the temporal and spatial variations of infiltration.

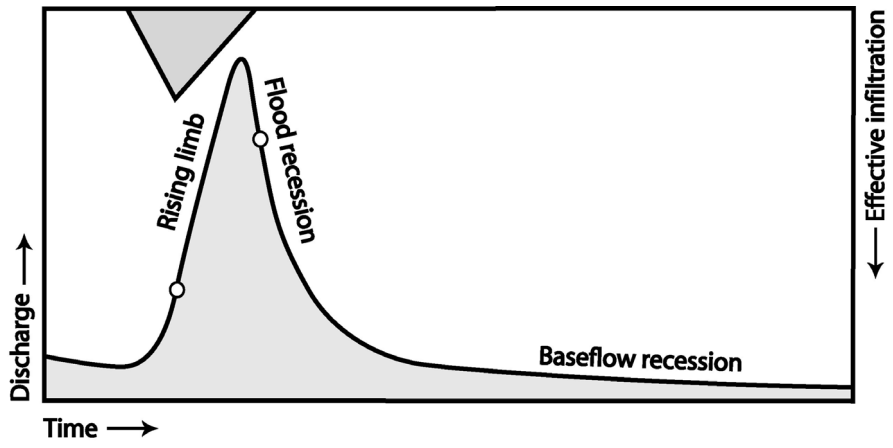

Figure 5-2. Typical features of a spring hydrograph. White dots indicate inflexion points that belong to the maximum infiltration state and to the end of the infiltration respectively.

Quantification and interpretation of spring hydrographs has been of a high interest for a long time. The mathematical interpretation of spring hydrographs, the definition of the recession coefficient, and the most important global modeling approaches are briefly presented in Chapter 2.

5.2.1. QUANTITATIVE INTERPRETATION OF THE RECESSION COEFFICIENTS DEPENDENCE ON AQUIFER PROPERTIES

Although the mathematical description and the interpretation of the fast recession is varying (Chapter 2), the baseflow recession is generally described by the classical exponential formula of Maillet (1905), and is believed to reflect the drainage of the saturated low-permeability fissured matrix. Consequently, the baseflow recession must be dependent on the material properties of the low-permeability fissured matrix. Analytical and semi-analytical expressions were developed by several authors for expressing this dependence.

Berkaloff (1967) gave a solution for diffusive flux from a one-dimensional conductive block having fix-head boundary conditions at one extremity, and steady-state initial conditions over the block (**Fig. 5-3**). This may be expressed as follows:

$$Q = \frac{2TR_0}{SL}\sum_{n=1}^{\infty} e^{-(n-\frac{1}{2})^2 \pi^2 \frac{Tt}{SL^2}} \tag{5-1}$$

where T is hydraulic transmissivity [L^2T^{-1}] , S is storativity [-], R_0 is the initial constant recharge expressed as [L], and L is the length of the one-dimensional block [L]. Neglecting the higher order terms of the series, the discharge can be approximated as:

$$Q_{(t)} = \frac{2TR_0}{SL} e^{-\frac{\pi^2 Tt}{4SL^2}} \tag{5-2}$$

The one-dimensional block recession coefficient is thus:

$$\alpha_b = \frac{\pi^2 T}{4SL^2} \tag{5-3}$$

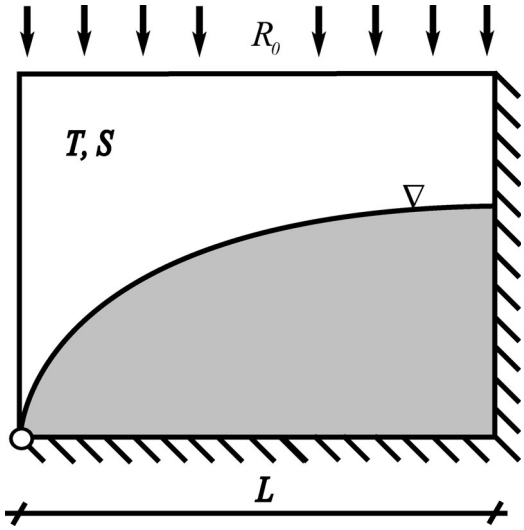

Figure 5-3. The one-dimensional model of Berkaloff (1967).

Bagarić (1978) provided an analytical solution for diffusive flux from a one-dimensional conductive block that has fix-head boundary condition at one edge. Contrary to the model of Berkaloff (1967), no infiltration was applied in this concept. According to Bagaric, the discharge of the block may be expressed as follows:

$$Q_{(t)} = Q_0 e^{-\frac{2T}{SL^2}t} \tag{5-4}$$

Based on **Equation (5-4),** the recession coefficient of a one-dimensional block may be equated to transmissivity and storage as follows:

$$\alpha_b = \frac{2T}{SL^2} \tag{5-5}$$

This solution is quite similar to that of Berkaloff (1967) expressed by the **Equation (5-3).**

5.2.2. QUALITATIVE INTERPRETATION OF THE RECESSION COEFFICIENTS DEPENDENCE ON AQUIFER PROPERTIES

The analytical formulae discussed in the previous section, consider the recession process as exclusively dependent on the hydraulic parameters of the low-permeability matrix, and neglect the effect of the conduit network geometry and hydraulic properties of the karst conduits. Although mathematical formulation has not yet been provided which describes the influence of the conduit network on the recession coefficient so far, some sensitivity analyses have been performed to describe this process qualitatively.

The first distributive modeling code capable of combining conduit flow and diffuse flow was created by Király & Morel (1976a) and Király (1985, 1988). These authors performed some sensitivity analyses too (Király & Morel, 1976b), and concluded that the increase of the conduit network density results in higher baseflow recession coefficients.

Some additional analyses were performed by Eisenlohr (1996) and Eisenlohr et al. (1997a) who constructed a series of 2D synthetic models having different karst network densities. This study concluded that the baseflow recession coefficient increases, as the density of the conduit network increases.

Similar sensitivity analyses were completed by Cornaton (1999) using three-dimensional synthetic models. These simulations confirmed the results of Eisenlohr (1996).

According to further simulations of Eisenlohr (1996), an increase of the conduit network conductivity results in a corresponding rise in baseflow recession coefficient. Moreover, the simultaneous increase of the storage coefficients of both the low-permeability matrix and the karst conduit network results in the decrease of the recession coefficient. Eisenlohr (1996) did not investigate the effect of the separate variation of the capacitive parameters of the low-permeability volume or the karst conduit network. Cornaton (1999) carried out such tests using 3D synthetic models and concluded that an increase in either the matrix storage coefficient or conduit storage coefficient resulted in a lower recession coefficient.

Eisenlohr (1996) investigated the effect of the *recharge function* on the discharge curve by simulating the effect of three different discharge functions on the hydrograph. Application of triangular, rectangular and hyperbolic recharge functions having the same integral value showed the followings: Until the durations of the recharge functions were identical, and the simulations did not involve slow retarded seepage from the upper capacitive volumes, the baseflow recession coefficients were similar. However, the fast recession limb showed a strong variation. In the case of where the recharge function implied retarded seepage, the baseflow recession coefficient decreased also.

Eisenlohr (1996) also constructed synthetic models having the same conduit network density, but different orientations of the network. These simulations showed that the baseflow recession coefficient increased as the orientation of conduit network corresponds more closely to the model domains longest orientation.

The above discussed studies demonstrated that contrary to the principal assumption of the analytical models of Berkaloff (1967) and Bagarić (1978) that neglected the effect of the conduit network, the baseflow recession coefficient may depend also on the hydraulic and geometric parameters of the conduit system. Although the above-mentioned sensitivity analyses demonstrated the variations of the recession coefficient according to the varying aquifer properties, they comprised only a tiny number of simulations. Consequently, these simulations could provide only a qualitative indication of the effect of the modification of certain aquifer parameters on spring hydrographs.

5.3. AN ANALYTICAL SOLUTION FOR DIFFUSIVE FLUX FROM A TWO-DIMENSIONAL HOMOGENEOUS SQUARE BLOCK

Since the one-dimensional analytical formulae described in Section 5.2.1. involve a number of simplifications, an analytical solution for diffusive flux from two-dimensional conductive blocks is provided below. Though this solution still involves simplifications, it provides a more realistic view of the dependence of the recession coefficient on geometric characteristics and hydraulic parameters of the low-permeability blocks encircled by high-permeability karst conduits.

The solution of diffusive flux from a homogeneous two-dimensional square block (**Fig. 5-4**) is derived from the heat flow equation solution of Carslaw & Jaeger (1959), using the following formula:

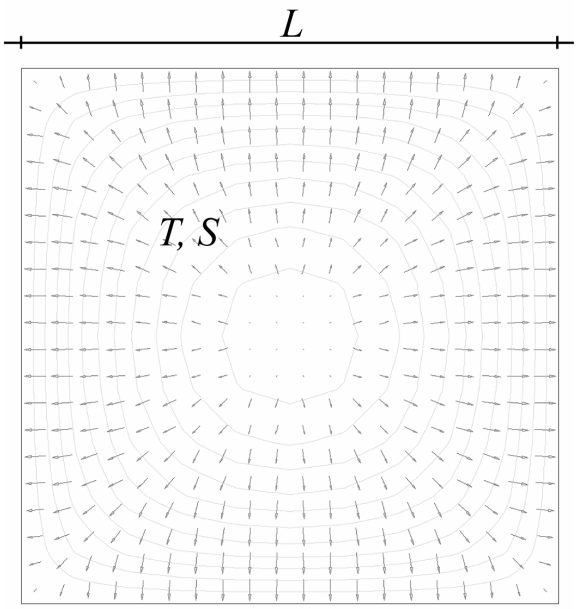

Figure 5-4. Diffusive flux from a two-dimensional homogeneous block having encircling uniform head boundary. L is the size of the domain [L], T is hydraulic transmissivity [L^2T^{-1}], S is storativity [-].

$$Q_{(t)} = \frac{128}{\pi^2} T \sum_{n=0}^{\infty} e^{-(2n+1)^2 \pi^2 \frac{Tt}{SL^2}} \sum_{n=0}^{\infty} \frac{e^{-(2n+1)^2 \pi^2 \frac{Tt}{SL^2}}}{(2n+1)^2} \tag{5-6}$$

where constant uniform hydraulic heads are assumed as boundary conditions along the sides of the square shape block, and initial conditions comprise uniform hydraulic heads over the block surface. Assuming that

$$a = \frac{\pi^2 Tt}{SL^2} \tag{5-7}$$

It follows from **Equation (5-6)** that

$$Q_{(t)} = \frac{128}{\pi^2} T(e^{-a} + e^{-9a} + e^{-25a} + ...)(e^{-a} + \frac{e^{-9a}}{9} + \frac{e^{-25a}}{25} + ...) \tag{5-8}$$

Neglecting the higher order terms of the series the discharge can be approximated as

$$Q_{(t)} = \frac{128}{\pi^2} T(e^{-2\pi^2 \frac{Tt}{SL^2}}) \tag{5-9}$$

Substituting this solution into the classical Maillet (1905) formula (**Eq. 2-1**), the recession coefficient of a two-dimensional homogeneous block may be expressed as

$$\alpha_b = \frac{2\pi^2 T}{SL^2} \tag{5-10}$$

5.3.1. VALIDATION OF THE ANALYTICAL SOLUTION BY NUMERICAL MODELS

Some simple numerical simulations have been performed to confirm the analytical solution given in **Equation (5-10)** for diffusive flux from a homogeneous two-dimensional square block. The parameters *T, S*, and *L* were systematically changed and results were compared with the analytical solution (**Figure 5-5**).

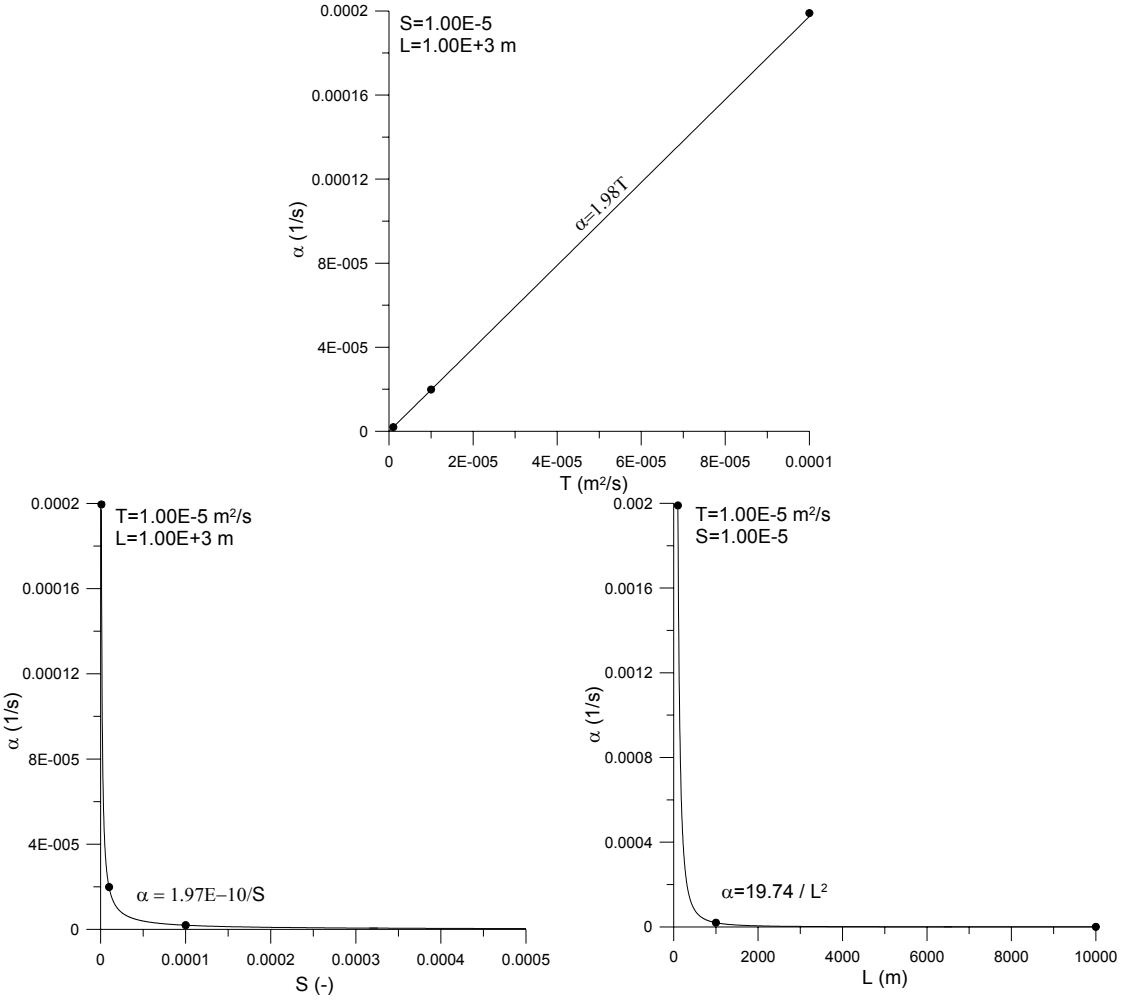

Figure 5-5. Comparison between numerically simulated and analytically calculated recession coefficients of homogeneous 2D square blocks. Solid lines: analytical solutions, dots: numerical simulations.

As shown in **Figure 5-5**, numerically calculated and analytically calculated recession coefficients are very similar for every parameter configuration indeed, in all cases the error on α never exceeds 1%.

5.4. EFFECT OF CONDUIT PARAMETERS ALTERATION ON RECESSION COEFFICIENT

Using **Equation (5-10)**, the analytical solution was evaluated for the flux from a homogeneous square block. The recession of an entire karst system can be determined using this approach if the conductive capacity of the water drainage system is assumed to be sufficiently high and the storage in the conduit network is neglected. Furthermore, the discharging waters from low-permeability blocks is assumed to reach the domain outlet instantaneously. In order to check the domain of validity for this simplification and the effect of changing conduit characteristics on the recession coefficient, several numerical models were constructed. Using an initial set of simulations, the sensitivity of the recession coefficient to the conduit conductivity was investigated. A second series of simulations was performed in order to investigate the sensitivity of the recession coefficient to conduit frequency. Conduit storage coefficients were calculated from relevant conduit apertures assuming water compression alone, using **Equation (2-29)**.

As demonstrated in **Figure 5-6**, an increase in conduit conductivity results in a rise in recession coefficient, until reaching the value of the analytical solution for a single homogeneous block. By exceeding a threshold value, the increase of the conduit conductivity has no further effect on the recession coefficient, and the recession process is constrained by the hydraulic parameters of the low-permeability blocks alone. This case coincides with the domain of validity of the analytical solution for diffusive flux from a homogeneous block.

This means, that in the case of where the conduit conductivity is sufficiently high, further increases do not influence the recession process, since the discharging capacity of the low-permeability blocks remains lower than that of the conduits. A threshold value of conduit conductivity must exist for any model configuration.

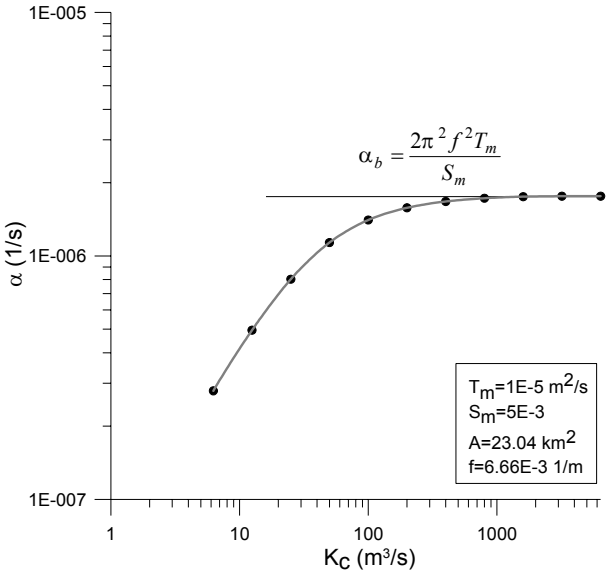

Figure 5-6. Dependence of the recession coefficient on conduit conductivity. Simulation results are represented by dots.

By exceeding this value, the hydraulic gradient in the conduits is negligible during the recession process, and conduit flow has no influence on the hydraulic gradient over the low-permeability blocks. The conduits act as fix-head boundary conditions as assumed by the analytical model (Section 5.3.). This flow condition is hereby denominated *matrix-restrained flow regime (MRFR)*, and the set of parameter configurations corresponding to such baseflow conditions is thus referred to as *matrix-restrained baseflow domain.* In the case where the conduit hydraulic conductivity is below the threshold value, the recession coefficient is strongly dependent on the conduit conductivity, and the analytical **Equation (5-10)** is no longer valid. This flow condition is hereby denominated *conduit-influenced flow regime (CIFR)*, and the set of parameter configurations corresponding to such baseflow conditions is referred to as *conduit-influenced baseflow domain.* This case is further investigated in Section 5.5.

The effect of changing conduit frequencies on recession coefficient follows similar principles as the alteration of conduit conductivity. However, the alteration of conduit frequency involves not only the change of the total length of high-conductivity features, but also the alteration of the low-permeability block size. That's why although low frequency domains can be characterized by **Equation (5-10)**, any change of conduit frequency influences the value of recession coefficients (**Fig. 5-7**). A threshold value of conduit frequency exists for any hydraulic parameter configuration, and above this threshold, the change of conduit frequency entails the change of the recession coefficient according to an unknown function to be developed in Section 5.5.

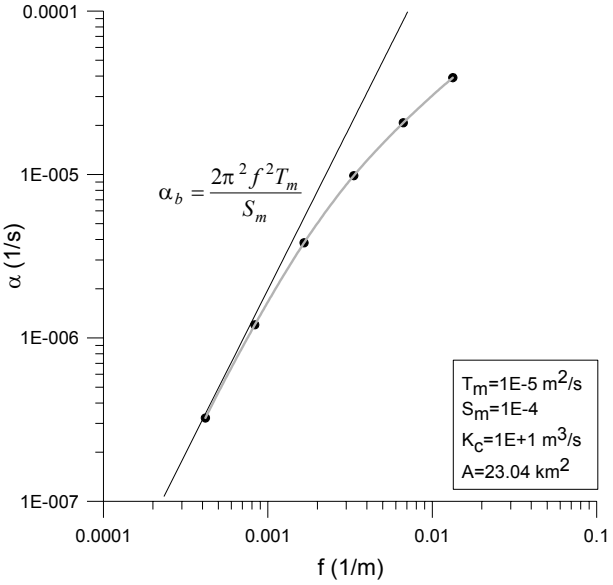

Figure 5-7. Dependence of the recession coefficient on conduit frequency.

5.5. CHARACTERIZATION OF THE RECESSION OF HETEROGENEOUS DOMAINS

Finding the link between heterogeneous domain recession coefficient and aquifer hydraulic and geometric parameters is the principal goal of this chapter. Based on the consequences of Section 5.4, heterogeneous aquifers having sufficiently high contrast between the conductive capacity of the conduits and the conductive capacity of low permeability blocks (matrix-restrained baseflow domain), can be characterized by **Equation (5-10)**. The principals of the recession process in aquifers where the system heterogeneity is insufficiently high (conduit-influenced baseflow domain) were investigated by assuming that aquifers global response can be approximated by the application of the equivalent porous medium concept, with further restrictions. The domains of validity of equivalent formulae were then tested and the formulae were corrected based on the results of a series of sensitivity analyses.

5.5.1. EQUIVALENT POROUS MEDIUM APPROACH FOR EVALUATING RECESSION COEFFICIENT IN THE CONDUIT-INFLUENCED BASEFLOW DOMAIN

By arranging porous media hydraulic parameters in a manner that an elementary volume of the aquifer transmits the same specific yield and releases the same amount of water from storage as that of a heterogeneous domain, a theoretically equivalent porous medium can be constructed (**Fig. 5-8**).

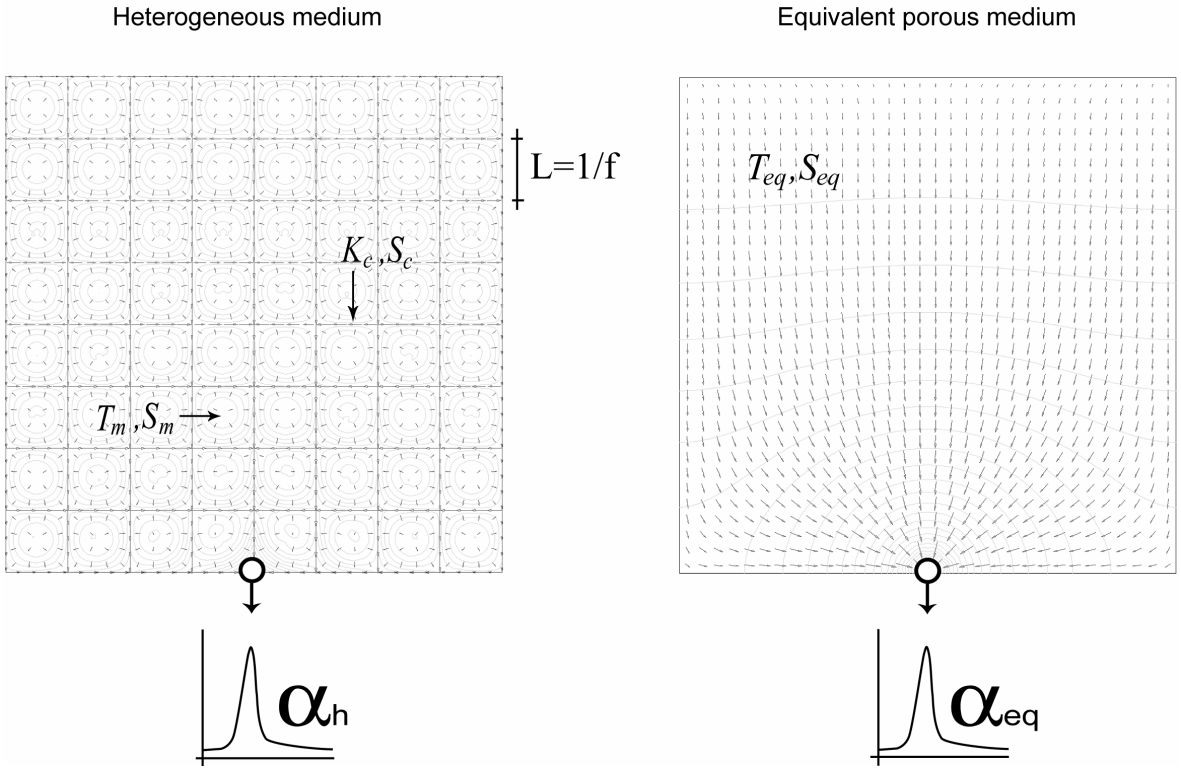

Figure 5-8. Graphical representation of heterogeneous and porous equivalent media. The recession coefficients of these domains are supposed to be a function of the same equivalent aquifer parameters.

Although the characterization of diffusive flux from a homogeneous domain having point-like head boundary condition is far simpler than that of a strongly heterogeneous domain, the lack of analytical formulae describing this phenomenon necessitated the development of an empirical formula.

5.5.1.1. DIFFUSIVE FLUX FROM A HOMOGENEOUS SQUARE DOMAIN

The empirical formula describing diffusive flux from a homogeneous domain having point-like head boundary condition (**Fig. 5-9**) was developed by constructing a variety of synthetic homogeneous models, altering hydraulic parameters, and subsequently deducing the equation governing the flux by fitting each parameter.

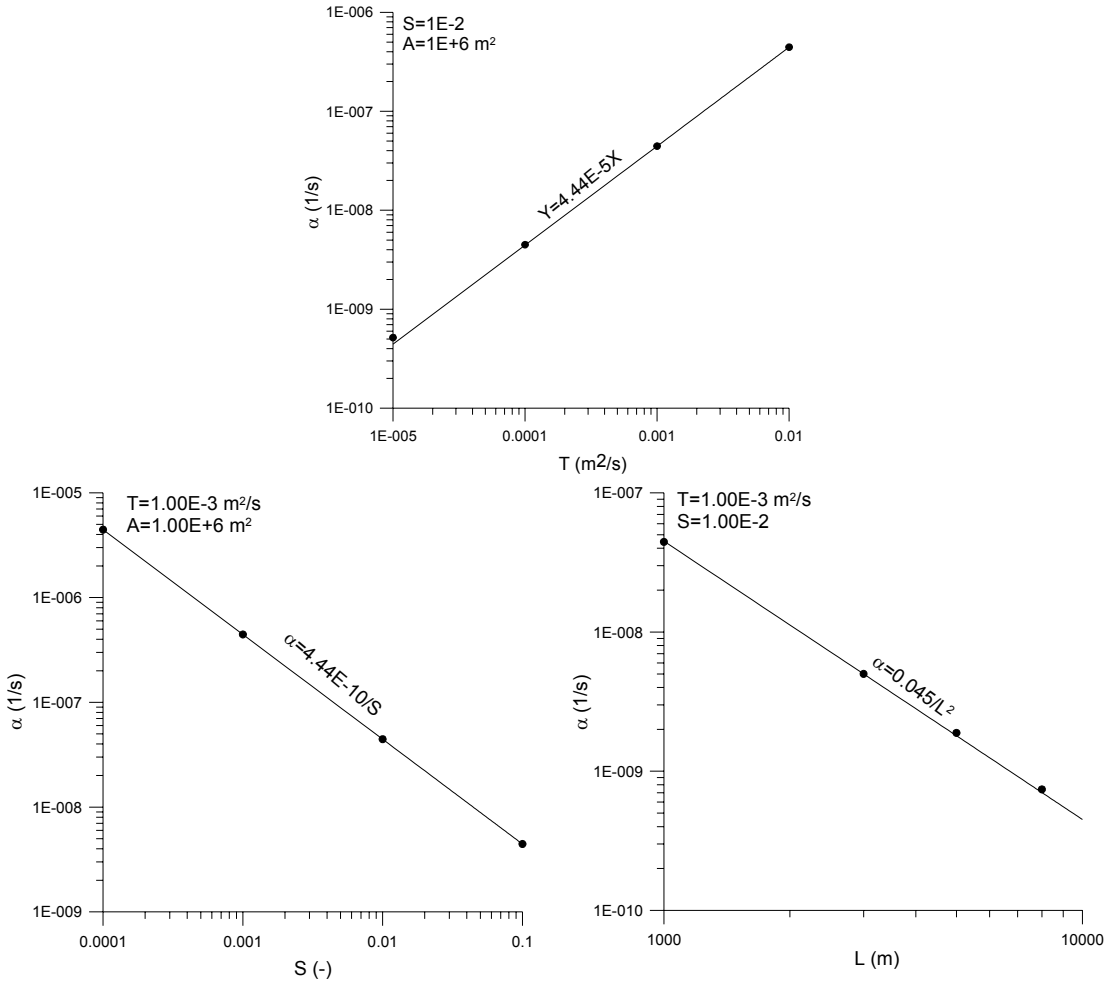

Figure 5-9. Dependence of recession coefficient on homogeneous domain parameters. Recession coefficient shows a direct proportionality to transmissivity, and inverse proportionality to storativity and domain size.

According to the simulation results presented in **Figure 5-9,** the formulation of diffusive flux from a homogeneous domain with a point-like head boundary is similar to the formulation of diffusive flux from a homogeneous block with encircling head boundary, with a different geometric factor (γ). The formulation of recession coefficient related to diffusive flux from a homogeneous block takes the following general form:

$$\alpha_{eq} = \frac{\gamma T_{eq}}{S_{eq} A} \tag{5-11}$$

where γ is the geometric factor [-] dependent on domain shape and boundary conditions, and A is the domain area [L^2].

For two-dimensional square domains having point-like head boundary condition, the geometric factor is $\gamma = 4/9$.

5.5.1.2. DIFFUSIVE FLUX FROM A HETEROGENEOUS DOMAIN

Supposing that the recession of a heterogeneous domain can be approached by the drainage of an equivalent porous domain of the same dimensions and same boundary conditions, the equivalent transmissivity parallel to karst conduits may be expressed as follows:

$$T_{eq} = K_c f + T_m \tag{5-12}$$

Similarly, as there are two intersecting conduits for each block, the equivalent storage can be expressed in the following form:

$$S_{eq} = S_m + 2S_c f \tag{5-13}$$

Substituting the equivalent parameters into the formulation of the recession coefficient (**Eq. 5-11**), the equivalent recession coefficient becomes

$$\alpha_h = \frac{\gamma}{A}\frac{(K_c f + T_m)}{(S_m + 2S_c f)} \tag{5-14}$$

where the transmissivity of the low permeability matrix is usually several order of magnitude lower than the equivalent conductivity of the conduit system. Similarly, in the case of phreatic karst systems, the equivalent storage of the conduits is much smaller than the storativity of the matrix. Consequently, the formula can be further simplified by neglecting these terms:

$$\alpha_h = \frac{\gamma}{A}\frac{(K_c f + T_m)}{(S_m + 2S_c f)} \approx \gamma\frac{(K_c f + T_m)}{S_m A} \approx \gamma\frac{K_c f}{S_m A} \tag{5-15}$$

Because of the introduction of heterogeneity into the model, the geometric parameter γ is expected to differ from the empirically obtained value for porous equivalent domains. Furthermore, the formulation of diffusive flux obtained from homogenous domains should be tested on a large variety of heterogeneous models. Consequently, several numerical model simulations was performed. The results of these analyses are presented in the following section.

5.5.2. EVALUATION OF THE GEOMETRIC PARAMETER IN THE CONDUIT-INFLUENCED BASEFLOW DOMAIN

In order to test the validity of **Equation 5-15**, a large variety of numerical tests was performed. The effect of systematic modification of each hydraulic and geometric parameter was investigated. The investigated parameter configurations are summarized in **Table 5-1**. The results of each numerical simulation are presented in Appendix 3.

Simulation results confirm the existence of two, significantly different flow domains, previously explained in Section 5.4, for the alteration of any parameters. While the matrix-restrained baseflow domain can be described by the analytical **Equation 5-10**, the conduit-influenced baseflow domain is approachable by the general formula provided in the previous section (**Eq. 5-15**). In order to test the validity of this formula, and to obtain the value of the geometric parameter γ, the simulation results falling into these two distinct baseflow domains were separated, and only the conduit-influenced baseflow domain was considered during the evaluation process. Among 78 flow simulations, 52 simulations were carried out in the conduit-influenced domain.

Model series	A (m^2)	T_m (m^2/s)	S_m (-)	K_c (m^3/s)	S_c (m)	1/f (m)
chgKc_1E+2	2.30E+07	1.00E-05	1.00E-04	1.00E+02	2.14E-07	75,150,300,600,1200,2400
chgKc_5E+1	2.30E+07	1.00E-05	1.00E-04	5.00E+01	1.70E-07	75,150,300,600,1200,2400
chgKc_1E+1	2.30E+07	1.00E-05	1.00E-04	1.00E+01	9.95E-08	75,150,300,600,1200,2400
chgKc_1E+0	2.30E+07	1.00E-05	1.00E-04	1.00E+00	4.62E-08	75,150,300,600,1200,2400
chgTm_1E-2	2.30E+07	1.00E-02	1.00E-02	1.00E+02	2.14E-07	75,150,300,600,1200,2400
chgTm_1E-3	2.30E+07	1.00E-03	1.00E-02	1.00E+02	2.14E-07	75,150,300,600,1200,2400
chgTm_1E-4	2.30E+07	1.00E-04	1.00E-02	1.00E+02	2.14E-07	75,150,300,600,1200,2400
chgSm_1E-1	2.30E+07	1.00E-05	1.00E-01	1.00E+02	2.14E-07	75,150,300,600
chgSm_1E-2	2.30E+07	1.00E-05	1.00E-02	1.00E+02	2.14E-07	75,150,300,600,1200
chgSm_1E-3	2.30E+07	1.00E-05	1.00E-03	1.00E+02	2.14E-07	75,150,300,600,1200,2400
chgSm_1E-4	2.30E+07	1.00E-03	1.00E-04	1.00E+02	2.14E-07	75,150,300,600,1200,2400
chgA_2400	2.40E+03	1.00E-04	1.00E-02	1.00E+02	2.14E-07	75,150,300,600,1200
chgA_9600	9.60E+03	1.00E-04	1.00E-02	1.00E+02	2.14E-07	150,300,600,1200,2400
chgA_19200	1.92E+04	1.00E-04	1.00E-02	1.00E+02	2.14E-07	300,600,1200,2400

Table 5-1. Parameter configurations of heterogeneous numerical models constructed to test analytical formulae.

Rearranging the **Equation 5-15** in a dimensionless manner yields:

$$\alpha_h A \frac{(S_m + 2S_c f)}{T_m} \approx \alpha_h A \frac{S_m}{T_m} = \gamma \left(\frac{K_c}{T_m} f + 1 \right) \approx \gamma \frac{K_c f}{T_m} \tag{5-16}$$

where the value of γ is represented by the slope of the line fitted to the simulation results (**Fig. 5-10**)

Curve fitting yields the value of γ=2/3. Although slight deviations in simulation results from the fitted curve occur, the final formula for the recession coefficient of the conduit-influenced baseflow domain can be expressed as follows:

$$\alpha_h = \frac{2}{3} \frac{(K_c f + T_m)}{A(S_m + 2S_c f)} \approx \frac{2}{3} \frac{(K_c f + T_m)}{S_m A} \approx \frac{2}{3} \frac{K_c f}{S_m A} \tag{5-17}$$

Equation (5-17) provides a quite good approximation of the recession coefficient (**Fig. 5-10**). The slight deviation in the simulation results from the fitted line is very probably due to differences in model discretization.

The plot of recession coefficients calculated using **Equation (5-17)** against the numerically obtained values is shown on **Figure 5-11.**

Equation (5-17) underestimates the value of the recession coefficient for several parameter configurations. Its average error is about 25 %, although the maximum error never exceeds 68 % even for the most unrealistic parameter configurations. As the difference between the two extremes of simulated recession coefficients is more than 5 orders of magnitude and the formula error is in the same range as the natural variation of the recession coefficient, **Equation (5-17)** gives a reasonable estimate of aquifer parameters.

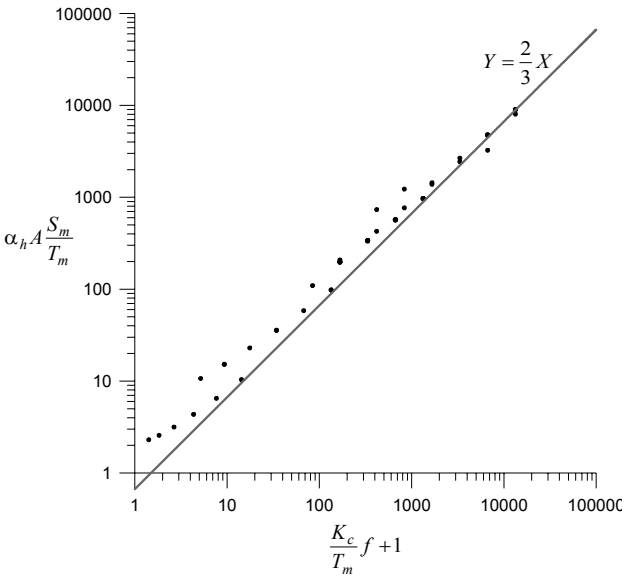

Figure 5-10. Evaluation of the strongly heterogeneous domain geometric parameter (γ) from numerical sensitivity analyses by the means of curve fitting.

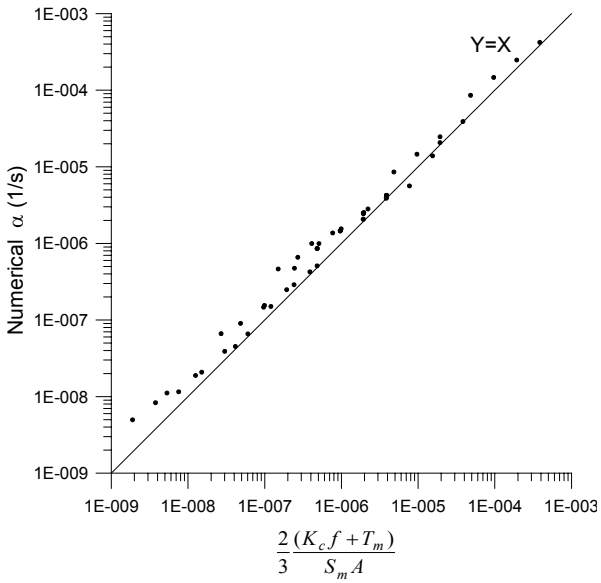

Figure 5-11. The plot of recession coefficients calculated using **Equation (6-17)** against the numerically obtained values.

5.6. GENERAL MATHEMATICAL CHARACTERIZATION OF THE RECESSION PROCESS

Previous sections have demonstrated that the alteration of aquifer hydraulic and geometric properties results in changing recession coefficients. The dependence of recession coefficient on aquifer properties follows two fundamentally different principles:

The MRFR flow regime is controlled by the hydraulic parameters of the low-permeability medium. This case can be mathematically characterized by the drainage of a homogeneous block (**Equation 5-10**).

The CIFR flow regime is mainly controlled by the conductive capacity of the drainage system. This case can be mathematically characterized by **Equation (5-17).**

The two principal baseflow domains are linked by a transition zone in which recession coefficient follows neither of the corresponding functions, but a mathematically unspecified intermediate function.

The existence of these two distinct flow domains is the manifestation of the "duality of groundwater flow field" defined by Király (1994) as the direct consequence of the heterogeneity of the hydraulic conductivity field.

The "heterogeneity" of a karst system changes not only with the alteration of the contrasts in hydraulic conductivity, but also with the alteration of the frequency of high-conductivity features. Consequently, a transition between the two principal baseflow domains exists for the alteration of both of these parameters.

The threshold separating the two principal flow domains can be mathematically expressed by equating the matrix-restrained (**Equation 5-10**) and the conduit-influenced (**Equation 5-17**) recession coefficients. This can be expressed as follows:

$$\alpha_b = \alpha_h \tag{5-18}$$

thus

$$\frac{2\pi^2 T_m f^2}{S_m} = \frac{2}{3}\frac{(K_c f + T_m)}{A(S_m + 2S_c f)} \approx \frac{2}{3}\frac{(K_c f + T_m)}{S_m A} \approx \frac{2}{3}\frac{K_c f}{S_m A} \tag{5-19}$$

where the threshold value of conduit conductivity (K_c^*) neglecting the storage in karst conduits can be expressed as follows :

$$K_c^* = 3\pi^2 T_m A f - \frac{T_m}{f} \approx 3\pi^2 T_m A f \tag{5-20}$$

For smaller values of K_c the flux is mainly restrained by the conductive capacity of the high-permeability conduit network, while for higher values of K_c, flux is restrained by the diffusivity of the low-permeability matrix. The graphical representation of recession coefficients dependence on conduit conductivity is demonstrated in **Figure 5-12.**

Similarly to the conductivity domain, a threshold value dividing the two principal flow domains can be defined in the frequency domain. This can be expressed as follows:

$$f^* = \frac{K_c + \sqrt{K_c^2 + 12\pi^2 A T_m^2}}{6\pi^2 T_m A} \approx \frac{K_c}{3\pi^2 T_m A} \tag{5-21}$$

where f^* is the threshold frequency dividing matrix-restrained and conduit-influenced baseflow domains. For smaller values of *f,* the recession is constrained by the diffusivity of the low-permeability matrix, while for higher values of *f*, recession is mainly constrained by the conductive capacity of the high-permeability conduit network. The graphical representation of recession coefficients dependence on conduit frequency is demonstrated in **Figure 5-13.**

The value of the recession coefficient corresponding to the threshold point and its physical meaning is discussed in the following section.

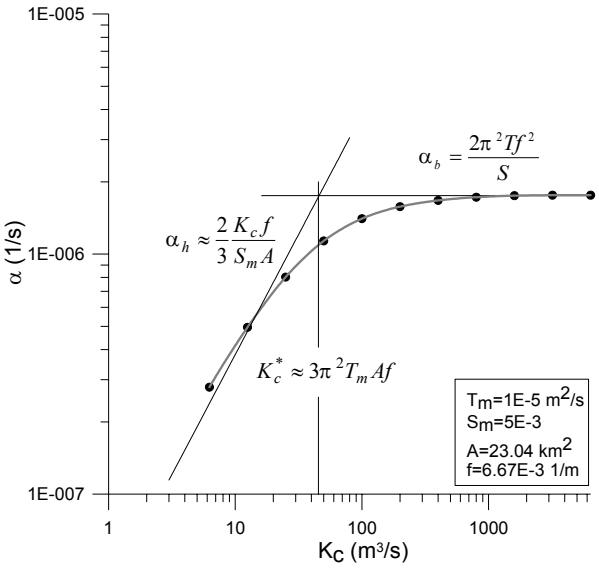

Figure 5-12. Graphical representation of the recession coefficients dependence on conduit conductivity. The simulated values of recession coefficient (dots), are approached by the functions α_b and α_h. The threshold value (K_c^*) dividing these flow domains was obtained by equating the **Equations (5-10)** and **(5-17)**.

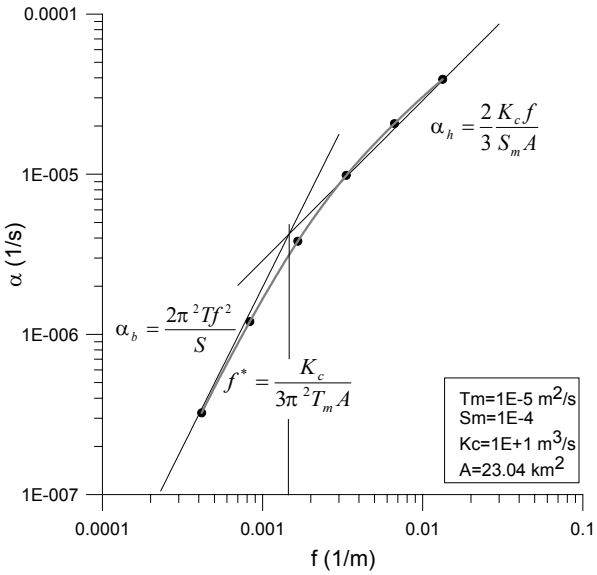

Figure 5-13 . Graphical representation of the recession coefficients dependence on conduit frequency. The simulated values of recession coefficient (dots), are approached by the functions α_b and α_h. The threshold value (f^*) dividing these flow domains was obtained by equating the **Equations (5-10)** and **(5-17)**.

The evaluation of threshold parameters facilitates the quantitative classification of karst systems: While MRFR flow regime is a characteristic of *mature karst systems* under baseflow conditions, *premature karst systems* exhibit CIFR baseflow.

5.7. VALIDITY OF EQUIVALENT MODELS

The validity and applicability of equivalent models is a crucial question in modeling fissured and karst systems. Not only because the estimation of the conduit hydraulic and geometric parameters is difficult, but also because the appropriate modeling code may not be available. Equivalent porous medium models are often used without adequate test of their applicability, and the application of equivalent discrete-continuum models may be a consequence of the false estimation of conduit frequency. The fundamental difference between equivalent porous medium and equivalent discrete-continuum models is demonstrated in **Figure 5-14**.

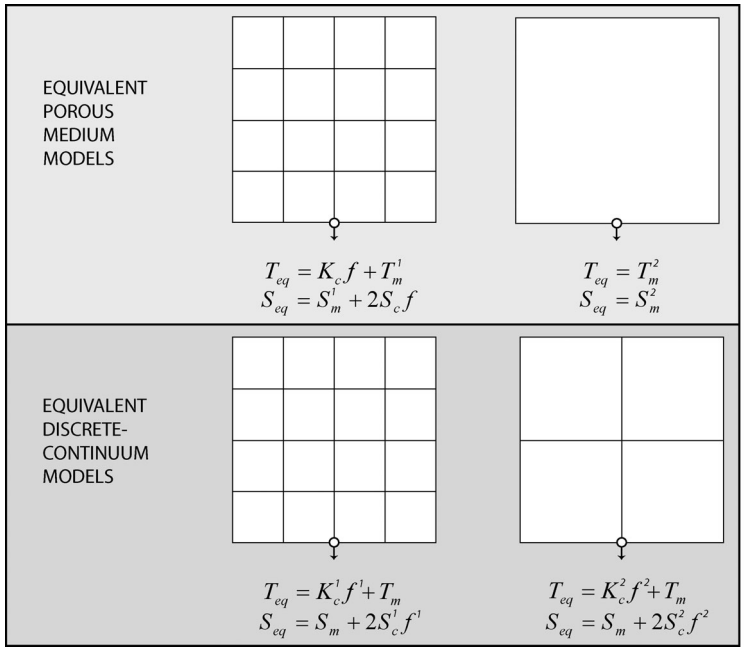

Figure 5-14. Evaluation of equivalent parameters for equivalent porous medium and equivalent discrete-continuum models.

As it was explained in the previous sections, the principles governing flux from heterogeneous systems are far more complicated than those of which govern flux from homogeneous systems. While the recession of homogeneous systems always follows the same principles, the evaluation of the global response of heterogeneous systems requires the discussion of flow parameters and the selection of the appropriate equation. Furthermore, the dominant flow regime of mature karst systems may change with time during the recession process.

In order to demonstrate the variations of the recession coefficient for domains having the same equivalent hydraulic parameters but different conduit geometries and conduit conductivities, a series of numerical tests was performed on equivalent discrete-continuum models. The results of these simulations are shown in **Figure 5-15**.

These numerical tests demonstrated that in the matrix-restrained baseflow domain the equivalent discrete-continuum models yield systematically different recession coefficients, as they follow **Equation (5-10)**, which is dependent exclusively on block size and matrix hydraulic properties. In this baseflow domain none of the equivalent models has validity. In the conduit-influenced baseflow domain, all of the equivalent discrete-continuum models yield the same result. Between these fundamentally different baseflow domains a transition zone exists. In the centre of this zone, the threshold parameters designate an inflection point, which coincides with the recession coefficient of the equivalent porous medium model. That means that heterogeneous systems having hydraulic and geometric parameters corresponding to the threshold values behave like equivalent porous medium. This is the only point of validity of the equivalent porous medium approach when simulating the recession process of karst systems.

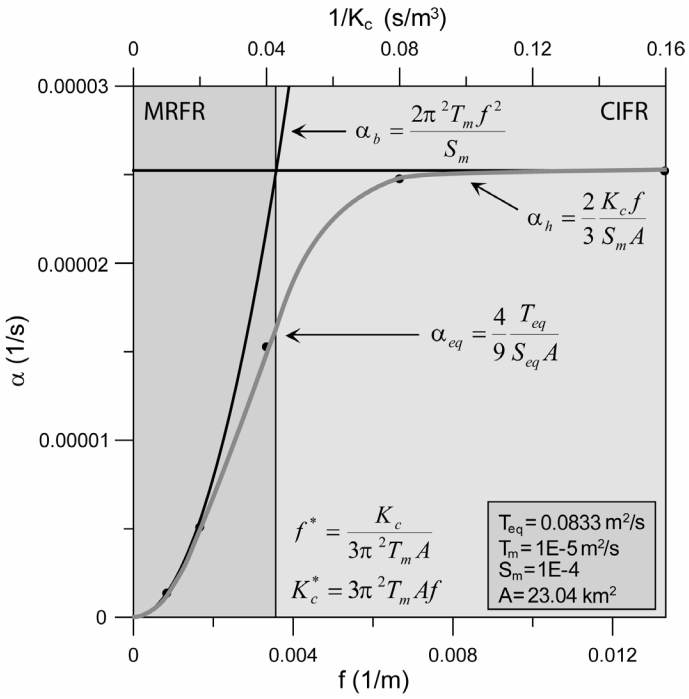

Figure 5-15. Variation of the recession coefficients for equivalent discrete-continuum domains. Each model (results represented by black dots) has the same equivalent hydraulic parameters, but different conduit conductivities and frequencies. The recession coefficient of the porous equivalent medium model is identical to the recession coefficient of the threshold parameter discrete-continuum model, and designates an inflection point of the curve.

5.8. A FAST GRAPHICAL METHOD FOR THE ESTIMATION OF AQUIFER PARAMETERS

The principles governing recession process have been mathematically defined in previous sections. In order to facilitate a fast estimation of desired parameters, a graphical representation of parameter dependences is provided in **Figure 5-16**.

Parameter dependences represented in this figure involve the negligence of storage related to the drainage of vertical shafts and variably saturated conduits. Furthermore, the equations represented in this figure were derived from two-dimensional models, and their correct application requires the transformation of measured field parameters into two-dimensional model parameters. For example, the conduit conductivity of multi-level karst systems must be multiplied by the number of active conduit horizons. Similarly, two-dimensional transmissive and capacitive parameters of the low-permeability matrix must be specified respecting the average thickness of the saturated zone.

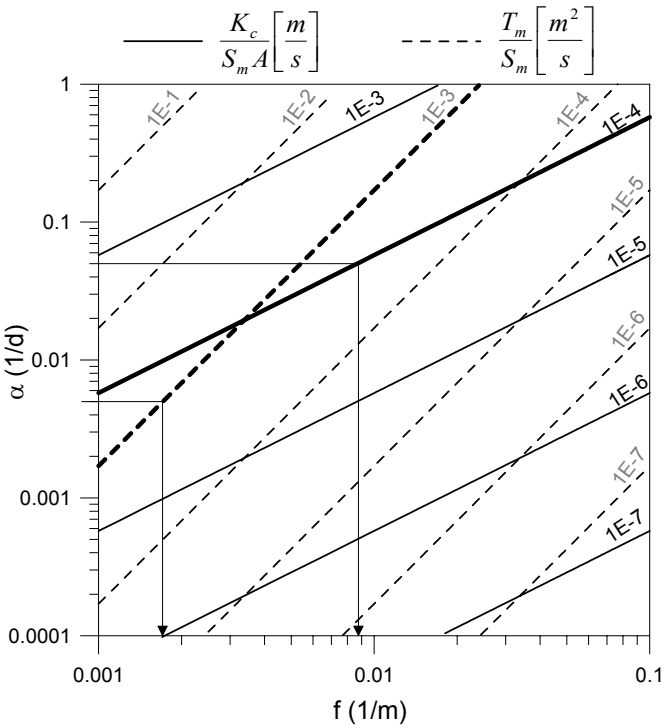

Figure 5-16. Graphical representation of the relationship between aquifer hydraulic and geometric parameters and baseflow recession coefficient. Subsequently to the identification of the two intersecting lines corresponding to field measurements, the lowermost line must be selected for the evaluation of the desired parameter. For example the parameter set of K_c=100 m^3/s , T_m=1E-5 m^2/s , S_m=1E-2 and A=1E+8 m^2, and the measured value of α=0.005 1/day yields f= 1.7E-3 1/m, while α=0.05 1/day yields f= 8,7E-3 1/m.

5.9. CONCLUSIONS

The global hydraulic behavior of heterogeneous systems such as karst aquifers is strongly dependent on aquifer hydraulic and geometric parameters.

Spring hydrograph recession coefficient is a characteristic global parameter of an aquifer, and supplies important information concerning the system's hydraulic and geometric parameters. As these parameters are rarely measurable, discharge time series represent a very important means of determining of information about the overall structure of a karst system.

The recession of strongly heterogeneous systems follows two, significantly different principles depending on the overall configuration of the hydraulic and geometric parameters.

The most important geometric parameters that control the recession process are the exposed area of an aquifer and conduit spacing. Aquifer shape plays an insignificant role.

The baseflow recession of mature karst systems is controlled by the hydraulic parameters of the low-permeability matrix, and by the conduit spacing. This flow condition is referred to as matrix-restrained flow regime (MRFR). The baseflow recession of premature karst systems is influenced by the hydraulic parameters of both conduits and low-permeability blocks, by the conduit spacing, and by the aquifer surface. This flow condition has been defined as conduit-influenced flow regime (CIFR). Between these two extremes a transitional domain exists which is mathematically difficult to characterize. However, the centre of the transition zone represents a threshold between matrix-restrained and conduit-influenced domains, and corresponds to the recession of an equivalent porous medium.

The diffusive flux from an aquifer can be described by a general exponential model, with the following recession coefficient:

$$\alpha = \frac{\gamma T}{SA}$$

where γ is a geometric factor that depends mainly on the boundary conditions, and also on aquifer shape. For square blocks surrounded by constant head boundary conditions $\gamma=2\pi^2$, for square blocks with punctual head boundary condition γ=4/9. Recession coefficients of heterogeneous aquifers in the conduit-influenced baseflow domain can be calculated by substituting equivalent hydraulic parameters, and by evaluating the appropriate geometric factor. For square shape heterogeneous domains with punctual head boundary γ=2/3.

The validity of equivalent models is strongly restricted. While equivalent discrete-continuum models may lead to adequate baseflow recession coefficients in the conduit-influenced baseflow domain, there is only one parameter configuration that yields appropriate recession coefficient in the matrix-restrained baseflow domain. Consequently, the applicability of equivalent discrete-continuum models is precluded in the case of mature karst systems. The global response of equivalent porous medium models corresponds to the transition between matrix-restrained and conduit-influenced flow regimes. Consequently, the equivalent porous medium approach cannot be directly applied for modeling karst aquifers.

6. TRANSIENT GROUNDWATER FLOW SIMULATIONS OF THE MILANDRINE AMONT CATCHMENT BY REGULAR CONDUIT NETWORK MODELS

ABSTRACT

Combined discrete-continuum type groundwater flow simulations of the Milandrine amont karstic catchment been performed by applying a regular conduit network to demonstrate the application of analytical formulae for estimating geometric and hydraulic aquifer parameters. Flow simulations demonstrated a significant difference in hydraulic behavior between mature and premature karst systems. Simulations reproducing "typical" karstic hydraulic behavior require matrix-restrained conditions during baseflow periods, designating mature systems. These phenomena could not be confidently detected in premature systems. Although the recession coefficient of mature systems depends exclusively on low-permeability matrix hydraulic parameters and conduit frequency, simulated flood peaks for such systems show a strong dependence on conduit hydraulic conductivity and the proportion of concentrated recharge. It is presumed that a transition between matrix-restrained and conduit-influenced flow regimes occurs during flood events, and the conduit conductivity can be estimated from measured discharge and hydraulic gradient during high water periods. Integrated epikarst and saturated zone model simulations demonstrated that the subcutaneous layer can modify the global hydraulic response of the entire system, by decreasing its recession coefficient. Parameter estimation of these systems using analytical formulae requires the separate observation of the global hydraulic response of the epikarst, or a reasonable estimate of the recession coefficient of the epikarst from its hydraulic and geometric parameters by analytical formulae.

Keywords: Groundwater flow modeling, Karst aquifers, Conduit network, Hydraulic parameters, Spring hydrograph, Analytical formulae, Milandrine amont

6.1. INTRODUCTION

The Milandrine Amont is the largest catchment in the Milandrine cave system, canton Jura, NW-Switzerland. Its zone of contribution has been delineated by tracing experiments. High resolution time-series of underground discharge measurements makes this site suitable for performing transient flow simulations. The purpose of the modeling experiments performed on the Milandrine amont catchment was to provide an example for the application of the analytical formulae expressing the nexus between aquifer characteristics and global response (Chapter 5). These analytical formulae were based on simplified conceptual models that involve darcian flow conditions in the conduit network, and do not take into account the temporary water storage in either the epikarst zone or in karst conduits. Consequently, model simulations are believed to be very approximate, and do not precisely reproduce either measured hydrographs, or observed piezometric levels. The aim of these models was rather to demonstrate the dramatic difference between matrix restrained and conduit influenced model configurations, to demonstrate the consequences of certain parameter configurations, and to propose a methodology for the rapid estimation of effective model parameters. As the epikarst zone is assumed to influence the global hydraulic response of the entire karst system, it has been integrated into the model in order to demonstrate the effect of the infiltration process on simulation results.

6.2. AQUIFER HYDRAULIC PARAMETERS

The total aerial extent of the Milandrine amont catchment delineated by tracing experiments (Grasso & Jeannin, 1994b; Favre, 2001) is 4.65 km^2 **(Fig. 3-9)**. Aquifer thickness varies between 60 and 200 m, with an average value of 100 m (**Fig. 3-8**). The average saturated zone thickness is 30 – 50 m. In the eastern part of the catchment, shallow karst conditions occur, while in the southern region the saturated zone thickness exceeds 100 m (**Fig. 3-11**).

The hydraulic conductivities determined from borehole tests vary between 1E-8 and 5E-4 m/s, but usually are in the range of 1E-7 – 1E-6 m/s (Jeannin, 1995; Flury & Allemann, 1991). The effective porosity of the low permeability matrix has been estimated by Jeannin & Grasso (1995a) to be in the range of 0.7 – 1 %. This value has been directly used as storativity parameter in two-dimensional models.

The one-dimensional laminar hydraulic conductivity of the karst channels can be estimated from the discharge and the average hydraulic gradient in the conduit network as follows:

$$K_c \approx \frac{Q}{I} \tag{6-1}$$

where K_c is the one-dimensional, laminar conductivity of karst channels [L^3T^{-1}] (see: Chapter 2), Q is spring discharge [L^3T^{-1}], and I is hydraulic gradient [-].The approximate difference in hydraulic heads between the spring and the distal part of the conduit network is 100 m over the distance of 5000 m. The average approximate 1D laminar hydraulic conductivity of the main karst channel throughout the explored part of the cave system estimated in this manner is K_c=5 m^3/s under baseflow conditions, and K_c=100 m^3/s under flood conditions.

However, this estimation is very approximate, as the hydraulic gradient in the conduits is influenced by the topography of the riverbed, and head-loss takes place at several underground cascades. Consequently, the hydraulic gradient provided is too high.

Furthermore, turbulent flow conditions may exist, and thus conduit conductivities calculated in this manner do not reflect real conduit properties, but they are equivalent parameters to be used in laminar flow models.

6.3. ASSESSMENT OF DOMINANT FLOW DOMAIN

As explained in Chapter 5, karst aquifers behave in two distinct ways during the recession process. The global hydraulic response of a karst aquifer depends on the geometric configuration of the conduit system, and the hydraulic parameter distribution. The threshold value of conduit conductivity (K_c^*) separating these two principal flow domains can be evaluated using **Equation (5-20)** as follows:

$$K_c^* \approx 3\pi^2 T_m A f \tag{6-2}$$

where T_m is the transmissivity of the low-permeability matrix [L^2T^{-1}], A is aquifer area [L^2], f is the frequency of conduits [L^{-1}]. Conduit conductivities (K_c) lower than the threshold value (K_c^*) reflect the influence of the conduit conductivity on the recession process (CIFR flow regime), while higher values provide an indication of matrix-restrained baseflow conditions. However, the transition between matrix-restrained and conduit influenced baseflow domains is relatively smooth, and the transition zone is not quantitatively characterized. Considering the hydraulic parameters provided above, the average transmissivity of the low-permeability matrix is in the range of $T_m = Kb \approx$ 5E-6 – 5E-5 m^2/s where the average saturated zone thickness (b) is approximately 50 m. The catchment area is A = 4.65E+6 m^2, and assuming an average distance of 200 m between karst channels based on cave maps and fault geometry, the threshold value of conduit conductivity varies between $3 < K_c^* < 30$ m^3/s.

Based on the available conduit conductivity data it is very difficult to classify the Milandrine system either into a conduit-influenced or into a matrix-restrained baseflow domain. In fact, the real parameter configuration can fall in the transition zone as well. In order to estimate the real parameter configuration, flow simulations have been performed in both the conduit-influenced and the matrix-restrained baseflow domains.

6.4. DISTRIBUTIVE MODEL CHARACTERISTICS

Flow simulations have been performed using the FEFLOW 5.0 groundwater modeling code (WASY Ltd., 2002). This simulation system facilitates the implementation of one-dimensional finite elements into two- or three-dimensional element network, thus permitting the simulation of groundwater flow in karst aquifers using the combined discrete-continuum approach.

Applied distributive model geometry comprises a regular conduit network with 200 m conduit spacing (**Fig. 6-1**). These high-conductivity features are represented by one-dimensional finite elements embedded in the network of two-dimensional finite elements that represent low permeability matrix. Darcian flow was considered to be operative both in the matrix and in the conduit network.

No-flow Neumann type boundary conditions were applied along the model boundary, except the outlet of the Milandrine amont catchment, where fix-head Dirichlet type boundary condition was imposed.

Uniform hydraulic parameters were applied throughout the low-permeability matrix and also in the conduit network. The hydraulic response of the model domain during a two weeks infiltration period (11.02.1996 – 23.02.1996) was simulated. The resulting discharge time series plotted for the model outlet was compared to measured spring hydrographs. Because of the negligible evapotranspiration during the winter months at the research site (Jeannin & Grasso 1995b), 100 % of the precipitation (1000 mm/y for steady-state models) was applied as effective recharge over the model. Precipitation data originates from the Fahy meteorological station (located in 5 km distance from the model area, **Fig. 3-2**), and it was extrapolated to the entire model domain as a uniform infiltration function. 50 % of the total precipitation was distributed over the low-permeability matrix, while the remaining portion was injected directly into the conduit network (Jeannin & Grasso 1995b).

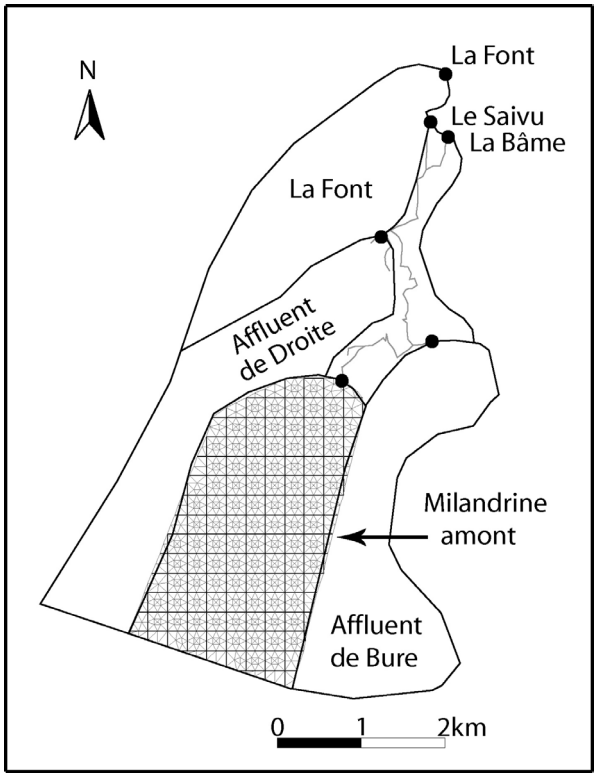

Figure 6-1. Model configuration and finite element mesh geometry. Gray elements represent the low-permeability fissured matrix; conduit network is represented by a regular network of one-dimensional finite elements (black).

The storage coefficient of the conduits is usually a calibration parameter, and integrates the storage within the epikarst, in vertical shafts hydraulically connected to the conduit system, as well as in deep phreatic conduits (if present). In the case of the Milandrine amont system, no deep-phreatic conduits were observed, and the epikarst subsystem was integrated into certain model versions. However, some conduit-related storage is suspected to take place, but is assumed to be negligible compared to the matrix storage. Consequently, only water compression-related storage is considered in the conduit network of the following models.

6.5. SIMULATIONS IN THE CONDUIT-INFLUENCED BASEFLOW DOMAIN

From the measured value of the recession coefficient (α=0.0028 1/d) (Grasso & Jeannin 1994) and the hydraulic parameters provided above (S_m=0.01, f=0.005 1/m, A=4.65E+6 m^2) (**Table 6-1**), using the analytical **Equation (5-17),** the conduit conductivity K_c can be estimated as follows:

$$K_c \approx \frac{3}{2}\frac{\alpha S_m A}{f} \tag{6-3}$$

This equation yields K_c=0.45 m^3/s. In order to fulfill the domain constraints defined by **Equation 5-10**, the hydraulic transmissivity of the low-permeability matrix (T_m) must exceed 6.5E-7 m^2/s for the above parameter configuration. The average measured value of T_m is 1E-5 m^2/s, which is safely within the conduit-influenced domain, and this value has been applied in the following numerical model (Model CIFR).

MODEL	T_m (m^2/s)	S_m (-)	K_c (m^3/s)	A (m^2)	f (1/m)	α (1/d)
reference	5E-6 - 5E-5	0.007 - 0.01	5 - 100	4.65E+6	0.005	0.0028
CIFR	1E-5	0.01	0.45	4.65E+6	0.005	0.0031
MRFR_1	6.5E-7	0.01	5	4.65E+6	0.005	0.0035
MRFR_2	6.5E-7	0.01	50	4.65E+6	0.005	0.0035
MRFR_3	6.5E-7	0.01	200	4.65E+6	0.005	0.0035
EPIK	6.5E-7	0.01	200	4.65E+6	0.005	0.0012
MRFR_4	2.0E-6	0.01	200	4.65E+6	0.005	0.0085

Table 6-1. Observed aquifer hydraulic parameters (reference) and model simulation results.

Figure 6-2 shows the simulated steady-state hydraulic head distribution of the conduit-influenced model. A comparison of the simulated discharge time series and the measured hydrograph is demonstrated in **Figure 6-3**. Although the conduit-influenced model configuration yields very reasonable hydraulic head distribution and a recession coefficient almost identical (α_{sim}=0.0031 1/d) to the measured value, it completely fails to simulate excessive discharge rates during flood events even if applying 100 % concentrated recharge to the conduits. Simulated hydrograph peaks are one order of magnitude smaller than those measured. This is because the conduit-influenced baseflow domains karst conduits cannot even transmit as much water as the low-permeability blocks can release. Consequently, additional waters originating from concentrated recharge can not either be instantaneously drained by the conduit network.

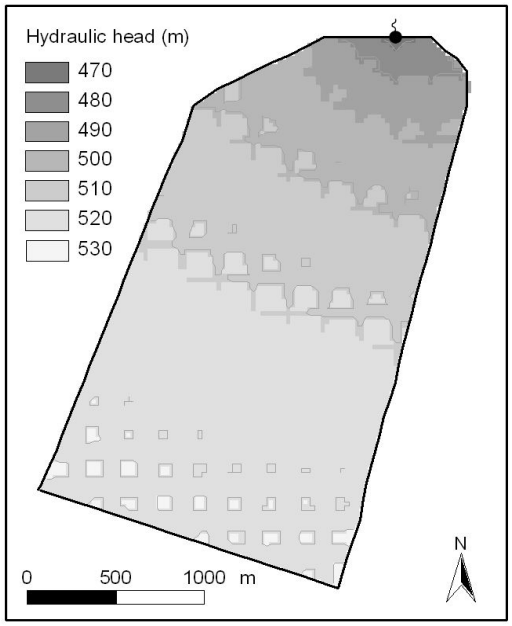

Figure 6-2. Hydraulic head distribution simulated by the steady-state conduit-influenced model (Model CIFR).

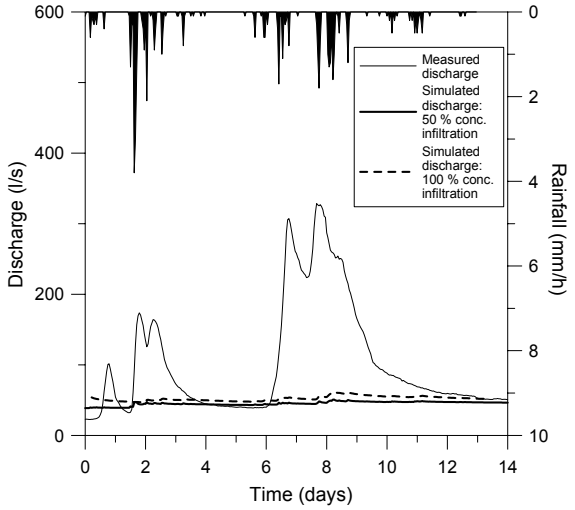

Figure 6-3. Comparison of measured hydrograph with simulated discharge time series in the conduit influenced flow domain (Model CIFR), generated applying 50 % and 100 % concentrated infiltration.

These phenomena demonstrate that the Milandrine amont is not a premature system with conduit-influenced baseflow recession. Furthermore, any karst systems with typically "karstic" global response [a typical karstic global response hydrograph has an instantaneous increase of recharge by often more than one order of magnitude during flood events, and fast peak descent] can be presumably characterized by matrix-restrained baseflow recession. Reasonable simulations of the Milandrine amont catchment can be also most likely expected in the matrix-restrained baseflow domain. The lower value of conduit conductivity (K_c=0.45 m^3/s) calculated by **Equation (6-3)** than both the approximate domain threshold value ($3<K_c^*<30$ m^3/s) obtained from **Equation (6-2),** and field observations ($K_c \geq 5$ m^3/s) support this assumption. The matrix-restrained domain hypothesis is tested in the following section.

6.6. SIMULATIONS IN THE MATRIX-RESTRAINED BASEFLOW DOMAIN

From the measured hydraulic parameters (S_m=0.01, f=0.005 1/m) the value of the matrix transmissivity (T_m) corresponding to the measured recession coefficient (α=0.0028 1/d) can be expressed using the analytical **Equation (5-10)** describing the matrix-restrained baseflow domain as follows:

$$T_m = \frac{\alpha S_m}{2\pi^2 f^2} \tag{6-4}$$

According to this calculation, the matrix-restrained hydraulic transmissivity evaluated using the above data is calculated as T_m=6.5E-7 m^2/s. This value is one order of magnitude lower than that approximately calculated from pumping tests. In order to fulfill the domain constraints defined by **Equation 5-20**, the conduit conductivity must exceed K_c=0.45 m^3/s. Several simulations have been performed applying different conduit conductivities higher than this threshold value (models MRFR_1-3). 50 % of total infiltration (Jeannin & Grasso 1995b) was applied as concentrated infiltration in conduits. The steady-state hydraulic head

distribution simulated in the matrix restrained baseflow domain is indicated in **Figure 6-4**. This figure clearly shows that the hydraulic gradient in the conduit network under MRFR conditions is very low, and that conduits act as head boundary conditions around the low-permeability blocks. However, the general shape of simulated water table does not agree with observations (**Fig. 3-10**). This is because shallow karst conduits of the Milandrine system are perched on the Oxfordian Marls surface, and thus impose different boundary conditions from those applied in the model. Furthermore, uniform hydraulic transmissivity has been applied for a medium with varying saturated zone thickness. However, the model reflects fundamental characteristics of the flow field. At the same time, the simulated hydraulic gradient between blocks and neighboring conduits is considerably high (up to 0.5), and the hydraulic head difference between these latter features reaches up to 40-60 m. According to the observations of Jeannin (1995a), the hydraulic head differences between conduits and the low-permeability blocks lie in the range of 30-40 m. However, this author also reports hydraulic gradients as high as 5-6 [-] in the vicinity of karst channels. Model simulations slightly overestimate the hydraulic head differences between blocks and conduits; this can be a result of the underestimation of matrix transmissivity, but also a result of numerical effects related to finite element discretization.

All of the matrix-restrained parameter configurations yield the same recession coefficient (α=0.0035 1/d) that closely approaches the analytical value. However, as demonstrated in **Figures 6-5, 6-6 & 6-7**, the simulated hydrographs of these models are very different. The increase of the conduit conductivity results in successively higher flood peaks, while the fast recession limbs of discharge peaks get steeper. The increase of the proportion of concentrated recharge results the same changes. This clearly indicates that although the baseflow recession of mature karst systems is independent on the conduit hydraulic conductivity, the hydraulic behavior of the same systems during flood events strongly depends on the conduit hydraulic parameters. This observation suggests that a transition of flow regimes takes place, and matrix-restrained baseflow domains perform CIFR flow regime during high water periods.

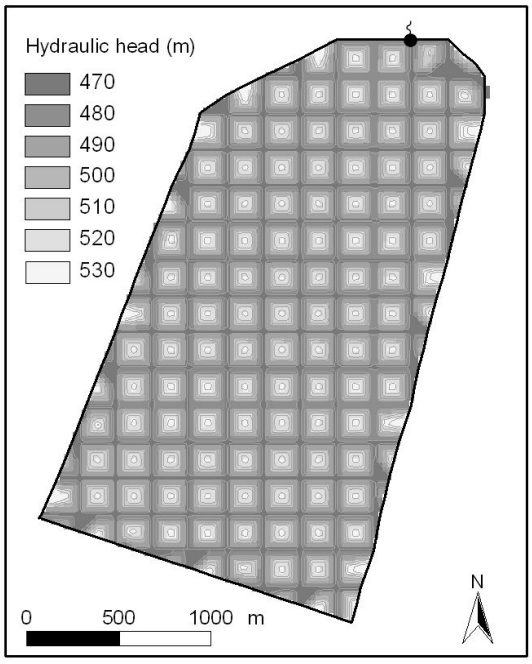

Figure 6-4. Steady-state simulated hydraulic head distribution in the matrix-restrained domain (Models MRFR_1-3).

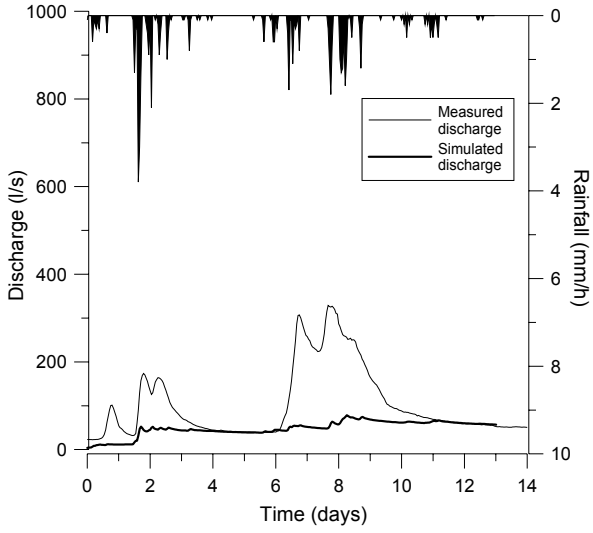

Figure 6-5. Measured and simulated hydrographs in the matrix-restrained baseflow domain (Model MRFR_1).

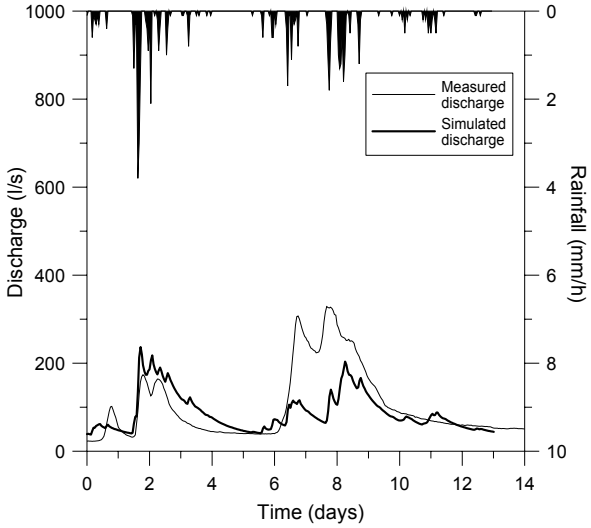

Figure 6-6. Measured and simulated hydrographs in the matrix-restrained baseflow domain (Model MRFR_2).

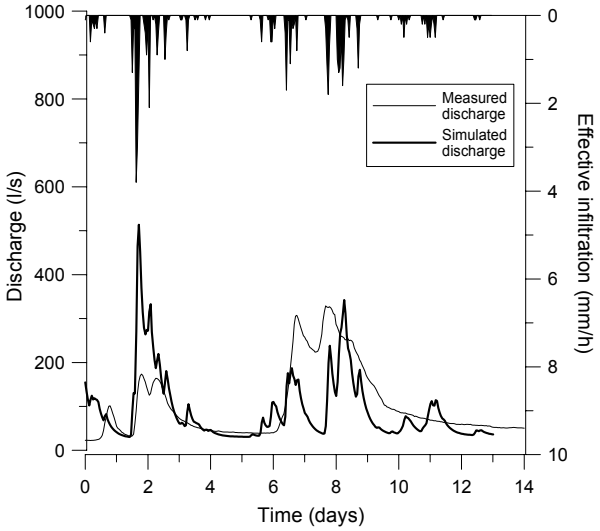

Figure 6-7. Measured and simulated hydrographs in the matrix-restrained baseflow domain (Model MRFR_3).

Although the simulated discharge curve of model MRFR_3 shows a more nervous behavior than the observed spring hydrograph, this model provides the most reasonable simulated hydraulic response. The difference between the relative amplitudes of the two principal discharge peaks is probably the result of the inappropriate extrapolation of the precipitation data measured at a meteorological station located outside of the model area. Alternatively, it may reflect other infiltration-related processes such as snow-melting.

Above simulations demonstrated that while the baseflow recession process of mature karst systems is independent on conduit hydraulic conductivity, the amplitude of discharge peaks and the fast recession process are strongly influenced by the hydraulic parameters of the conduit network. The effective conduit conductivity of mature karst systems can be estimated from hydraulic gradients and spring discharges measured during flood events (see: Chapter 7.3). The similarity between the estimated value of equivalent laminar conduit conductivity presented in Section 6.2. and the conduit conductivity of the best-fitting matrix-restrained model version supports this hypothesis.

6.7. THE EPIKARST MODEL

As demonstrated in **Figures 6-5, 6-6 & 6-7**, the global hydraulic response of the saturated zone models shows a more "nervous" behavior than observed spring hydrograph. This is the consequence of the oversimplification of the infiltration process. Although the approximate distribution of effective infiltration between diffuse and concentrated recharge was respected in the above models, recharging waters reached the aquifer instantaneously, and the infiltration-retarding effect of the epikarst was neglected.

In order to test the effect of the epikarst on the hydraulic response of the Milandrine amont system, a simple, two-dimensional epikarst model proposed by Perrin (2002) has been integrated with the two-dimensional model of the saturated zone. This combined model considers the epikarst as a porous medium of three, progressively declining permeabilities with increasing depth (**Fig. 6-8**). The vertical conductivities of these layers vary between 1E-4 and 1E-6 m/s. Horizontal conductivities are one order of magnitude lower than vertical

conductivities. A uniform storage coefficient of S_s=0.01 1/m has been applied in every layer. The recharge is uniformly distributed over the model surface. A permanent outflow is located in the lowermost layer, while a temporary outflow is configured in the uppermost layer. The model representing an epikarstic block is 10 m long. The thickness of the entire epikarst was assumed to be 3.5 m.

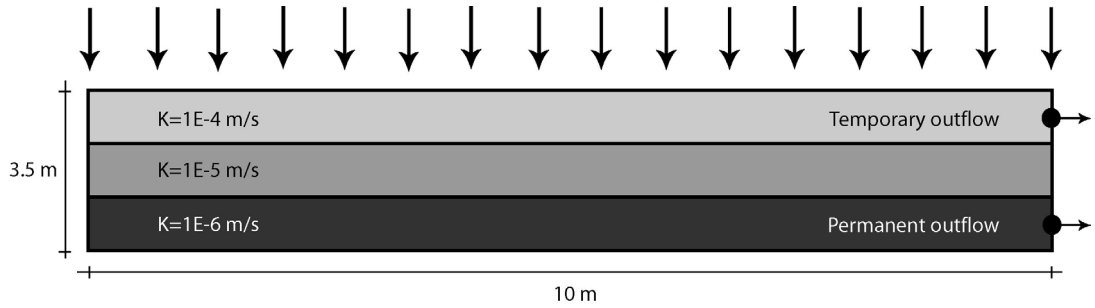

Figure 6-8. The epikarst model configuration.

The simulated discharge of the permanent outflow has been distributed over the low-permeability blocks of the saturated zone model. This item represents diffuse discharge along the base of the epikarst through small fractures. The simulated discharge of the temporary outflow was directly injected into the conduit network of the saturated zone model. This volume represents concentrated discharge into vertical shafts connecting the epikarst to the conduit network of the saturated zone.

The global response of the epikarst model is represented in **Figure 6-9**. The simulated recession coefficient resulting from the epikarst is in the same order of magnitude (α_{epi}=0.004 1/d) as the measured recession coefficient of the entire system. This agrees with some of the sporadic field observations obtained by Perrin (2002), Puech (1996), and Thierrin (1996) from the Bure test site.

Since epikarst is a strongly heterogeneous system with karstic reactions and dual hydraulic behavior, the above porous epikarst model is schematic and oversimplified. However, it reproduces the most important hydraulic functions of the epikarst, i.e. it distributes recharge, retards diffuse infiltration, stores water, and behaves as a threshold gate. As demonstrated in **Figure 6-10**, the combined model (model EPIK) smoothes discharge peaks and suppresses excessive discharges in the simulated hydrograph of the system. The integrated epikarst model yields more realistic hydrograph characteristics than the pure saturated zone model.

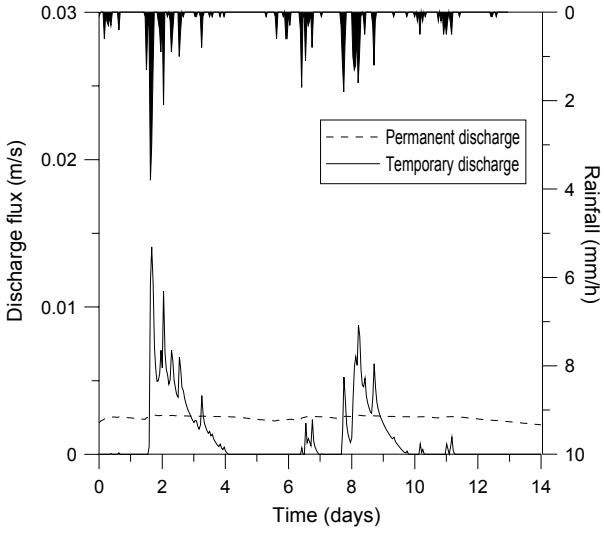

Figure 6-9. Simulated diffuse (permanent outflow) and concentrated (temporary outflow) discharge fluxes of the epikarst model.

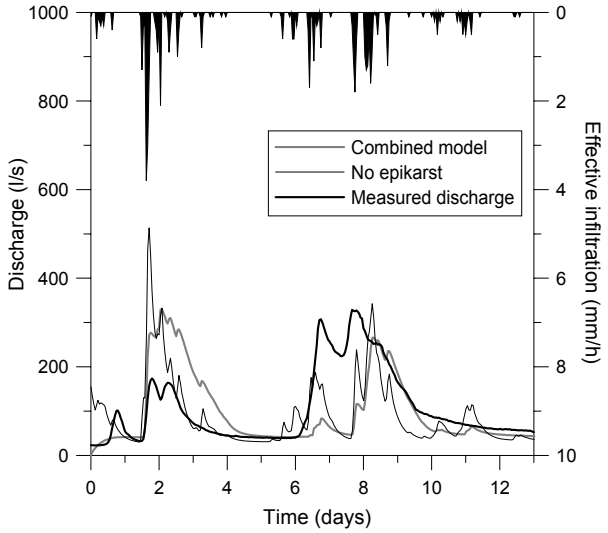

Figure 6-10. Comparison of hydrographs simulated by the integrated model (model EPIK) and the pure saturated zone model (Model MRFR_3).

However, the recession coefficient obtained from the integrated epikarst model is lower (α_{sim}=0.0012 1/d) than either the pure saturated zone models recession coefficient or the measured value. This is the logical consequence of the slow retarded discharge of water from the epikarst. Concomitant with the slow drainage of the saturated low-permeability blocks, the epikarst also releases water from storage and thus prolongs the recession process of the saturated zone. Although the available information on the hydraulic behavior of the epikarst is generally incomplete, retarded discharge of water from the epikarst could significantly influence the global response of the entire system and thus may result in an inaccurate estimation of hydraulic and geometric properties of the aquifer by assuming that the saturated zone influences alone recession. In such cases, proper parameter estimation requires information not only on the global response of the entire system, but the separate observation of the global hydraulic response of the epikarst, or a reasonable estimate of the recession coefficient of the epikarst from its hydraulic and geometric parameters using analytical **Equations (5-10)** and **(5-17)**.

Although the parameter estimation of the Milandrine amont system based on the uni-component (saturated zone) analytical model yields reasonable results, the underestimation of matrix transmissivity that results in slightly excessive hydraulic heads can be a consequence of the negligence of the epikarst layer. Although there is insufficient data for calibrating an epikarst model of the Milandrine amont system, a good estimation of the saturated zone matrix transmissivity can be obtained by steady-state parameter calibration based on mean observed hydraulic head difference between conduits and low-permeability blocks. A more reasonable steady-state hydraulic head distribution (**Figure 6-11**) can be simulated by applying an increased transmissivity value of T_m=2E-6 m^2/s, instead of the value T_m=6.5E-7 m^2/s predicted by direct application of the analytical **Equation (5-10).**

The calculation of the analytical value of the saturated zone recession coefficient by applying an increased value of transmissivity yields α=0.0085 1/d, a value higher than the measured one. The graphical representation of the Milandrine amont hydraulic and geometric parameters coupled with the estimated effect of the epikarst on the aquifers global response is demonstrated in **Figure 6-12**.

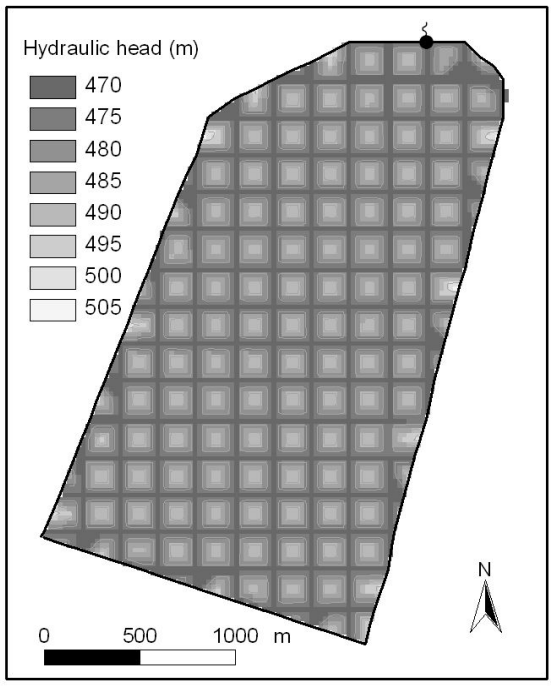

Figure 6-11. Steady-state hydraulic head distribution simulated by an increased transmissivity saturated zone model (T_m=2E-6 m^2/s).

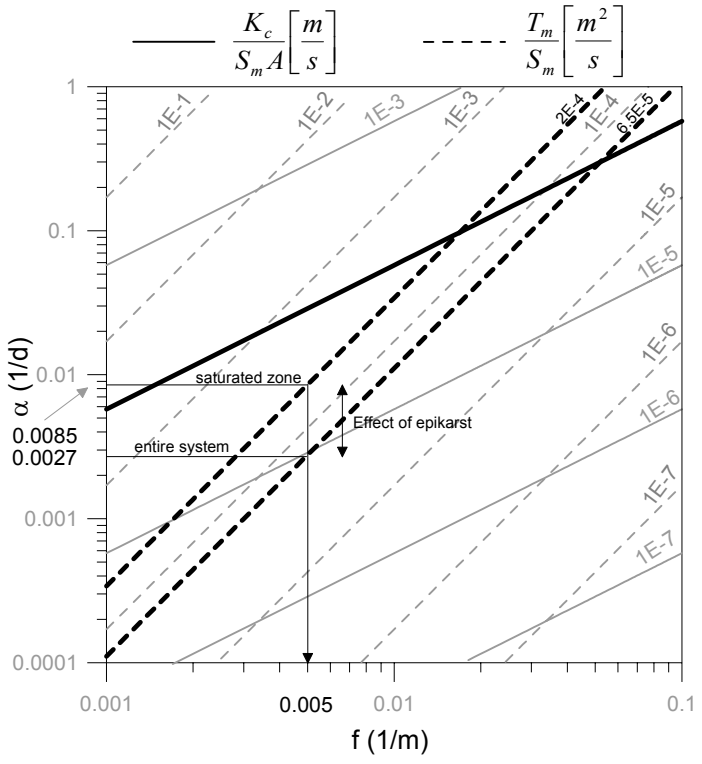

Figure 6-12. The graphical representation of the Milandrine amont catchments hydraulic parameters. Figure demonstrates that every reasonable parameter configuration falls in the matrix-restrained baseflow domain (dashed lines). The difference between measured and calibrated recession coefficients is probably the result of retarded infiltration from the epikarst. Applied hydraulic parameters: S_m=0.01, T_m=6.5E-7 m^2/s, T_m^{sat}=2.0E-6 m^2/s, K_c=5 m^3/s, f=0.005, A=4.65E+8.

6.8. CONCLUSIONS

The estimation of aquifer geometric and hydraulic parameters using analytical formulae made the transient groundwater flow simulation of the Milandrine amont karstic catchment possible using the combined discrete-continuum approach. The application of regular conduit network geometry and uniform hydraulic parameter fields facilitated the direct verification of analytical formulae introduced in Chapter 5. Although this approach does not allow for the simulation of the exact water table, it provides a direct link between aquifer hydraulic parameters, temporal variations of discharge, and certain characteristics of the observed hydraulic head distribution. These comprise the mean and maximum hydraulic heads in karst conduits, over low-permeability blocks and throughout the entire aquifer. Because the conduit network of the Milandrine amont karst system is perched on the aquifer basement, this approach cannot reflect the general shape of water table over this aquifer without introducing karst conduits as head boundaries.

Flow simulations demonstrated that "typical" karstic hydraulic behavior can not be simulated in the conduit-influenced baseflow domain, but it requires MRFR flow conditions during baseflow periods. It is presumed that a transition between MRFR and CIFR flow regimes occurs during flood events, since simulated flood peaks of mature systems show a strong dependence on conduit hydraulic conductivity. The equivalent laminar conduit conductivity of such systems can be estimated from measured discharge and hydraulic gradient during flood events, and this equivalent laminar value can be also used for the initial evaluation of the respective baseflow domain.

The integration of the epikarst into the numerical model demonstrated that retarded discharge from the subcutaneous layer modifies the global hydraulic response of the entire system, and decreases recession coefficient. Consequently, the parameter estimation of these systems requires the separate observation of the global hydraulic response of the epikarst, or a reasonable estimate of the recession coefficient of the epikarst layer from its hydraulic and geometric parameters by analytical formulae.

The numerical simulations of the Milandrine amont catchment suggest that this system is characterized by matrix-restrained baseflow (mature system). The equivalent laminar conduit conductivity estimated from flood discharges and hydraulic gradients agrees with calibrated model values. However, this parameter does not reflect real conduit properties, as it does not consider turbulent flow. The estimation of aquifer geometric and hydraulic parameters by analytical formulae provides acceptable simulation results. However, the negligence of the epikarst results in slightly underestimated matrix transmissivities and excessive simulated hydraulic heads.

7. GENERAL CONCLUSIONS AND OUTLOOK

7.1. OVERVIEW

Karst aquifers are highly complex hydrogeological systems. The high solubility of carbonates in water results in the development of dissolution void networks, and is responsible for the strong heterogeneity of karstified media. The coexistence of two different permeability media (host rock and voids) results in a spatial and temporal duality of karst-hydrogeological processes.

However, karst systems may be hierarchically organized, both in vertical and horizontal directions. This hierarchical organization allows for the characterization of karst hydrodynamic processes. Mathematical models are exact tools for quantitatively characterizing hydrodynamic phenomena. There are two distinct approaches for modeling karst hydrodynamics. Distributive models facilitate the spatial representation of hydraulic parameter fields, and provide a link between hydraulic input, groundwater flow field and global hydraulic response. Consequently, distributive models are the most coherent and detailed quantitative representation of real karst hydrogeological systems. However, field data necessary for specifying distributive model parameters are generally not available.

The scarcity of appropriate field data necessary for constructing distributive flow models requires information to be derived by alternative means. Global models consist of the analysis of discharge time-series, and are believed to provide information about aquifer structure and hydraulic parameters. However, the interpretation of global models has been hitherto qualitative.

The most important outcome of this research is the establishment of the link between global and distributive models, by quantitatively characterizing the relationship between systems global response and aquifer properties, thus providing a tool for the estimation of distributive model parameters. This has been achieved by deducing analytical solutions for the global hydraulic response of simple two-dimensional model geometries, and testing these formulae using numerical models. Resulting formulae express the connection between the hydraulic and geometric properties of a karst system and the spring hydrograph recession coefficient, which is believed to be a characteristic parameter of a systems global response.

7.2. RELATION BETWEEN AQUIFER PARAMETERS AND GLOBAL RESPONSE

The global hydraulic response of an aquifer is strongly dependent on hydraulic parameters, aquifer extent, and the spatio-temporal distribution of recharge. In the case of karst systems it also depends on the density of the conduit network, and the proportion of diffuse and concentrated recharge. Baseflow recession is believed to be independent of the recharge phenomena. Consequently, it only reflects aquifer characteristics (however, it can be influenced by retarded recharge from higher order sub-systems such as the epikarst). The temporal evolution of diffusive flux from an aquifer can be closely approximated by the following exponential formula (Maillet, 1905):

$$Q_{(t)} = Q_0 e^{-\alpha t} \tag{2-1}$$

where the recession coefficient (α) depends on aquifer parameters. For two-dimensional porous aquifers, this relation can be expressed as follows:

$$\alpha = \frac{\gamma T}{SA} \tag{5-11}$$

where the geometric parameter (γ) is typically dependent on boundary conditions and aquifer shape.

The drainage process of karst aquifers follows similar rules; however, there is a significant difference between porous and karst systems. While the drainage of porous systems is always dependent on the extent of the entire aquifer, the drainage of karst aquifers depends either on the extent of the entire aquifer or on the extent of individual low-permeability fissured blocks surrounded by karst conduits. The respective law that characterizes the drainage of a karst system is dependent on the overall geometric configuration of the aquifer and of the karst conduit system, and on the distribution of hydraulic parameters.

If the "heterogeneity" of a karst system is lower than a quantitatively defined threshold, the conduits cannot effectively drain the low-permeability matrix. Such system behaves similarly to a porous system; the drainage process is dependent on the entire aquifer area, and equivalent hydraulic parameters can be used to express the recession coefficient. (However, the geometric parameter (γ) is different from that of an equivalent porous system). This has been defined as *conduit-influenced flow regime (CIFR),* and is typical during the baseflow of fissured systems, or weakly karstified systems, defined as *premature karst systems*. The recession coefficient of conduit-influenced baseflow domains can be expressed as follows:

$$\alpha \approx \frac{2}{3}\frac{K_c f}{S_m A} \tag{5-17}$$

where a regular perpendicular conduit distribution is assumed.

If the heterogeneity of a karst system exceeds the threshold value, karst conduits do not longer influence the drainage of individual low-peremability blocks. Conduits behave as fix-head boundary conditions, and the drainage process is influenced by the low-permeability blocks alone. This flow condition has been defined as a *matrix-restrained flow regime (MRFR),* and is typical for highly karstified systems during baseflow periods. These systems have been referred to as *mature karst systems*. The baseflow recession coefficient of two-dimensional matrix-restrained systems can be expressed as follows:

$$\alpha = \frac{2\pi^2 T_m f^2}{S_m} \tag{5-10}$$

As a consequence of direct infiltration during flood periods, a transition between MRFR and CIFR flow regimes may occur in mature karst systems. This transition is assumed to be reflected by steep exponential or non-exponential components of spring hydrographs. However, the flood recession coefficient cannot be expressed by the above analytical formulae, due to the strongly turbulent flow conditions in karst conduits during flood events.

7.3. PARAMETER ESTIMATION AND NUMERICAL MODELING OF KARST SYSTEMS

The hydraulic parameters of the low-permeability fissured matrix derived from borehole tests, and the baseflow recession coefficient measured at karst springs are probably the most reliable hydraulic data that can be obtained in karst aquifers. Supplementary data may consist of hydraulic heads in the low-permeability matrix and different parts of the conduit system. Approximate information concerning the conduit network density can be obtained from cave maps and structural analyses.

Indirect information obtained by the means of steady-state numerical modeling of the Bure aquifer illustrated some general geometric characteristics of karst systems. These model simulations suggest that conduit networks extend horizontally below that part of the aquifer that is exposed to infiltration. Karst networks belonging to adjacent karst springs extend to catchment boundaries. Steady-state simulations also demonstrated that higher spring discharges of adjacent sub-catchments involve higher conduit conductivities.

Although the quantity and precision of available information about aquifer parameters is usually far from satisfactory, the purposive step-by-step application of the above proposed analytical formulae, and the recurrent comparison of calculated values with available field measurements make the verification and completion of field observations possible. Combined with preliminary numerical tests, this approach makes the quantitative synthesis of aquifer hydrodynamics into a coherent deterministic groundwater flow model possible.

The first step of any modeling study should be the evaluation of the dominant baseflow domain. The shape of the hydrograph and hydraulic gradients in the karst channels provide a preliminary estimate of the baseflow domain (however, mature shallow karst systems may manifest artificially high conduit hydraulic gradients, similar to those of premature systems). The domain threshold is expressed by the following analytical formula:

$$K_c^* \approx 3\pi^2 T_m A f \tag{5-20}$$

Higher values of measured laminar equivalent conduit conductivities designate matrix-restrained baseflow domain, while lower values indicate conduit-influenced baseflow domain. This formula requires information on conduit frequency, and conduit conductivity. Since the conductive capacity of partially constrained (free-surface flow) karst conduits is attained during flood events, the estimation of an equivalent laminar conduit conductivity requires conduit hydraulic gradient data and spring discharges during high-water events.

The analytical formulae and a large number of sensitivity analyses demonstrated that none of the equivalent approaches are appropriate for modeling groundwater flow in mature karst systems. There can be only one parameter set that reflects observed spatio-temporal reactions of mature systems. The conduit frequency can be verified or estimated from matrix hydraulic parameters and recession coefficient, using **Equation (5-10).** A double-check is possible, by testing hydraulic head differences between low-permeability blocks and conduits by applying measured matrix hydraulic parameters and overestimated conduit conductivities (in order to ensure MRFR conditions) in steady-state groundwater flow models. Equivalent laminar conduit conductivity can be estimated from measured flood discharge and conduit hydraulic gradients as proposed above. This parameter can be verified and adjusted by modeling realistic infiltration events, and comparing simulated discharge peak amplitudes with those measured. However, the numerical value of conduit conductivity does not reflect real conduit properties, but it is an equivalent parameter to be used in laminar flow models.

Evaluation of turbulent conduit conductivity from calibrated laminar model conduit conductivity is possible by assuming identical measured and calibrated hydraulic gradients and spring discharges. In this case the turbulent conduit conductivity can be expressed from the Darcy flow-law and the Darcy-Weissbach friction law (**Equation (2-33**)) as follows:

$$K_c^{'} = K_c \sqrt{I} \tag{7-1}$$

or

$$K_c^{'} = \sqrt{K_c Q} \tag{7-2}$$

An estimation of the "real" conduit diameter from turbulent conduit conductivity, or the estimation of turbulent conduit conductivity from measured conduit diameter is possible using either the Louis formula (**Equation (2-34)**) or the Strickler formula (**Equation (2-35)**). Both of these approaches yield realistic conduit diameters or turbulent conductivities. However, the direct transformation between conduit diameter and laminar conduit conductivity during strongly turbulent flow conditions using the Hagen-Poiseuille law (**Equation (2-32)**) yields false results.

In the case of premature karst systems, the equivalent transmissivity that is dependent mainly on conduit frequency and conductivity, determine the hydraulic head distribution over the entire aquifer. Consequently, when information on one of these parameters is available, the other parameter can be calibrated by adjusting simulated steady-state hydraulic head distribution. However, any combination of these parameters that provides the same equivalent transmissivity, yield the same recession coefficient as well. The storativity parameter can be verified or calculated from the calibrated values of conduit frequency and conductivity, using the analytical **Equation (5-17)**. The matrix transmissivity, which has negligible effect on both the global response and on the large-scale hydraulic head distribution in premature systems, can be calibrated by adjusting hydraulic head difference between low-permeability blocks and neighboring conduits. Equivalent discrete-continuum models can be used for modeling groundwater flow in premature systems. The global response of equivalent porous medium models corresponds to the transition between MRFR and CIFR flow regimes. Consequently, the EPM approach cannot be directly applied for modeling such systems.

Transient model simulations have demonstrated that retarded seepage from the epikarst may significantly modify the global hydraulic response of the entire karst system. In the case if the saturated zone model based on observed hydraulic parameters yields a significantly increased recession coefficient, epikarst storage may not be neglected. The effect of the epikarst can be taken into account in a distributive groundwater flow model in two different ways.

An indirect approach may consist of distributing recharge between diffuse infiltration and concentrated recharge, and artificially increasing conduit storage. This method provides only limited information on the hydraulic functioning of the epikarst. However, it facilitates modeling of either global or spatio-temporal behavior of entire karst systems.

A deterministic approach consists of representing the epikarst by a separate distributive model, and feeding the saturated zone by simulated diffuse and concentrated discharges of the epikarst model. Saturated zone and epikarst models can also be integrated. Since the epikarst has similar karstified structure to the saturated zone, the analytical formulae linking aquifer hydraulic and geometric parameters with global response may also be applied for the epikarst. However, this approach requires supplemental information concerning the baseflow recession of the epikarst zone.

7.4. RESEARCH SITE HYDROGEOLOGY

A detailed hydrogeological revaluation of the Bure plateau and data synthesis into a coherent conceptual and numerical model has been performed. This has involved the construction of a hydrostratigraphical map, several cross-sections and structural surfaces. Furthermore, the mean water table, mean and minimum saturated zone thicknesses, and the mean unsaturated zone thickness have been determined, and catchment boundaries have been redefined. These calculations located the regional groundwater divide along the Porrentruy – Bure – Croix axis, and designated extended shallow karst zones in the area of Buix and Croix.

Tracing experiments demonstrated that the two Kimmeridgian marl horizons do not act as aquicludes, and they do not influence regional flow patterns, nor do the Sequanian Astarte Marls influence groundwater flow field in the unconfined zone. However, their role in the confined zone remains uncertain.

Steady-state groundwater flow simulations based on realistic hydraulic parameters demonstrated that the Milandrine cave is only a small portion of an extended cave system. Each spring has its own conduit network, which extends to its catchment boundaries.

Transient flow simulations demonstrated that the Milandrine amont catchment is a mature karst system. It is highly probable that the other subcatchments of the Milandrine system are also matrix-restrained baseflow systems. Baseflow hydraulic gradients measured in the conduit network of the Milandrine amont catchment are much higher than those either simulated by the groundwater flow model, or usually measured in such sysems. This confirms that the Milandrine amont catchment contains “shallow karst” zones, i.e. some parts of the system are perched on the top of the Astarte marls. Integrated numerical models of the Milandrine amont catchment demonstrated that considerable water storage can be assigned to the epikarst layer.

7.5. OUTLOOK

Although this work has demonstrated some important characteristics of karst hydrogeological systems, several questions and problems also arose. These issues require further field data and more complex modeling techniques, which were not available at the time of writing, or could not be achieved within the framework of this research.

Assuming laminar groundwater flow in karst conduits during the baseflow recession gives a reasonable approximation of real phenomenon observed in the field. However, the same assumption can not be applied during strongly turbulent flood conditions. Model results suggest that a transition between MRFR and CIFR flow regimes occurs during high-water periods. The change of flow regimes is supposed to manifest itself in spring hydrographs, and conduit hydraulic parameters could possibly be expressed from flood recession hydrograph components determined by decomposition techniques, assuming turbulent flow in the conduit system. The resulting combined technique would facilitate more complex parameter estimation. Consequently, the determination and verification of analytical formulae under turbulent flow conditions would largely increase the efficiency of the parameter-estimation method proposed here.

The analytical formulae presented in this thesis are based on two-dimensional conceptual models. The extension of two-dimensional formulae to three spatial dimensions would increase the precision of the proposed parameter estimation technique. This would require the evaluation of the geometric parameter (γ) for three-dimensional aquifer configurations.

While real conduit networks are irregular and may be hierarchically organized, the conduit frequency parameter has been derived assuming regular conduit networks of uniform conductivity. As the direct application of regular networks in distributive models is hardly realistic, the frequency parameter is intended to be used for conditioning stochastic network generators.

According to numerical tests, slow retarded seepage from the epikarst can significantly influence the global response of the entire aquifer. Since the parameter estimation method proposed here is based on global response, the improvement of our knowledge concerning the structure and hydraulic parameters of the epikarst is crucial. Supplementary information on the global hydraulic behavior of the epikarst would facilitate the estimation of epikarst hydraulic parameters and structure by means of analytical formulae.

Finally, a transition from conduit-influenced to matrix-restrained baseflow domains is a logical consequence of the karstification phenomenon. It would be important to investigate, how this change in hydraulic behavior influences natural evolution of karst aquifers at its early stage, in order to better understand the karstification process.

ACKNOWLEDGEMENTS

I am indebted to my advisors, who largely contributed to the success of this doctoral research. Prof. **Pierre Perrochet**, the director of this thesis, gave indispensable help in solving hydraulic and mathematical problems that arose in the course of this research. His initiative ideas often served as keys to the final solution. Dr. **Pierre-Yves Jeannin**, the thesis co-director, guided the way for me all along the preparation of this work. His persistent enthusiasm about karst often held to maintain my motivation. Prof. **László Király** not only assisted my first steps in the thorny field of karst modeling, but provided the basic tools for my research. Without the FEN family of revolutionary modeling codes written by him, this thesis would not exist. His constructive criticism often prevented me to oversimplify hydrogeological problems, and helped to avoid mistakes.

I wish to thank Prof. **Martin Sauter** and Prof. **Daniel Hunkeler**. Their participation in my Ph.D. jury, and their helpful corrections improved the quality of the final version of this manuscript.

Many thanks to Prof. **François Zwahlen**, the director of our institute. His flexible and effective management permitted to fully concentrate on my research, without passing much time with administration.

I would like to thank Dr. **Mahmoud Bouzelboudjen** for remaining available to help me at any time and assisting me with the construction of a Geological Information Systems database.

Thank you to the collaborators of the CHYN, especially to Dr. **Ray Flynn** for his English corrections, suggestions and constructive criticism, and to Prof. **Imre Müller** and Dr. **François Vuataz** for their advice and interest in my research. I thank Dr. **Frank Bosch**, **Alain Pochon** and **Michael Sinreich** for translating the abstract of this thesis. The rapid and effective administration of **Michèle Jaquet** is also greatly appreciated.

The collaborators of the MFR Ltd. provided me with considerable data that were essential for the understanding of the Bure site hydrogeology. Thanks to **François Flury** and **Romain Christ** for their availability. I also had a chance to make a visit at the Colenco Ltd. I thank Dr. **Olivier Jaquet** and Dr. **Pascal Siegel** for fruitful discussions and the opportunity for using their MAGIC mesh generator.

My best thanks to my friends in Neuchâtel, particularly to **Frank**, **Nicolas**, **Ray** and **Tamás**.

Adrienn, you were by my side during the most challenging times. Your loveliness and sincerity gave me lots of motivation. Thank you for everything.

Most of all, I am perpetually indebted to **my parents** for their selfless and absolute love, assistance and solidarity.

This work was supported by the Swiss National Scientific Foundation under projects 2000-061717.00/1 and 2000-068066.02/1.

REFERENCES

Andersson, J. & Dverstorp, B. (1987): Conditional simulations of fluid flow in three-dimensional networks of discrete fractures. Water Resources Reasarch, 23(10), 1876-1886.

Armadillio, E., Massa, F., Caneva, G., Gambetta, M. & Bozzo, E. (1998): Modeling of karst structures by geophysical methods. An example: The doline of S. Pietro dei Monti (Western Liguria). Anali di Deophisica, 41(3), 389-397.

Bagarić, I., (1978): Determination of storage and transportation characteristics of karst aquifers. In: Milanović, P.T., (1981): Karst hydrogeology. Water Resources Publications, Littleton, CO, USA. 434 p.

Barrenblatt, G.I., Zheltow, I.P. & Kochina, I.N. (1960): Basic concepts in the theory of seepage of homogenous liquids in fissured rocks (strata). J. Appl. Math. Mech., 24, 1286-1303.

Bedinger, M.S. (1966): Electric analog study of cave formation. - Nat. speleol. Soc. Bull., 28(3), 127-132.

Berkaloff, E. (1967) : Limite de validité des formules courantes de tarissement de débit. Chronique d'Hydrogéologie, 10, 31-41.

Bezes, C. (1976): Contribution a la modélisation des systèmes aquifères karstiques. Thèse, Université des Sciences et Techniques du Languedoc, Montpellier.

Bosch, F-P. & Müller, I. (2001): Continuous gradient VLF measurements: A new possibility for high resolution mapping of karst structures. First Break, 19(6), 343-350.

Box, G.E.P. & Jenkins, G.M. (1976): Time series analysis: forecasting and control. Holden Day, San Francisco.

Carslaw, H.S. & Jaeger, J.C. (1959): Conduction of heat in solids (2nd ed.). Oxford University Press, London. 510p.

Cornaton, F. (1999): Utilisation de modèles continu discret et a double continuum pour l'analyse des reponses globales de l'aquifère karstique. Diplôma, CHYN, Université of Neuchâtel.

Cornaton, F. & Perrochet, P. (2002): Analytical 1D dual-porosity equivalent solutions to 3D discrete single-continuum models. Application to karstic spring hydrograph modeling. Journal of Hydrology, 262, 165-176.

Diebold, P., Laubscher, H.P., Schneider, A. & Tschopp, R. (1963): Atlas géologique de la Suisse à 1/25000. Carte 1085 (St-Ursanne). Kümmerly & Frey AG, Bern.

Doerfliger, N. & Zwahlen, F. (1995): Action COST 65 – Swiss National Report. Bulletin d'Hydrogéologie de l'Université de Neuchâtel, 14, 3-33.

Dreiss, S.J. (1989): Regional scale transport in karst aquifers. 2: Linear systems and time moment analysis. Water Resources Research, 25(1), 126-134.

Drogue, C. (1972): Analyse statistique des hydrogrammes de décrues des sources karstiques. Journal of Hydrology, 15, 49-68.

Drogue, C. (1974) : Structure de certains aquifères karstiques d'après les résultats de travaux de forage. Comptes Rendus Académie des sciences, Paris, D, 278, 2621-2624.

Drogue, C. (1980) : Essai d'identification d'un type de structure de magasins carbonates fissurées. Application à l'interprétation de certains aspects du fonctionnement hydrogéologique. Mémoires hors série Société Géologique de la France, 11, 101-108.

Dverstorp, B. & Andersson, J. (1989): Application of the discrete fracture network concept with field data: Possibilities of model calibration and validation. Water Resources Research, 25(3), 540-550.

Eisenlohr, L. (1996) : Variabilité des réponses naturelles des aquifères karstiques. Thèse, Université de Neuchâtel.

Eisenlohr, L., Király, L., Bouzelboudjen, M. & Rossier, I. (1997a): Numerical simulation as a tool for checking the interpretation of karst springs hydrographs. Journal of Hydrology, 193, 306-315.

Eisenlohr, L., Király, L., Bouzelboudjen, M. & Rossier, I. (1997b): Numerical versus statistical modeling of natural response of a karst hydrogeological system. Journal of Hydrology, 202, 244-262.

Favre, I. (2001): Base de données des essais de traçage du plateau karstique de Bure (JU), SIG, interprétations statistiques. Travail de diplôme, Université de Neuchâtel.

Fleury, F. (1984): Multitraçage sur le plateau de Bure (Ajoie, JU) à l'aide de bactériophages et de traceurs fluorescents. Bulletin d'Hydrogéologie de l'Université de Neuchâtel, 5, 91-105.

Fleury, F. & Allemann, R. (1991): Recherche d'eau par forages à Delémont. GWA, 71, 841-849.

Ford, D. & Williams, P. (1989): Karst geomorphology and hydrology. Unwin Hyman Ltd., London.

Forkasiewicz, J. & Paloc, H. (1967): Le régime de tarissement de la Foux-de-la-Vis. Etude préliminaire. Chronique d`Hydrogéologie, BRGM, vol. 3(10), 61-73.

Grasso, D.A. (1998): Interprétation des réponses hydrauliques et chimiques des sources karstiques. Thèse, Centre d'hydrogéologie, Université de Neuchâtel.

Grasso, D.A. & Jeannin, P-Y. (1994a): Etude critique des méthodes d'analyse de la réponse globale des systèmes karstiques. Application au site de Bure (JU, Suisse). Bulletin d'Hydrogéologie de l'Université de Neuchâtel, 13, 87-113.

Grasso, D. A. & Jeannin, P.-Y. (1994b): Estimation des pertes dans la partie aval du réseau karstique de la Milandrine: bilan hydrique au sein d'un aquifère karstique. Bulletin d'Hydrogéologie de l'Université de Neuchâtel, 13, 115-128.

Grasso, D.A. & Jeannin, P-Y. (1998): Statistical approach to the impact of climatic variations on karst spring chemical response. Bulletin d'Hydrogéologie de l'Université de Neuchâtel, 16, 59-74.

Gretillat, P.-A. (1996): Aquifères karstiques et poreux de l'Ajoie (Jura, Suisse). Thèse, CHYN, Université de Neuchâtel.

Guerin, R. & Benderitter, Y. (1995): Shallow karst exploration using MT-VLF and DC resistivity methods. Geophysical Prospecting 43, 635-653.

Guilbot, A. (1975): Modélisation des écoulement d`un aquifère karstique (liaisons pluie-debit), application aux bassins de Saugras et du Lez. Thèse, Université des Sciences et Techniques du Languedoc, Montpellier.

Gurk, M. & Bosch, F. (2001): Cave detection using Self-Potential-Surface (SPS) technique on a karstic terrain in the Jura Mountains (Switzerland). In: Proceedings of the Elektromagnetische Tiefenforschung, Burg Ludwigsstein, Germany, 19, Deutsche Geophysikalische Gesellschaft.

Huyakorn, P.S. & Pinder, G.F. (1983): Computational methods in subsurface flow. Academic Press, London.

Jeannin P-Y. (1995a): Comportement hydraulique mutuel des volumes de roche peu perméable et des conduits karstiques : conséquences sur l`étude des aquifères karstiques. Bulletin d'Hydrogéologie de l'Université de Neuchâtel, 14, 113-148.

Jeannin P-Y. (1995b): Action COST 65 – Projects Bure et Hölloch (Suisse): cadre théorique, position des problèmes, présentation des sites étudiés et des données disponibles. Bulletin d'Hydrogéologie de l'Université de Neuchâtel, 14, 53-81.

Jeannin, P-Y. (2001): Modeling flow in phreatic and epiphreatic karst conduits in the Hölloch Cave (Muotathal, Switzerland). Water Resources Research, 37(2), 191-200.

Jeannin, P.-Y. & Grasso, A.D. (1995a): Recharge respective des volumes de roche peu perméable et des conduits karstiques, rôle de l'epikarst. Bulletin d'Hydrogéologie de l'Université de Neuchâtel, 14, 95-111.

Jeannin, P.-Y. & Grasso, A.D. (1995b): Estimation dés infiltrations efficaces journalières sur le bassin karstique de la Milandrine (Ajoie, JU, Suisse). Bulletin d'Hydrogéologie de l'Université de Neuchâtel, 14, 83-89.

Jeannin, P-Y. & Maréchal, J-C. (1995): Lois de pertes de charge dans les conduits karstiques: base théorique et observations. Bulletin d'Hydrogéologie de l'Université de Neuchâtel, 14, 149-176.

Jeannin, P-Y. & Sauter, M. (1998): Analysis of karst hydrodynamic behavior using global approaches: A review. Bulletin d'Hydrogéologie de l'Université de Neuchâtel, 16, 31-48.

Jenkins, G.M. & Watts, D.G. (1968): Spectral analysis and its applications. Holden Days, San Francisco.

Kinzelbach, W. (1986): Groundwater modeling. Elsevier, Int. Edition.

Király, L. (1969): Anisotropie et hétérogénéité de las perméabilité dans les calcaires fissurés. Eclogae Geologica Helvetiae, 62(28), 613-619

Király, L. (1973): Notice explicative de la carte hydrogéologique de canton de Neuchâtel. Supplément au Bulletin de la Société neuchâteloise des sciences naturelles, 96, 16p.

Király, L. (1975): Rapport sur l'état actuel des connaissances dans le domaine des caracteres physique des roches karstique. In: Burger, A. & Dubertet, L.: Hydrogeology of karstic terrains, Int. Union of Geol. Sciences, B, 3, 53-67

Kiraly, L. (1979): Remarques sur la simulation des failles et du réseau karstique par éléments finis dans les modèles d'écoulement. Bulletin d'Hydrogéologie de l'Université de Neuchâtel, 3, 155-167.

Király, L. (1985): FEM-301 – A three dimensional model for groundwater flow simulation. NAGRA Technical Report 84-49, 96 p.

Király, L. (1988): Large-scale 3D groundwater flow modeling in highly heterogeneous geologic medium. In: Custoido et al. Eds., Groundwater flow and quality modeling, 761-775, D. Riedel Publishing Company.

Király, L., (1994): Groundwater flow in fractures rocks: models and reality. In: 14th Mintrop Seminar über Interpretationsstrategien in Exploration und Produktion, Ruhr Universität Bochum 159, 1-21.

Király, L., (1998a): Modeling karst aquifers by the combined discrete channel and continuum approach. Bulletin d'Hydrogéologie de l'Université de Neuchâtel, 16, 77-98.

Király, L. (1998b): Introduction à l'hydrogéologie des roches fissurées et karstiques. Bases théoriques à l'intention des hydrogéologues. Manuscrit, Université de Neuchâtel.

Király, L., (2002): Karstification and Groundwater Flow. In: Proceedings of the Conference on Evolution of Karst: From Prekarst to Cessation. Postojna-Ljubljana. 155-190.

Király, L. & Morel, G. (1976a): Etude de régularisation de l'Areuse par modèle mathématique. Bulletin d'Hydrogéologie de l'Université de Neuchâtel, 1,19-36.

Király, L. & Morel, G. (1976b): Remarques sur l'hydrogramme des sources karstiques simule par modèles mathématiques. Bulletin d'Hydrogéologie de l'Université de Neuchâtel, 1, 37-60.

Király, L., Matthey, B. & Tripet, J.P. (1971): Fissuration et orientation des cavités souterraines. Région de la Grotte Milandre. Bull. Soc. Neuchât. Sci. Nat. 94, 99-114.

Király, L., Perrochet, P. & Rossier, Y. (1995): Effect of epikarst on the hydrograph of karst springs: a numerical approach. Bulletin d'Hydrogéologie de l'Université de Neuchâtel, 14, 199-220

Kovács, A., & Jeannin, P-Y. (2003): Hydrogeological overview of the Bure Plateau, Ajoie, Switzerland. Eclogae Geologicae Helvetiae, accepted

Kraemer, S.R. & Haitjema, H.M. (1989): Regional modeling of fractured rock aquifers. In: Josuma et al. Eds., Groundwater contamination: Use of models in decision-making, 467-476. Kluwer Academic Publishers.

Labhart, T. & Decrouez, D. (1997): Géologie de la Suisse. Delachaux et Niestlé SA, Lausanne – Paris.

Lang, U. (1995): Simulation regionaler stromungs und transportvorgange in karstaquiferen mit hilfe des doppelkontinuum-ansatzes: Methodenentwicklung und parameteridentifikation. Ph.D. thesis, University of Stuttgart.

Larocque, M., Mangin, A., Razack, M. & Banton, O. (1998): Characterization of the La Rochefoucauld karst aquifer (Charente, France) using correlation and spectral analysis. Bulletin d'Hydrogéologie de l'Université de Neuchâtel, 16, 49-57.

Laubscher, H.P. (1963): Erläuterungen zum Geologischen Atlas der Schweiz. 1085 St-Ursanne. Kümmerly & Frey AG, Bern.

Liniger, H. (1969): Atlas géologique de la Suisse à 1/25000. Carte 1065 (Bonfol). Kümmerly & Frey AG, Bern.

Liniger, H. (1970): Erläuterungen zum Geologischen Atlas der Schweiz. 1065 Bonfol. Kümmerly & Frey AG, Bern.

Long, J.C.S., Remer, J.S., Wilson, C.R. & Witherspoon, P.A. (1982): Porous media equivalents for networks of discontinuous fractures. Water Resources Research, 18(3), 645-658.

Long, J.C.S, Gilmour, P. & Witherspoon, P.A. (1985): A model for steady fluid flow in random three-dimensional networks of disc-shaped fractures. Water Resources Research, 21(8), 1105-1115.

Louis, C. (1968): Etude des écoulements d'eau dans les roches fissurées et de leurs influences sur la stabilité des massifs rocheux. Bull. Dir. Étud. Rech. Electr. Fr., A, 3, 5-132.

Maillet, E. (1905): Essais d`hydraulique souterraine et fluviale. Hermann, Paris.

Mangin, A. (1971): Etude des débits classés d'exutoires karstiques portant sur un cycle hydrologique. Annales de spéléologie, 28(1), 21-40.

Mangin, A. (1975): Contribution a l`étude hydrodynamique des aquifères karstiques. Thèse, Institut des Sciences de la Terre de l`Université de Dijon.

Mangin, A. (1981): Utilisation des analyses correlatoire et spectrale dans l'approche des systèmes hydrologiques. Comptes Rendus de l'Académie des Sciences, Série III, 293, 401-404.

Mangin, A. (1982): L'approche systémique du karst, conséquences conceptuelles et méthodologiques. Proc. Réunion Monographica sobre el karst, Larra, 141-157

Mangin, A (1984): Pour une meilleure connaissance des systèmes hydrologiques à partir des analyses corrélatoire et spectrale. Journal of Hydrology, 67, 25-43.

Mero, F. (1963): Application of the groundwater depletion curves in analyzing and forecasting spring discharges influenced by well fields. Symposium on surface waters, General assembly of Berkeley of IUGG, 63, 107-117. IAHS Publication.

Mero, F. (1969): An approach to daily hydrometeorological water balance computations for surface and groundwater basins. Proceedings ITC-UNESCO, Seminar for integrated river basin development.

Mero, F. & Gilboa, Y. (1974): A methodology for the rapid evaluation of groundwater resources, Sao Paulo State, Brazil. Bulletin des Sciences Hydrogéologiques, 19(3), 347-358.

MFR Géologie-Géotechnique SA. (1993) : N16 Sections 1-2. Etude géologique et hydrogéologique. Campagne de sondages 1991 (Rapport géologique N°4). Service des Ponts et Chaussées, Delémont, 19 p.

MFR Géologie-Géotechnique SA. (1996): N16 Sections 1-3. Secteur Boncourt - Courtedoux. Reconnaissances par sondages carottés Campagne 1993-Lots 20.10 et 2.011. Etude géologique et géotechnique. Dossier de référence des sondages. Service des Ponts et Chaussées, Delémont.

Militzer, H., Rsler, R. & Lsch, W. (1979): Theorethical and experimental investigations for cavity research with geoelectrical resistivity methods. Geophys. Prosp., 27, 640-652.

Mohrlok, U. (1996): Parameter-identifikation in doppel-kontinuum-modelen am beispiel von karstaquiferen. Ph.D. thesis, University of Tubingen.

Mohrlok, U. & Teutsch, G. (1997): Double continuum porous equivalent (DCPE) versus discrete modeling in karst terranes. In: Günay & Johnson eds., Karst waters and environmental impacts, Balkema, Rotterdam.

Müller, I. (1982) : Rôle de la prospection électromagnétique VLF (Very Low Frequency) pour la mise en valeur et la prospection des aquifères calcaires. Annales Scientifiques de l'Université de Besançon, 1, 367-380.

Neuman, S.P. & De Marsily, G. (1976): Identification of linear system response by parametric programming. Water Resources Research, 12(2), 253-262.

Padilla, A. & Pulido-Bosch, A. (1995): Study of hydrographs of karstic aquifers by means of correlation and cross-spectral analysis. Journal of Hydrology, 168, 73-89.

Perrin, J. (2002): A conceptual model of flow and transport in a karst aquifer based on spatial and temporal variations of natural tracers. Ph.D. thesis, CHYN, Université de Neuchâtel. 158 p.

Perrochet, P. (1994): Modélisation des écoulements souterrains: Méthodes de simulation numérique. Manuscrit, Université de Neuchâtel.

Puech, V. (1996) : Etude préliminaire à une classification des zones épikarstiques en fonction de leurs propriétés hydrauliques. Travail de diplôme. CHYN, Université de Neuchâtel. 104 p.

Sauter, M. (1992): Quantification and forecasting of regional groundwater flow and transport in a karst aquifer (gallusquelle, malm, SW. Germany). Ph.D. thesis, University of Tübingen.

Service Géologique National Francais (1985): Carte géologique de la France à 1/50000, Delle. Bureau de Recherches Géologiques et Minières, Orléans.

Snow, D.T. (1969) : Anisotropic permeability of fractured media. Water Resources Research, 5(6), 1273-1289.

Strickler, A. (1923): Beitrage zur frage der geschwindigkeitsformel und der rauhigkeitszahlen für störme, kanale und geschlossene leitungen. Mitt. Amt. für Wasserwirt, 16, 21-38.

Teutsch, G. (1988): Grundwassermodele im karst: Praktische ansatze am beispiel zweier einzugsgebiete im tiefen und seichten malmkarst der Swabischer Alb. Ph.D. thesis, University of Tubingen.

Teutsch, G. & Sauter, M. (1991): Groundwater modeling in karst terranes: Scale effects, data aquisistion and field validation. 3rd Conference on hydrology, ecology, monitoring and management of ground water in karst terranes, Nashwille, USA.

Teutsch, G. & Sauter, M. (1998): Distributed parameter modeling approaches in karst-hydrological investigations. Bulletin d'Hydrogéologie de l'Université de Neuchâtel, 16, 99-109.

Thrailkill, J., Sullivan, S.B. & Gouzie, D.R. (1991): Flow parameters in a shallow conduit-flow carbonate aquifer, Inner Bluegrass Karst Region, Kentucky, USA. Journal of Hydrology, 129, 87-108.

Tierrin, R. (1996) : Contribution à l'étude de la circulation hzdraulique dans l'épikarst, site du Maira (JU). Travail de diplôme. CHYN, Université de Neuchâtel. 44 p.

Turberg, P. & Müller, I. (1992) : La méthode inductive VLF-EM pour la prospection hydrogéologique en continu du milieu fissuré. Annales Scientifiques de l'Université de Besançon, Mémoire hors série 11, 207-214.

Wang, H.F. & Anderson, M.P. (1982): Introduction to groundwater modeling. W.H. Freeman and Co., San Francisco, USA

Warren, J.E. & Root, P.J. (1963): The behavior of naturally fractured reservoirs. Soc. Pet. Eng. J., 3, 245-255.

WASY Ltd. (2002): FEFLOW 5.0 – A finite element subsurface flow and transport simulation system. Program package and reference manual. Berlin.

Witherspoon, P.A., Wang, J.S.Y., Iwai, K. & Gale, J.E. (1980): Validity of cubic law for fluid flow in a deformable rock fracture. Water Resources Reasarch, 16(6), 1016-1024

LIST OF SYMBOLS

A	Aquifer area [L^2]
A_c	Cross-sectional area of a conduit [L^2]
A_f	Cross-sectional area of a fracture [L^2]
a	Fracture aperture [L]
α	Recession coefficient [T^{-1}]
α_{epi}	Recession coefficient of the epikarst [T^{-1}]
α_b	Recession coefficient of a homogeneous block [T^{-1}]
α_{eq}	Recession coefficient of equivalent medium [T^{-1}]
α_h	Recession coefficient of heterogeneous medium [T^{-1}]
D_h	Hydraulic diameter [L]
E_w	Bulk modulus of water compression [$ML^{-1}T^{-2}$]
f	Conduit frequency [L^{-1}]
f^*	Threshold conduit frequency [L^{-1}]
g	Acceleration due to gravity [LT^{-2}]
γ	Geometric parameter [-]
H	Hydraulic head [L]
K	Laminar hydraulic conductivity [LT^{-1}]
K'	Turbulent hydraulic conductivity [LT^{-1}]
K_m	Matrix conductivity [LT^{-1}]
K_c	Laminar conduit conductivity [L^3T^{-1}]
K_c'	Turbulent conduit conductivity [L^3T^{-1}]
K_c^*	Threshold laminar conduit conductivity [L^3T^{-1}]
K_s	Strickler coefficient [$L^{1/3}T^{-1}$]
μ	Dynamic viscosity of water [$ML^{-1}T^{-1}$]
Q	Discharge [L^3T^{-1}]
r	Conduit radius [L]
R_h	Hydraulic radius [L]
ρ	Density [ML^{-3}]
S_s	Specific storage coefficient [L^{-1}]
S	Storativity [-]
S_m	Matrix storativity [-]
S_f	Fracture storativity [-]
S_c	Conduit storativity [L]
S_{eq}	Equivalent storativity [-]
T	Hydraulic transmissivity [L^2T^{-1}]
T_m	Matrix transmissivity [L^2T^{-1}]
T_{eq}	Equivalent transmissivity [L^2T^{-1}]
v	Average groundwater velocity [LT^{-1}]
w	Fracture width [L]

A GIS BASED INTEGRATED APPROACH FOR MODELING FLOW IN KARST AQUIFERS

1. INTRODUCTION

Different types of field data, the numerous conceptual models evaluations, and the large number of numerical simulations performed in the course of the present research (called KARSTMOD hereafter), required the application of a data management, data transformation and visualization tool. This tool has been employed for the following activities:

- transforming field observations into digital information accessible for further mathematical operations, and for groundwater flow modeling
- performing mathematical transformations of field data and of simulation results
- synthesis of geological, hydrogeological and geographical information for the research site
- establishing a database, which can easily be incorporated into future research activities
- facilitating the visualisation of field data and groundwater flow simulation results

These requirements have been satisfied by integrating a GIS system into the overall research procedure. In fact, GIS provided a crucial nexus between field data, conceptual models and numerical models as demonstrated in **Figure 1**.

2. FUNDAMENTALS OF GIS

A GIS (Geographical Information System) consists of a powerful set of tools for collecting, storing, retrieving, transforming and displaying real-world spatial data at will (Burrough, 1986).

Real-world data can be described in two, fundamentally different manners. *Vector data models* perceive the space as being occupied by entities which are described by their attributes or properties, and whose position can be mapped using a geometric coordinate system (1). The fundamental entity types in a vector data model are points, lines and polygons.

In contrast, *raster data models* represent an attribute of interest varying over the space as some continuous mathematical function or field (2). The fundamental entity types in a raster data model are pixels (in 2D) or voxels (in 3D).

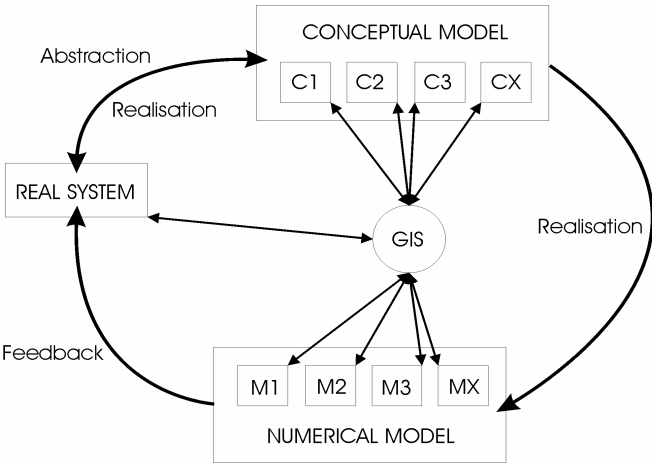

Figure 1. The role of GIS in the KARSTMOD research project. GIS provides a crucial nexus between field data, conceptual models (C_x) and numerical models (M_x)

Not all kinds of geographical data can be represented using both vector and raster data models. Certain data types such as spatial objects favor the use of the vector data model, while others (for example spatially varying data fields) are more conveniently represented using raster data models. The principal data types and their representation by vector and raster data models are summarized in **Figure 2**.

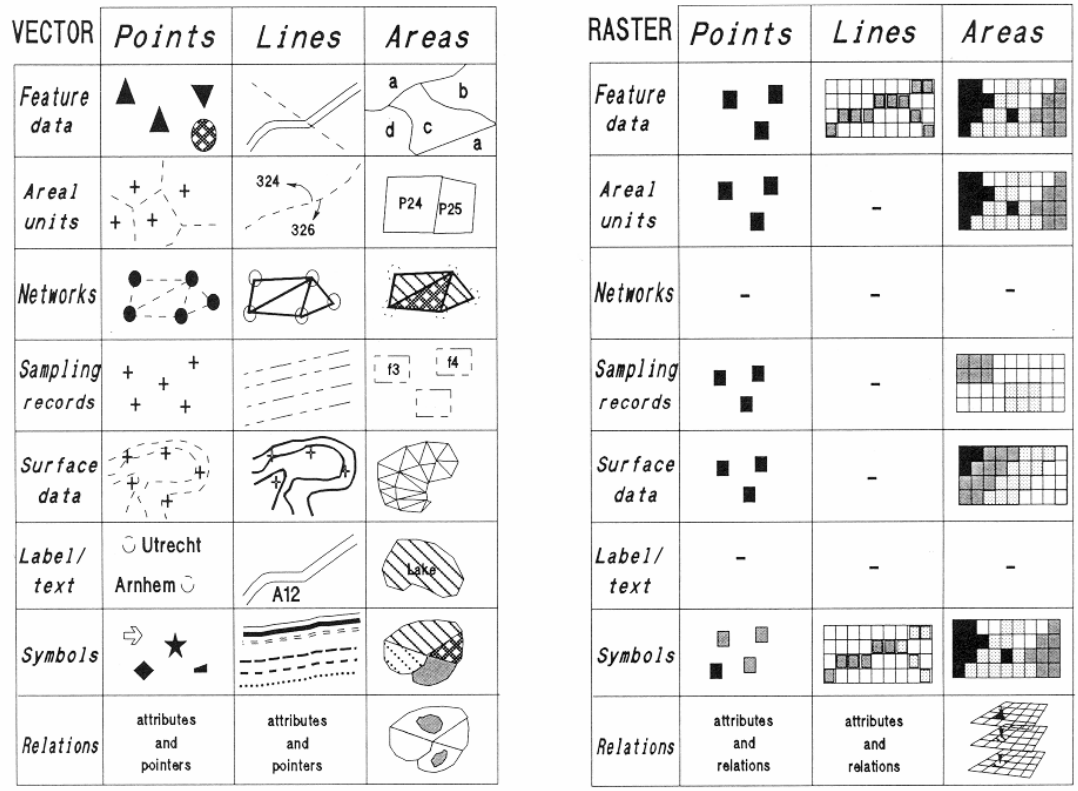

Figure 2. Different means of graphically displaying data encapsulated by vector and raster models. Borrough & McDonnel (1998).

The data linked to each of the entities have either qualitative or nominal attributes, and quantitative data or numbers. A computer program that is designed to store and manage these data is called a database management system (DBMS). There are four fundamental ways of organizing information in modern DBMS: hierarchical, network, relational or object-oriented schemata.

- Hierarchical database structure employs a parent/child or one-to-many relation. In this structure each part of the hierarchy can be reached using a key.
- In a network database structure the linkage of data is solved by ring pointer structures.
- In a relational database structure there are no pointers and has no hierarchy. Instead, the data are stored in simple records; known as tuples, which are sets of fields each containing an attribute.
- The object-oriented database structure is a further development of the network model, which enables the interconnectivity and ownership relations between spatial entities to be modeled effectively. The characteristics of an object may be described in the database in terms of its attributes as well as a set of procedures which describe its behavior.

3. THE KARSTMOD DATABASE

In the course of the present research the ArcView/ArcInfo GIS software package was applied. This GIS package involves a relational database system (INFO), which has the advantage that its structure is very flexible and may meet the demands of all queries. This system allows different kinds of data to be treated, combined, and compared. Addition or deletion of data is simple. The relational organization of data involved in the INFO database system is schematized in **Figure 3**.

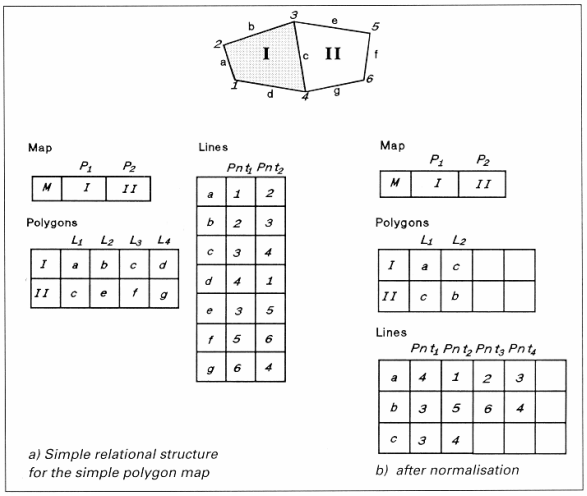

Figure 3. Relational organization of vector data. From Borrough & McDonnel (1998).

The spatial information involved in the KARSTMOD research include geomorphological, geophysical, geological, and hydrogeological data. The different entities or field values of identical type constituting these information are organized in themes (ArcView) or coverages (ArcInfo) (ESRI, 1992). Themes or coverages have the same coordinate reference system, and they constitute a multi-layer information structure as represented in **Figure 4**.

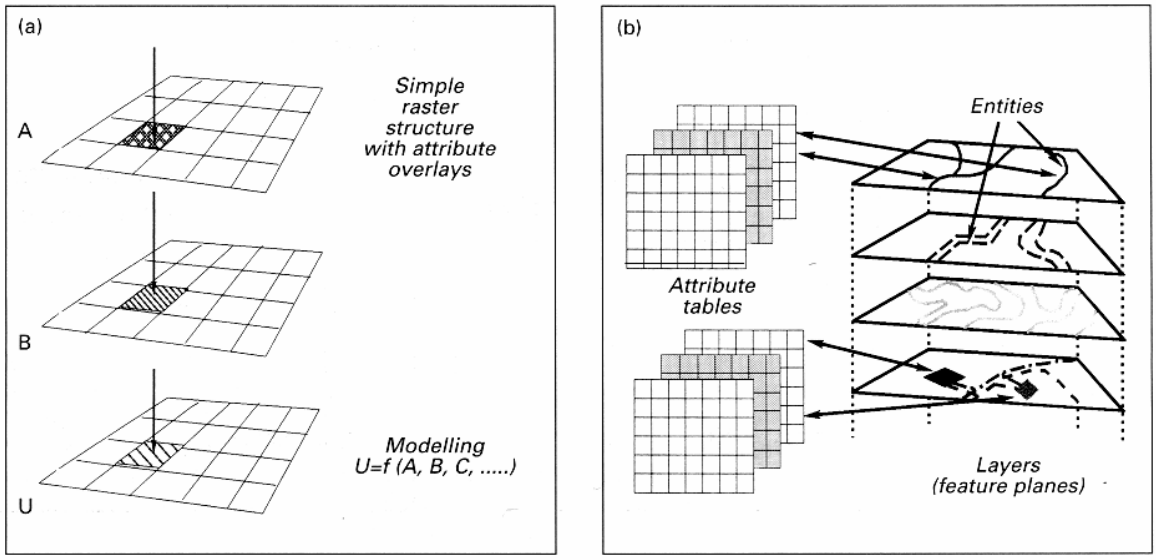

Figure 4. Organization of spatial data in data layers (represented by themes or coverages) in (a) raster and (b) vector data structures (Borrough & McDonnel 1998).

The information obtained and produced in the course of the KARSTMOD research has been organized in several themes. The themes containing the most important raw information that were used for further GIS operations and groundwater flow modeling are represented in **Table 1.**

TYPE OF INFORMATION	COVERAGE	ENTITY TYPE	DATA SOURCE	SCALE
Geographical	DEM	r	OFT (2000a)	1:25000
	landuse	ply	OFT (2000b)	1:25000
	cave geometry	lin	Heller (1983)	1:10000
	cave geometry	pnt	Heller (1983)	1:10000
	railways	lin	OFT (2000b)	1:25000
	roads	lin	OFT (2000b)	1:25000
	landmarks	pnt	OFT (2000b)	1:25000
	landmarks	lin	OFT (2000b)	1:25000
	hydrography	lin	OFT (2000b)	1:25000
Geological	geology	lin, ply	Kovács & Jeannin (2003)	1:25000
	tectonics	lin	Kovács & Jeannin (2003)	1:25000
	boreholes	pnt	MFR (2001)	1:25000
	quaternary sediments	ply	SGNF (1985), Laubscher (1963), Liniger (1970)	1:50000 1:25000
Hydrogeological	springs	pnt	Gretillat (1996)	1:25000
	piezometers	pnt	MFR (2001)	1:25000
	observation points	pnt	Perrin (2002)	1:25000
	site boundary	lin	Kovács & Jeannin (2003)	1:25000
	Tracer injections	pnt	Favre (2001)	1:10000
	Tracer observ.	pnt	Favre (2001)	1:10000
	Tracer flowpaths	lin	Favre (2001)	1:10000

Table 1. GIS information layers (themes) of raw data involved in the KARSTMOD research (DEM: digital elevation model, r: raster, pnt: point, lin: line, ply: polygon).

Higher order data themes have been obtained by simple or sometimes more complicated mathematical operations. These include GIS operations like raster data queries and calculations, interpolation, contouring, conversion between raster and vector data models, cleaning input data and building topology, geoprocessing (merge, clip, intersect, union), buffering, etc. Similarly, the results of spatial information obtained from numerical groundwater flow simulations have been transformed in raster data themes. Some of the most important themes involved in the KARSTMOD research are demonstrated in **Table 2**.

TYPE OF INFORMATION	COVERAGE	ENTITY TYPE	SCALE	RESOLUTION (m)
Geological	Top of Oxfordian Marls	ply, tin, r	1:25000	25
	Bottom of Astarte Marls	ply, tin, r	1:25000	25
	Top of Astarte marls	ply, tin, r	1:25000	25
	Aquifer thickness	r	1:25000	25
Hydrogeological	Water table	r	1:50000	100
	Saturated zone thickness	r	1:50000	100
	Unsaturated zone thickness	r	1:50000	100
	Shallow karst zones	ply	1:50000	-
	Minimum saturated thickness	r	1:50000	25
	Confined aquifer zones	ply	1:50000	-
	Confined flow zones	ply	1:50000	-
	Water catchments	ply	1:25000	-
	Simulated hydraulic heads	r	1:10000	25 – 100
	Discrete feature buffers	ply	1:10000	-
	Extended conduit networks	lin	1:25000	-
	Regular conduit netwoks	lin	1:25000	-
	Finite element supermeshes	lin, ply	1:25000	-
	Finite element meshes	lin, ply	1:10000	-

Table 2. GIS information layers (themes) of data obtained from GIS operations and groundwater flow modeling. (r: raster, lin: line, ply: polygon, tin: triangular irregular network).

Digital information included in a theme is usually organized in one or several files. Depending on the type of entities included in a theme and on the computer program it is generated by/for, several file formats are used in modern GIS systems. In order to allow efficient accessing and data retrieval, theme files have been further organized in the following folders:

- DIG_DATA: ASCII files of raw digitalized data (.dig)
- ASCII_DATA: ArcInfo generate files (.pnt, .lin,.ply)
- ARCINFO_DATA: Arcinfo coverages and interchange files (.e00)
- EXCEL_DATA: Pointwise data themes (.xls)
- DBF_DATA: Pointwise data themes (.dbf)
- GRID_DATA: ArcView/ArcInfo raster data themes
- SHP_DATA: ArcView shapefiles (.dbf, .shp, .shx)
- IMAGE_DATA: Georeferenced background images (.tif)
- ARCVIEW_PROJECT: Arcview project files (.apr)
- ARCVIEW_LEGENDS: ArcView legend files (.avl)

4. A GIS-BASED WORK SCHEME FOR MODELING KARST AQUIFERS

Any comprehensive hydrogeological study requires the synthesis of spatial information, and hydrogeological modeling which is not only a standard requirement, but often the only efficient tool for the coherent synthesis and interpretation of a hydrogeological situation; this always necessitates the management of digital data. Data management and groundwater flow modeling take up a significant part of the work effort and time, and an inappropriate planning of the work plan can entail considerable deficits and the deterioration of the quality of results.

The overall work plan for constructing efficient groundwater flow models of karst aquifers based on the experience gained in the course of this research is demonstrated in **Figure 5**. This schemata follows the steps below:

1. Reconnaissance mapping : Collection of geographical information such as topography, hydrography, and karstic landforms. Delimitation of hydraulic boundaries.
2. Synthesis of geological and geophysiscal data (maps, cross sections, borehole logs) into a three-dimensional structural-hydrostratigraphical model that contains aquifer bottom topography, fractures, and structural surfaces.
3. Retrieval of hydraulic and hydrochemical data : Piezometric levels in low-permeability blocks and in karst conduits, spring hydrographs, chemical components.
4. Transformation of geological, geographical and hyrdogeological data in a digital form: digitizing maps and observation points.
5. Clarification of raw digital maps and attribute data, building topology.
6. Generation of the extended regular or irregular conduit network based on the information obtained from analytical formulae (Chapter 5)
7. Unifying relevant hydraulic limits and discrete features: generation of the "superelement mesh".
8. Generation of the finite element mesh.
9. Implementation of the conduit network into the finite element mesh
10. Generation of continuous fields of aquifer structural surfaces and of matrix hydraulic parameters using geostatistical methods; extraction of field values to finite element nodes.
11. Model simulation
12. Extraction of simulation results
13. Verification of results by comparing simulation results with field measurements and critical surfaces such as surface topography and aquifer base. Calculation of simulated recession coefficient and comparison of simulated discharges with spring hydrographs.
14. Modification of input hydraulic parameters and repetition of steps 11-14 until obtaining satisfactory results.
15. Visualisation and interpretation of results.

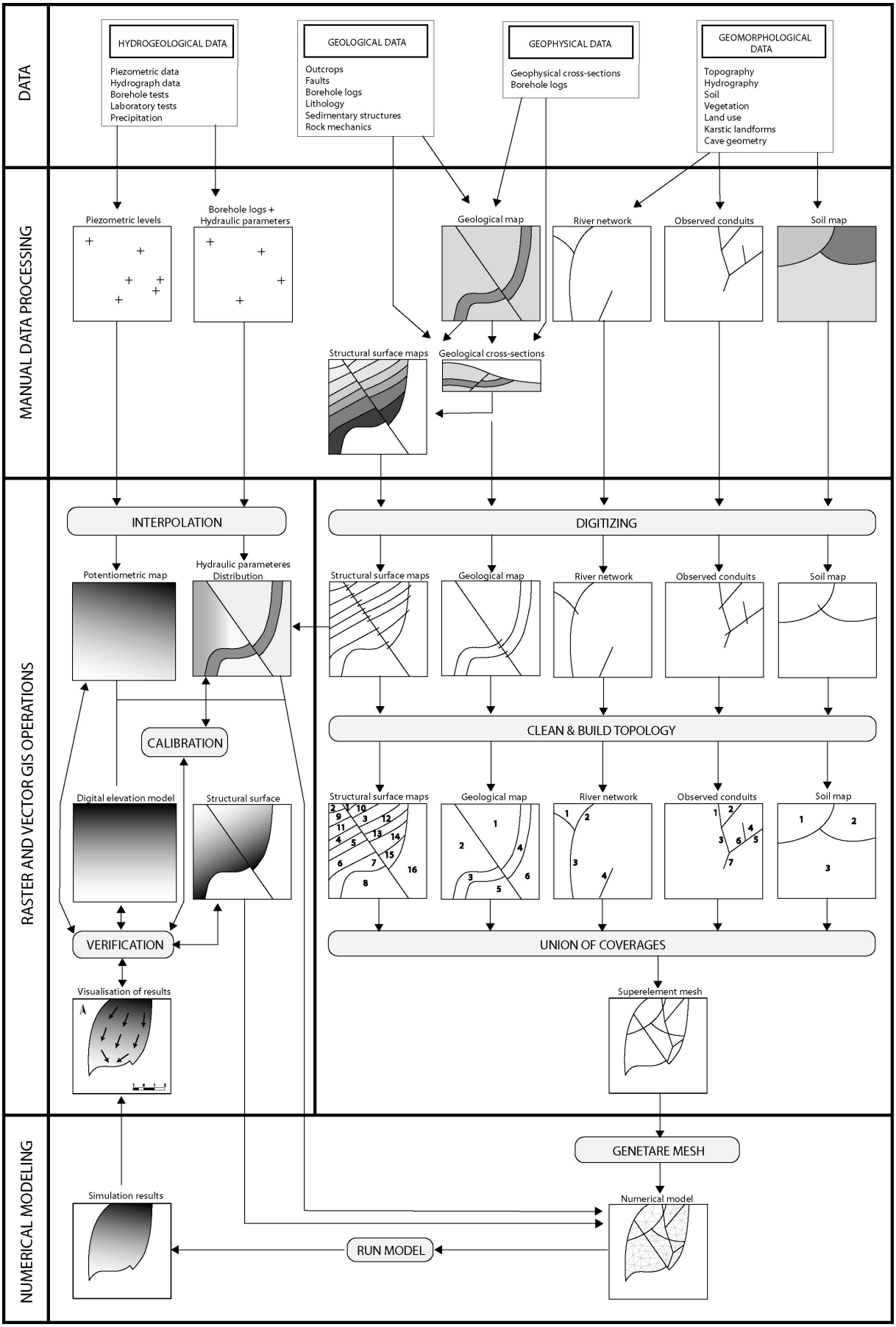

Figure 5. Work scheme for constructing efficient groundwater flow models of karst aquifers.

REFERENCES

Burrough, P.A. (1986): Principles of Geographical Information Systems for land resources assessment. Oxford University Press, Oxford.

Burrough, P.A. & McDonnel, R.A. (1998): Principles of Geographical Information Systems. Oxford University Press, New York.

Environmental System Research Institute (1992): Understanding GIS. Environmental System Research Institute, Redlands.

Favre, I. (2001) : Base de données des essais de traçage du plateau karstique de Bure (JU), SIG, interprétations statistiques. Travail de diplôme, Université de Neuchâtel.

Gretillat, P.-A. (1996) : Aquiferes karstiques et poreux de l'Ajoie (Jura, Suisse). Thèse, CHYN, Université de Neuchâtel.

Heller M., (1983) : L'ordinateur au service du spéléologue cartographe. Stalactite, 1983(1), 9-27.

Kovács A., & Jeannin P-Y. (2003): Hydrogeological overview of the Bure Plateau, Ajoie, Switzerland. Eclogae Geologicae Helvetiae, Accepted

Laubscher, H.P. (1963): Erläuterungen zum Geologischen Atlas der Schweiz. 1085 St-Ursanne. Kümmerly & Frey AG, Bern.

Liniger, H. (1970): Erläuterungen zum Geologischen Atlas der Schweiz. 1065 Bonfol. Kümmerly & Frey AG, Bern.

MFR Géologie-Géotechnique SA. (2001) : A16 Section 2 Projet définitif. Tunnel de Bure. Galerie de reconnaissance - Rapport géologique-géotechnique final. Tunnel - Etude géologique-géotechnique prévisionnelle. Service des Ponts et Chaussées. Rapport inedit, Delémont.

Office Fédéral de Topographie de la Suisse (2000a) : Atlas numérique de la Suisse, Modèle Numérique de Terrain a 25 m, feuilles 1064, 1065, 1084, 1085, Wabern.

Office Fédéral de Topographie de la Suisse (2000b) : Atlas numérique de la Suisse, Modèle Vectorielle, Wabern.

Perrin, J. (2002): A conceptual model of flow and transport in a karst aquifer based on spatial and temporal variations of natural tracers. Ph.D. thesis, CHYN, Université de Neuchâtel. 158 p.

Service Géologique National Français (1985) : Carte géologique de la France à 1/50000, Delle. Bureau de Recherches Géologiques et Minières, Orléans.

2D SYNTHETIC DISCRETE-CONTINUUM MODELS OF KARST SYSTEMS: APPLIED PARAMETERS AND SIMULATION RESULTS

MODEL	$A(m^2)$	T_m (m^2/s)	S_m (-)	K_C (m^3/s)	S_C (-)	f (1/m)	α_{sim} (1/d)	α_{MRFR} (1/d)	α_{CIFR} (1/d)	DOMAIN
chgKc_1E+2_a	2.30E+07	1.00E-05	1.00E-04	1.00E+02	2.14E-07	4.17E-04	2.97E-02	2.97E-02	1.04E+00	MR
chgKc_1E+2_b	2.30E+07	1.00E-05	1.00E-04	1.00E+02	2.14E-07	8.33E-04	1.21E-01	1.18E-01	2.08E+00	MR
chgKc_1E+2_c	2.30E+07	1.00E-05	1.00E-04	1.00E+02	2.14E-07	1.66E-03	4.63E-01	4.70E-01	4.15E+00	MR
chgKc_1E+2_d	2.30E+07	1.00E-05	1.00E-04	1.00E+02	2.14E-07	3.33E-03	1.74E+00	1.89E+00	8.33E+00	MR
chgKc_1E+2_e	2.30E+07	1.00E-05	1.00E-04	1.00E+02	2.14E-07	6.66E-03	6.09E+00	7.56E+00	1.67E+01	MR
chgKc_1E+2_f	2.30E+07	1.00E-05	1.00E-04	1.00E+02	2.14E-07	1.33E-02	1.83E+01	3.03E+01	3.33E+01	TR
chgKc_5E+1_a	2.30E+07	1.00E-05	1.00E-04	5.00E+01	1.70E-07	4.17E-04	2.96E-02	2.97E-02	5.22E-01	MR
chgKc_5E+1_b	2.30E+07	1.00E-05	1.00E-04	5.00E+01	1.70E-07	8.33E-04	1.16E-01	1.18E-01	1.04E+00	MR
chgKc_5E+1_c	2.30E+07	1.00E-05	1.00E-04	5.00E+01	1.70E-07	1.66E-03	4.44E-01	4.70E-01	2.08E+00	MR
chgKc_5E+1_d	2.30E+07	1.00E-05	1.00E-04	5.00E+01	1.70E-07	3.33E-03	1.58E+00	1.89E+00	4.16E+00	MR
chgKc_5E+1_e	2.30E+07	1.00E-05	1.00E-04	5.00E+01	1.70E-07	6.66E-03	4.91E+00	7.56E+00	8.33E+00	TR
chgKc_5E+1_f	2.30E+07	1.00E-05	1.00E-04	5.00E+01	1.70E-07	1.33E-02	1.25E+01	3.03E+01	1.67E+01	CI
chgSm_1E-3_a	2.30E+07	1.00E-05	1.00E-03	1.00E+02	2.14E-07	4.17E-04	2.90E-03	2.97E-03	1.04E-01	MR
chgSm_1E-3_b	2.30E+07	1.00E-05	1.00E-03	1.00E+02	2.14E-07	8.33E-04	1.20E-02	1.18E-02	2.08E-01	MR
chgSm_1E-3_c	2.30E+07	1.00E-05	1.00E-03	1.00E+02	2.14E-07	1.66E-03	4.60E-02	4.70E-02	4.15E-01	MR
chgSm_1E-3_d	2.30E+07	1.00E-05	1.00E-03	1.00E+02	2.14E-07	3.33E-03	1.74E-01	1.89E-01	8.33E-01	MR
chgSm_1E-3_e	2.30E+07	1.00E-05	1.00E-03	1.00E+02	2.14E-07	6.66E-03	6.09E-01	7.56E-01	1.67E+00	MR
chgSm_1E-3_f	2.30E+07	1.00E-05	1.00E-03	1.00E+02	2.14E-07	1.33E-02	1.84E+00	3.03E+00	3.33E+00	TR
chgSm_1E-4_a	2.30E+07	1.00E-03	1.00E-04	1.00E+02	2.14E-07	4.17E-04	1.89E+00	2.97E+00	1.07E+00	CI
chgSm_1E-4_b	2.30E+07	1.00E-03	1.00E-04	1.00E+02	2.14E-07	8.33E-04	4.10E+00	1.18E+01	2.11E+00	CI
chgSm_1E-4_c	2.30E+07	1.00E-03	1.00E-04	1.00E+02	2.14E-07	1.66E-03	7.42E+00	4.70E+01	4.18E+00	CI
chgSm_1E-4_d	2.30E+07	1.00E-03	1.00E-04	1.00E+02	2.14E-07	3.33E-03	1.27E+01	1.89E+02	8.35E+00	CI
chgSm_1E-4_e	2.30E+07	1.00E-03	1.00E-04	1.00E+02	2.14E-07	6.66E-03	2.14E+01	7.56E+02	1.67E+01	CI
chgSm_1E-4_f	2.30E+07	1.00E-03	1.00E-04	1.00E+02	2.14E-07	1.33E-02	3.64E+01	3.03E+03	3.34E+01	CI
chgKc_1E+1_a	2.30E+07	1.00E-05	1.00E-04	1.00E+01	9.95E-08	4.17E-04	2.80E-02	2.97E-02	1.05E-01	MR
chgKc_1E+1_b	2.30E+07	1.00E-05	1.00E-04	1.00E+01	9.95E-08	8.33E-04	1.04E-01	1.18E-01	2.09E-01	MR
chgKc_1E+1_c	2.30E+07	1.00E-05	1.00E-04	1.00E+01	9.95E-08	1.66E-03	3.30E-01	4.70E-01	4.15E-01	TR
chgKc_1E+1_d	2.30E+07	1.00E-05	1.00E-04	1.00E+01	9.95E-08	3.33E-03	8.50E-01	1.89E+00	8.33E-01	CI
chgKc_1E+1_e	2.30E+07	1.00E-05	1.00E-04	1.00E+01	9.95E-08	6.66E-03	1.79E+00	7.56E+00	1.67E+00	CI
chgKc_1E+1_f	2.30E+07	1.00E-05	1.00E-04	1.00E+01	9.95E-08	1.33E-02	3.38E+00	3.03E+01	3.33E+00	CI
chgSm_1E-2_a	2.30E+07	1.00E-05	1.00E-02	1.00E+02	2.14E-07	8.33E-04	1.20E-03	1.18E-03	2.08E-02	MR
chgSm_1E-2_b	2.30E+07	1.00E-05	1.00E-02	1.00E+02	2.14E-07	1.66E-03	4.70E-03	4.70E-03	4.15E-02	MR
chgSm_1E-2_c	2.30E+07	1.00E-05	1.00E-02	1.00E+02	2.14E-07	3.33E-03	1.75E-02	1.89E-02	8.33E-02	MR
chgSm_1E-2_d	2.30E+07	1.00E-05	1.00E-02	1.00E+02	2.14E-07	6.66E-03	6.08E-02	7.56E-02	1.67E-01	MR
chgSm_1E-2_e	2.30E+07	1.00E-05	1.00E-02	1.00E+02	2.14E-07	1.33E-02	1.83E-01	3.03E-01	3.33E-01	TR

MODEL	A(m^2)	T_m (m^2/s)	S_m (-)	K_C (m^3/s)	S_C (-)	f (1/m)	α_{sim} (1/d)	α_{MRFR} (1/d)	α_{CIFR} (1/d)	DOMAIN
chgTm_1E-4_a	2.30E+07	1.00E-04	1.00E-02	1.00E+02	2.14E-07	4.17E-04	2.80E-03	2.97E-03	1.05E-02	MR
chgTm_1E-4_b	2.30E+07	1.00E-04	1.00E-02	1.00E+02	2.14E-07	8.33E-04	1.04E-02	1.18E-02	2.09E-02	MR
chgTm_1E-4_c	2.30E+07	1.00E-04	1.00E-02	1.00E+02	2.14E-07	1.66E-03	3.30E-02	4.70E-02	4.15E-02	TR
chgTm_1E-4_d	2.30E+07	1.00E-04	1.00E-02	1.00E+02	2.14E-07	3.33E-03	8.50E-02	1.89E-01	8.33E-02	CI
chgTm_1E-4_e	2.30E+07	1.00E-04	1.00E-02	1.00E+02	2.14E-07	6.66E-03	1.79E-01	7.56E-01	1.67E-01	CI
chgTm_1E-4_f	2.30E+07	1.00E-04	1.00E-02	1.00E+02	2.14E-07	1.33E-02	3.38E-01	3.03E+00	3.33E-01	CI
chgSm_1E-1_a	2.30E+07	1.00E-05	1.00E-01	1.00E+02	2.14E-07	1.66E-03	4.70E-04	4.70E-04	4.15E-03	MR
chgSm_1E-1_b	2.30E+07	1.00E-05	1.00E-01	1.00E+02	2.14E-07	3.33E-03	1.76E-03	1.89E-03	8.33E-03	MR
chgSm_1E-1_c	2.30E+07	1.00E-05	1.00E-01	1.00E+02	2.14E-07	6.66E-03	6.10E-03	7.56E-03	1.67E-02	MR
chgSm_1E-1_d	2.30E+07	1.00E-05	1.00E-01	1.00E+02	2.14E-07	1.33E-02	1.84E-02	3.03E-02	3.33E-02	TR
chgTm_1E-3_a	2.30E+07	1.00E-03	1.00E-02	1.00E+02	2.14E-07	4.17E-04	1.90E-02	2.97E-02	1.07E-02	CI
chgTm_1E-3_b	2.30E+07	1.00E-03	1.00E-02	1.00E+02	2.14E-07	8.33E-04	4.10E-02	1.18E-01	2.11E-02	CI
chgTm_1E-3_c	2.30E+07	1.00E-03	1.00E-02	1.00E+02	2.14E-07	1.66E-03	7.40E-02	4.70E-01	4.18E-02	CI
chgTm_1E-3_d	2.30E+07	1.00E-03	1.00E-02	1.00E+02	2.14E-07	3.33E-03	1.26E-01	1.89E+00	8.35E-02	CI
chgTm_1E-3_e	2.30E+07	1.00E-03	1.00E-02	1.00E+02	2.14E-07	6.66E-03	2.13E-01	7.56E+00	1.67E-01	CI
chgTm_1E-3_f	2.30E+07	1.00E-03	1.00E-02	1.00E+02	2.14E-07	1.33E-02	3.64E-01	3.03E+01	3.34E-01	CI
chgKc_1E-0_a	2.30E+07	1.00E-05	1.00E-04	1.00E+00	4.62E-08	4.17E-04	1.89E-02	2.97E-02	1.07E-02	CI
chgKc_1E-0_b	2.30E+07	1.00E-05	1.00E-04	1.00E+00	4.62E-08	8.33E-04	4.10E-02	1.18E-01	2.11E-02	CI
chgKc_1E-0_c	2.30E+07	1.00E-05	1.00E-04	1.00E+00	4.62E-08	1.66E-03	7.40E-02	4.70E-01	4.18E-02	CI
chgKc_1E-0_d	2.30E+07	1.00E-05	1.00E-04	1.00E+00	4.62E-08	3.33E-03	1.26E-01	1.89E+00	8.35E-02	CI
chgKc_1E-0_e	2.30E+07	1.00E-05	1.00E-04	1.00E+00	4.62E-08	6.66E-03	2.13E-01	7.56E+00	1.67E-01	CI
chgKc_1E-0_f	2.30E+07	1.00E-05	1.00E-04	1.00E+00	4.62E-08	1.33E-02	3.64E-01	3.03E+01	3.34E-01	CI
chgTm_1E-2_a	2.30E+07	1.00E-02	1.00E-02	1.00E+02	2.14E-07	4.17E-04	4.00E-02	2.97E-01	1.29E-02	CI
chgTm_1E-2_b	2.30E+07	1.00E-02	1.00E-02	1.00E+02	2.14E-07	8.33E-04	5.70E-02	1.18E+00	2.33E-02	CI
chgTm_1E-2_c	2.30E+07	1.00E-02	1.00E-02	1.00E+02	2.14E-07	1.66E-03	8.60E-02	4.70E+00	4.40E-02	CI
chgTm_1E-2_d	2.30E+07	1.00E-02	1.00E-02	1.00E+02	2.14E-07	3.33E-03	1.34E-01	1.89E+01	8.58E-02	CI
chgTm_1E-2_e	2.30E+07	1.00E-02	1.00E-02	1.00E+02	2.14E-07	6.66E-03	2.19E-01	7.56E+01	1.69E-01	CI
chgTm_1E-2_f	2.30E+07	1.00E-02	1.00E-02	1.00E+02	2.14E-07	1.33E-02	3.68E-01	3.03E+02	3.36E-01	CI
chgA_2400_a	5.76E+06	1.00E-04	1.00E-02	1.00E+02	2.14E-07	8.33E-04	1.17E-02	1.18E-02	8.34E-02	MR
chgA_2400_b	5.76E+06	1.00E-04	1.00E-02	1.00E+02	2.14E-07	1.66E-03	4.50E-02	4.70E-02	1.66E-01	MR
chgA_2400_c	5.76E+06	1.00E-04	1.00E-02	1.00E+02	2.14E-07	3.33E-03	1.60E-01	1.89E-01	3.33E-01	MR
chgA_2400_d	5.76E+06	1.00E-04	1.00E-02	1.00E+02	2.14E-07	6.66E-03	4.87E-01	7.56E-01	6.66E-01	TR
chgA_2400_e	5.76E+06	1.00E-04	1.00E-02	1.00E+02	2.14E-07	1.33E-02	1.21E+00	3.03E+00	1.33E+00	CI

MODEL	A(m^2)	T_m (m^2 /s)	S_m (-)	K_C (m^3/s)	S_C (-)	f (1/m)	α_{sim} (1/d)	α_{MRFR} (1/d)	α_{CIFR} (1/d)	DOMAIN
chgA_9600_a	9.22E+07	1.00E-04	1.00E-02	1.00E+02	2.14E-07	4.17E-04	2.30E-03	2.97E-03	2.61E-03	CI
chgA_9600_b	9.22E+07	1.00E-04	1.00E-02	1.00E+02	2.14E-07	8.33E-04	6.10E-03	1.18E-02	5.21E-03	CI
chgA_9600_c	9.22E+07	1.00E-04	1.00E-02	1.00E+02	2.14E-07	1.66E-03	1.30E-02	4.70E-02	1.04E-02	CI
chgA_9600_d	9.22E+07	1.00E-04	1.00E-02	1.00E+02	2.14E-07	3.33E-03	2.50E-02	1.89E-01	2.08E-02	CI
chgA_9600_e	9.22E+07	1.00E-04	1.00E-02	1.00E+02	2.14E-07	6.66E-03	4.40E-02	7.56E-01	4.16E-02	CI
chgA_19200_a	3.69E+08	1.00E-04	1.00E-02	1.00E+02	2.14E-07	4.17E-04	1.00E-03	2.97E-03	6.53E-04	CI
chgA_19200_b	3.69E+08	1.00E-04	1.00E-02	1.00E+02	2.14E-07	8.33E-04	1.80E-03	1.18E-02	1.30E-03	CI
chgA_19200_c	3.69E+08	1.00E-04	1.00E-02	1.00E+02	2.14E-07	1.66E-03	3.37E-03	4.70E-02	2.60E-03	CI
chgA_19200_d	3.69E+08	1.00E-04	1.00E-02	1.00E+02	2.14E-07	3.33E-03	5.70E-03	1.89E-01	5.20E-03	CI

Table 1. Imposed hydraulic parameters, simulated recession coefficients (α_{sim}) and dominant flow domains of 2D synthetic square-shape discrete-continuum flow models. Analytically evaluated values of recession coefficient in the matrix-restrained and conduit-influenced baseflow domains are also demonstrated. Dominant baseflow domain is evaluated for each parameter configuration. CI: Conduit-Influenced baseflow domain, MR: Matrix-restrained baseflow domain, TR: transition zone.